Effects of Heat Treatment on Microstructure and Wear Resistance of Stainless Steels and Superalloys

Kuan Jiang

A thesis submitted to the Faculty of Graduate and Postdoctoral Studies
in partial fulfillment of the requirements for the degree of

MASTER OF APPLIED SCIENCE

in Mechanical Engineering

Ottawa-Carleton Institute for Mechanical and Aerospace Engineering
University of Ottawa
Ottawa, Canada

March 2013

Abstract

Slurry coating technique, as one of the most popular deposition methods, is widely used to produce various material coatings. This method includes two processes: spraying, brushing or dipping of slurry, and sintering heat treatment of the coated specimen. Superalloys and stainless steels are the most common materials used as either coating materials or substrate materials because of their excellent corrosion, wear, high-temperature and mechanical properties. This research is aimed at investigating the influence of the sintering heat treatment in the slurry coating process developed at Kennametal Stellite Inc. on the microstructure, hardness and wear behavior of superalloys and stainless steels. Low-carbon Stellite 22, cobalt-based Tribaloy T-400C, martensitic AISI 420 and AISI 440C stainless steels are studied in this research. The microstructure, hardness and wear resistance of these alloys before and after the heat treatment are investigated, stressing the influence of the heat treatment on these material characteristics. The hardness and wear tested are conducted on these alloys at both room temperature and at elevated temperatures. The worn surfaces of each specimen are analyzed using a Scanning Electron Microscope (SEM) with backscatter electron imaging (BEI) and energy dispersive X-ray (EDX) spectrum. It is demonstrated that the heat treatment alters the microstructures of these alloys differently; it increases the hardness but affects the wear resistance more complexly than hardness. At room temperature, the wear resistance of these alloys is governed by their microstructures. However, at high temperatures, oxidation, resulting in formation of oxide films on the specimen surface, influences the wear resistance significantly.

Acknowledgements

I would like to thank my advisor, Dr. Ming Liang for his guidance and support throughout my research in University of Ottawa. He was always accessible and willing to provide endless and tireless support whenever I need help.

I would also like to thank my co-supervisor Prof. Rong Liu at Carleton University and Dr. Kuiying Chen at NRC. The assistance from Prof. Rong Liu and Dr. Kuiying Chen and their expert knowledge of superalloy was truly invaluable. Their guidance and patience greatly inspired me in the research.

As well, I want to extend my thanks to the staffs of NRC specifically Dr. Qi Yang and Olga Lupandina. I appreciate their assistance and suggestions in providing me the instruments and technical experience during my time at NRC.

In addition, I would like to thank Kennametal Stellite Inc. in Belleville. I really appreciate the assistance from Dr. Matthew Yao and Rachael Collier in sample preparation, figuring out problems with the pin-on-disc instrument, and providing me deep knowledge about superalloys.

Lastly, a special thank you to my parents, friends, and especially my girlfriend, Tianjiao Li, all your encouragements and supports gave me endless enthusiasm and power through my hours of study and work.

Table of Contents

List of Tables

List of Figures

Nomenclature

V	Volume of worn material removed
L	Applied normal load on specimen
s	Total sliding distance
H	Hardness of the softer in a pair of materials
k	Wear coefficient
C	Circumference
D	Diameter of circular wear track
N	Rotational speed
t	Test duration
A	Cross-sectional area of worn track
T	Temperature

List of Acronyms

FCC	Face centered cubic
HCP	Hexagonal close packed
BCT	Body centered tetragonal
P/M	Powder metallurgy
HIP	Hot isostatic pressing
SEM	Scanning electron microscopy
EDX	Energy dispersive X-ray
BSE	Backscattered electron
WC	Tungsten carbide
HRC	Rockwell hardness
DSC	Differential scanning calorimetry
SE	Secondary electron
SFE	Stacking fault energy
ASTM	American society for testing and material
ASM	American society for metals

1 Introduction

1.1 Background of the Research

1.1.1 High-temperature wear of materials

Wear failure is a very common problem in mechanical applications of aerospace, automotive, oil production and oil refinery, chemical, nuclear, mining, and manufacturing industries. It degrades the performance and lifetime of mechanical components and results in economic loss. A statistic investigation shows that the wear failure of mechanical parts causes a great amount of economical loss which is estimated as much as 7% of gross national product costs in many industrialized nations every year [1]. In high temperature applications, where mechanical components operate in severe environments combining wear, corrosion and oxidation, the failure of some specific mechanical component is more common and it may be vital and catastrophic in many cases. A typical example is relevant to the aerospace industry, where a variety of degradation problems exist in aircraft engines as a result of metal to metal wear, fretting, hot corrosion, particle erosion plus others. This degradation is accelerated due to the high temperature conditions involved. The failure of any of these parts can have disastrous effects on the safety of the passengers and pilots in the aeroplane.

1.1.2 Materials for high-temperature wear resistance

For centuries, industry has an increasing need for high mechanical performance, more wear-resistant and corrosion-resistant materials for high-temperature applications. Stainless steels, a group of corrosion-resistant steels, differing from carbon steels by the amount of chromium present, were developed and applied in the second and third decades of the 20th century and served as a starting point for the satisfaction of high-temperature engineering

requirements [2]. Stainless steels possess excellent resistance to corrosion and staining, and also good wear resistance and high temperature oxidation resistance, as well as low cost, which make them popularly used in various industries.

Superalloys, consisting of nickel-, iron-nickel-, and cobalt-based alloys, were developed in the early 1900s. They are generally used when operating temperatures are beyond about 540 ℃ (1000 ℉) [3]. The crucial characteristics of all types of superalloys include superior tribological properties, excellent mechanical strength, outstanding resistance to loading under static, fatigue, and creep conditions; good surface stability, superb oxidation and corrosion resistance, and good phase stability at high temperatures. Over the years, a large number of superalloys have been developed and employed in various applications, typically in gas turbine engines, oil production and refining, and mechanical manufacturing.

Stellite alloy is a group of cobalt-based superalloys, containing chromium and tungsten or molybdenum and also a small amount of carbon. There are a large number of Stellite alloys composed of various amounts of cobalt, chromium, tungsten, molybdenum, nickel, iron, aluminum, boron, carbon, manganese, phosphorus, sulphur, silicon, and titanium, in various proportions, most alloys containing four to six of these elements. The main differences in the current Stellite alloy grades are carbon and tungsten contents, hence the amount and type of carbide formation in the microstructure during solidification [3]. The chief difference among the individual Stellite wear-resistant alloys is carbon content and, thus, carbide volume fraction in the materials.

Tribaloy alloy is another group of superalloys, usually hypereutectic and containing the

primary intermetallic Laves phase in a range of 30 ~ 70 vol% evenly dispersed in a softer eutectic matrix. The main alloying elements of Tribaloy alloys are chromium and molybdenum. Silicon is a minor (~ 3%) constituent of Tribaloy alloys. The carbon content in Tribaloy alloys is kept low to prevent carbides forming in preference to the Laves phase. The hard primary phase is a ternary Laves phase of the C-14 ($MgZn_2$) type having a melting point of about 1560°C, and its compositions are approximately Co_3Mo_2Si or CoMoSi for the Co-Mo-Cr-Si Tribaloy family. Because the Laves phase is so abundant in these alloys, its presence governs all the material properties. Accordingly, the effects of the matrix composition in these alloys are less pronounced than in the case of the cobalt-based carbide-type alloys, that is, Stellite alloys. The Laves phase is specifically responsible for outstanding abrasion resistance, but it severely limits the material ductility and the impact strength [4]. However, the presence of chromium and molybdenum, and the cobalt or nickel matrix provide Tribaloy alloys with excellent corrosion and high temperature properties.

1.1.3 Surface coatings

In many high temperature applications, mechanical components have to combat with multi-attacks from wear, corrosion and oxidation etc. Although stainless steels and superalloys have their own outstanding characteristics for wear, corrosion and high temperature protection, they still cannot fulfill the need to the best in all aspects. For instance, stainless steels are designed primarily for corrosion protection, but they are rarely found in the fields requiring high wear resistance. In the applications serving in extreme corrosive and wear environments, in an attempt to achieve the maximum combined properties of wear, corrosion, and oxidation resistance, as well as mechanical strength, one wise option is to

fabricate wear or corrosion resistant coatings on properties-balanced high temperature stainless steels and superalloys. On the other hand, superalloys and stainless steels can also be applied as coating materials. For example, stainless steels are usually coated with superalloys for better strength; carbon steels are coated with stainless steels for improved corrosion resistance, and superalloy are coated with hard tungsten carbides (WC) for enhanced wear resistance. The coating protection systems can extend the lifetime of superalloys and stainless steels in various different environments, with improved high temperature oxidation, wear resistance, enhanced erosion resistance and corrosion resistance, excellent creep resistance and reduction of thermal and mechanical fatigue.

Coating deposition techniques include slurry coating, chemical vapor deposition, physical vapor deposition, thermal spraying, optical coatings, laser coating, etc. Within various coating techniques, slurry coating is a popular, simple, low cost method to create protective coating for large size and complex shapes. As one of the traditional methods to fabricate coatings, this technique has been applied in gas turbine manufacturing process for several decades [5]. In the slurry coating fabrication process, slurry, formed by mixing metal powders with a liquid carrier, is deposited onto a substrate by spraying, brushing or dipping. The coated specimen is then placed into an oven to dry out the coating suspension. After that, it is processed with a sintering heat treatment to produce functional coating on the substrate. The heat treatment includes two steps. In the first step, the coated specimen is diffusion annealed at a certain elevated temperature, hold for several hours, in order to implement debinding or degassing and to release the liquid carrier out from the coating. Finally, the coated specimen is continuously heated up to the sintering temperature, held for a period of

time and then cooled down slowly. Through the sintering process, the metal powders are solid bonded onto the substrate forming a uniform coating. The slurry process utilizes simple equipment and techniques to create coating layers in an easier way so that it has potential to be automated in the future.

1.2 Introduction of the Research

1.2.1 Significance

Kennametal Stellite Inc. utilizes the slurry technique to produce various materials coatings; superalloys and stainless steels are the most popular because of their excellent corrosion, wear and mechanical properties. In many cases of industrial application, mechanical components operate in a corrosive, wear and high temperature combined environment, which requires the materials for these components to possess the properties against the synergetic attacks in the environment. Superalloys and stainless steels are the best options for this type of application environment. However, in order to further enhance the performance of these components, for example, high-temperature wear resistance, the surfaces of the components can be hardened by applying an effective coating such as WC. Therefore, superalloys and stainless steels have been employed as either coating materials or substrate materials in the coating products of Kennametal Stellite Inc.

The sintering cycle in the slurry coating process that Kennametal Stellite Inc. designed for superalloys and stainless steels has a relatively high sintering temperature (> 1000^{o}C) that is below the melting points of the alloys since higher temperature expedites atom diffusion of the

metallic powders. This heat treatment process may alter the microstructure and the properties of superalloys and stainless steels, thus influence the lifetime of the coated mechanical components.

1.2.2 Objectives

In this research, two superalloys and two stainless steels were selected to investigate their heat treatment influence on the microstructure, hardness and wear resistance. The thermal cycle of the heat treatment was exactly identical to the sintering cycle of the slurry coating process used by Kennametal Stellite Inc. for superalloys and stainless steels. The selected superalloys included a low-carbon Stellite alloy, designated as Stellite 22, and a cobalt-based Tribaloy alloy, named T-400C; the stainless steels were martensitic AISI 420 and AISI 440C. In consideration of the application environment of these materials coatings, the hardness and wear resistance of these alloys were evaluated at both room temperature and elevated temperatures.

1.2.3 Methodologies

This research is based on an experimental approach. The heat treatment process was implemented in an Oxy-Geo Industries High Temperature Vacuum Furnace. The microstructural analysis was performed using a Tescan Vega-II XMU Scanning Electron Microscope (SEM), equipped with an Oxford X-ray detection system (INCA EDX) for elemental analysis and quantitative mapping. The high-temperature hardness of these alloys was investigated using a Microhardness Tester Unit, Model SMT-X7 Dual Indenter, equipped with a microscope and with a Clemex video camera that allowed the hardness test made on

individual phases of a microstructure. The high temperature environment was created by attaching a Hot Stage to the indentation table with the temperature capacity of 700°C. The sliding wear resistance of the alloys was evaluated on a Nanovea Pin-On-Disc Tribometer. For high temperature wear test, a furnace was added to the system to keep the specimen in a specific temperature environment. The furnace could operate up to 500^{o}C and was controlled by a high temperature heating/holding system. To explore the wear mechanisms of each alloy at the different temperature environments and investigate the influence of the heat treatment on the wear behavior of these alloys in these environments, the worn surfaces of each specimen were studied using the Tescan Vega-II XMU Scanning Electron Microscope (SEM) with an Oxford X-ray detection system (INCA EDX).

1.2.4 Tasks

To achieve the objectives of this research, the following tasks have been completed:

(1) Half of the as-received specimens, including as-cast Stellite 22 and T-400C, and as-wrought AISI 420 and AISI 440C, experienced the heat treatment.

(2) Microstructural analysis was conducted on each as-received specimen and each heat-treated specimen of each alloy for comparison using SEM/EDX.

(3) Microhardness test was performed on individual phases and overall microstructure of as-received specimens and heat-treated specimens at both room temperature and elevated temperatures of 250°C, 450°C and 600°C.

(4) Wear behavior of each specimen was investigated on a pin-on-disc tribometer at room temperature and elevated temperatures of 250°C and 450°C.

(5) Worn surfaces of each specimen were examined using SEM to obtain the morphologies

and studied using EDX to analyze the elemental contents.

(6) Analysis of the influence of the heat treatment on the microstructure development of each alloy by comparing the change of the microstructures before and after the heat treatment.

(7) Analysis of the effect of the heat treatment on the hardness of each alloy at room temperature and at elevated temperatures.

(8) Analysis of the effect of the heat treatment on the wear resistance of each alloy at room temperature and at elevated temperatures.

(9) Discussion on the correlations between microstructure, hardness, wear resistance and temperature of these alloys, with emphasis on the heat treatment influence on these relations

1.3 Outline of the Thesis

This thesis can be considered a comprehensive report of this research. It is divided into eight chapters covering the introduction of this research, literature review in related research areas, main experimental procedures including heat treatment, metallographic examination, microhardness test, and pin-on-disc sliding wear test, experimental data collection and results, discussions on experimental results, conclusions and future work. The contents of the thesis are summarized below:

Chapter 1 is an introduction to the present research. It consists of general information on the background, significance, objectives, methodologies and tasks of this research.

Chapter 2 presents a literature review relevant to this research project. A brief introduction to stainless steels and superalloys is given in this chapter, including chemical composition, classification, microstructure, features, properties and applications. It also presents a detailed review over the previous research in the effects of heat treatments on stainless steels and superalloys.

Chapter 3 describes the details of experimental procedures in the study, including specimen preparation, heat treatment, metallographic analysis, hardness test, wear test and worn surface analysis. Various testing facilities employed in this research are also introduced in this chapter.

Chapter 4 reports the results of microstructural analysis. Both SEM microstructure images and EDX spectra for each specimen are provided. The results are explained.

Chapter 5 reports the results of microhardness test. Various plots are made on these results to facilitate analysis and comparison.

Chapter 6 reports the results of wear test and worn surface analysis. Various plots are made on the wear test results to facilitate analysis and comparison. SEM morphologies and EDX spectra for each specimen are provided. The results are explained.

Chapter 7 discusses the results obtained from the experiments. The effects of the heat treatment on the microstructure, hardness and wear resistance of these alloys are highlighted. The temperature-dependence of these material properties is discussed in regard of the heat treatment effect on these alloys.

Chapter 8 summarizes the research results and presents the conclusions drawn from this research. It also proposes the future work to further study the heat treatment effects.

2 Literature Review

2.1 Materials for High Temperature Resistance

2.1.1 Types of materials

Mechanical components operating in aerospace, automotive, oil production and oil refinery, chemical, nuclear, mining, and manufacturing industries often require strength to withstand the synergetic attack combining wear, corrosion and high temperature. In order to extend the service lifetime of the mechanical components in high temperature applications, various materials have been designed and developed purposefully to fulfill the increasing need for stronger, more wear-resistant materials in industry. The most well-known high temperature material is the superalloy family. These high performance materials are a group of iron-nickel-, nickel-, and cobalt-base alloys used above about 1000^{o}F (540^{o}C) for high temperature applications [3]. Another notable family for high temperature applications is stainless steels, which contain a minimum of 10.5% chromium with at least 50% iron. Owing to high chromium content, stainless steels exhibit the "stainless" characteristic and have strong resistance for corrosion and high temperature (up to 800^{o}C for some specific types) attack. Nowadays, due to their unique combination of mechanical, wear/corrosion resistance and high temperature properties, superalloys and stainless steels are widely used in various high temperature applications.

2.1.2 Superalloys

Based on the different balance material elements, superalloys are generally classified into three categories: iron-nickel-based, nickel-based, and cobalt-base. Stellite alloys and Tribaloy alloys are two main groups of superalloys designed for wear and corrosion resistance. Stellite

alloys are a range of cobalt-chromium alloys containing tungsten or molybdenum and a small amount of carbon. Unlike Stellite alloys, Tribaloy alloys consist of a great amount of molybdenum and silicon, and carbon is limited to as less as possible in the chemical compositions.

Stellite alloys are a group of cobalt-based superalloys designed for high temperature, wear, corrosion and oxidation resistance. They are derived from the Co-Cr-W and Co-Cr-Mo alloys which investigated by Elwood Haynes in early 1900 and now the trademark of Kennametal Stellite Company. The chemical compositions of Stellite alloys are typically composed of cobalt, chromium, tungsten or molybdenum and a small amount of carbon. Table 2-1 lists the nominal chemical compositions of various Stellite alloys that are commonly used in different fields. It can be seen that the most important agent, carbon, varies between 0.1 ~ 2.5 wt% among the alloys. The difference of carbon content between Stellite alloys results in the variety of carbides constitution and volume fraction in the material. For example, Stellite 3 with a high carbon level of 2.4wt% has a microstructure of primary chromium-rich M_7C_3 carbides in an interdendritic eutectic matrix with solid solution and tungsten-rich M_7C_3 carbides [6], as shown in Figure 2-1, while hypo-eutectic Stellite 6 with 1wt% carbon content consists of primary cobalt dendrites with eutectic chromium-rich M_7C_3 carbides network.

Table 2-1: Nominal chemical compositions (wt%, Co in balance) of various Stellite alloys [7]

Alloy	Process	Cr	W	Mo	C	Fe	Ni	Si	Mn	Others
Stellite 1	Cast	30	13	0.5	2.5	3	1.5	1.3	0.5	
Stellite 3	P/M	30.5	12.5		2.4	5	3.5	2	2	1B
Stellite 6	Cast	29	4.5	1.5	1.2	3	3	1.5	1	
Stellite 6	P/M	28.5	4.5	1.5	1	5	3	2	2	1B
Stellite 21	Cast	27		5.5	0.25	3	2.75	1	1	
Stellite 20	Cast	33	17.5		2.45	2.5	2.5		1	
Stellite 22	Cast	27		11	0.25	3	2.75	1	1	
Stellite 25	Cast	20	15		0.1	3	10	1	1.5	
Stellite 80	Cast	33.5	19		1.9					1B
Stellite 188	Cast	22	14		0.1	3	22	0.35	1.25	0.03La
Stellite 720	Cast	33		18	2.5	3	3	1.5	1.5	0.3B
Stellite 706K	Wrought	29		6	1.4	3	3	1.5	1.5	
Stellite 6B	Wrought	30	4	1.5	1	3	2.5	0.7	1.4	
Stellite 6K	Wrought	30	4.5	1.5	1.6	3	3	2	2	

As the balance element, cobalt plays a very important role in Stellite alloys. Owing to the instable crystal structure and very low stacking fault energy of cobalt, cobalt-based alloys have various distinct features such as high yield strengths, high work-hardening rates, limited fatigue damage under cyclic stresses and the ability to absorb stresses [3].

Other alloying elements such as chromium, tungsten and molybdenum exert their own influence on Stellite alloys. For example, chromium acts as the predominant carbide former and the most important alloying element in the γ matrix. It provides additional strength to the matrix and contributes to the enhancement of resistance to corrosion and oxidation. Tungsten and molybdenum improve the corrosion/oxidation resistance of the Stellite alloys. They strengthen the matrix owing to their unique characteristic of large atom size. Moreover, when present in large quantities, tungsten and molybdenum participate in the formation of carbides during alloy solidification and promote the precipitation of M_6C [3].

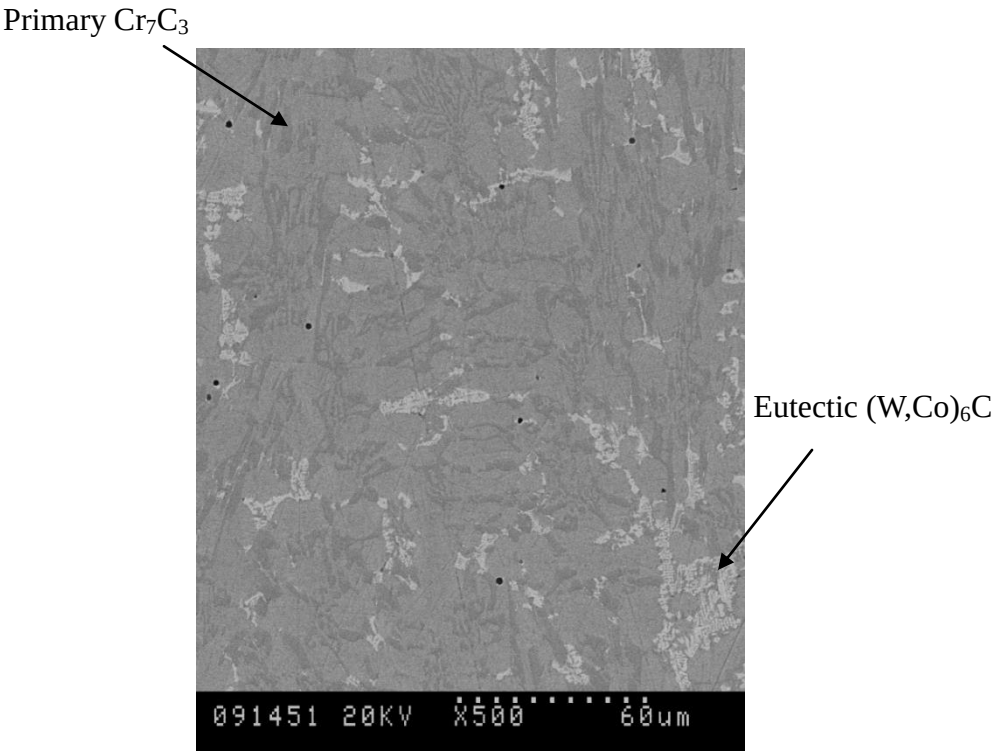

(a)

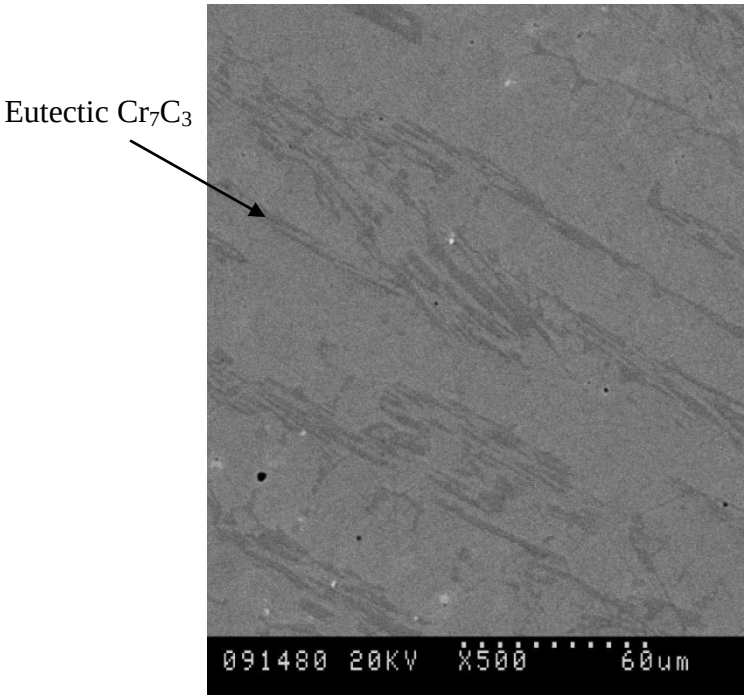

(b)

Figure 2-1: SEM images of microstructure: (a) Stellite 3 and (b) Stellite 6 [7].

Tribaloy alloys are also a group of cobalt-based or nickel-based superalloys designed for high temperature, wear and corrosion applications, but they differ from Stellite alloys in that they are strengthened with hard intermetallic phase, known as Laves phase, instead of carbides, as shown in Figure 2-2. The hard primary phase is a ternary Laves phase of the C-14 ($MgZn_2$) type having a melting point of about 1560^{o}C, and its compositions are approximately Co_3Mo_2Si or CoMoSi [8]. The intermetallic Laves phase has a hexagonal closed packed (hcp) crystal structure. Because the Laves phase is so abundant in these alloys (35 – 70 vol%), its presence governs all the material properties [3]. Laves phase is hard and brittle, which provides Tribaloy alloys with several high performance properties such as hardness, strength, wear resistance and corrosion resistance. On the other hand, the ductility and impact strength of Tribaloy alloys are limited by Laves phase severely. Table 2-2 presents nominal chemical

compositions of various Tribaloy alloys. Cobalt and nickel are based-material to form a solid solution matrix. The solid solution is strengthened by chromium and molybdenum. In Tribaloy alloys, chromium exists in the solid solution matrix, contributing to the corrosion resistance and the matrix strengthening. Molybdenum is used to impart high temperature strength to the matrix. Molybdenum and chromium, by reducing the stacking fault energy, enhance the plastic deformation that is induced by the fcc to hcp crystal structure transformation in the cobalt-based matrix [9-12]. In addition, as shown in Table 2-2, unlike other cobalt-based alloys (i.e. Stellite alloys), a great amount of molybdenum and silicon are added in Tribaloy alloys to promote the precipitation of the intermetallic Laves phase. Carbon content is quite a tiny part in Tribaloy alloys with the purpose to keep carbide formation as less as possible.

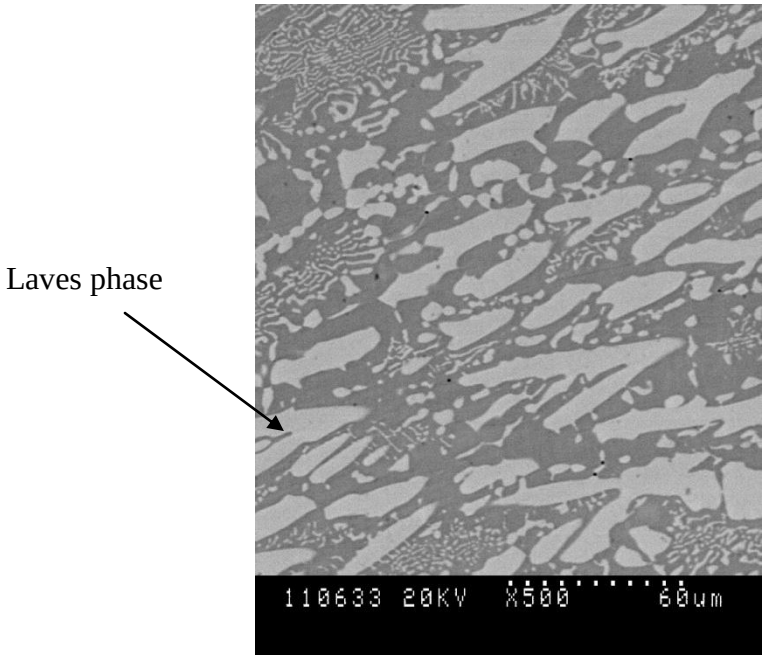

Figure 2-2: SEM image of the microstructure of T-400 [7].

Table 2-2: Nominal chemical compositions (wt%) of Tribaloy alloys [7]

Tribaloy alloy	Co	Ni	Cr	Mo	Si	Laves phase content (vol%)
T-100	55			35	10	~65
T-400	62		8.5	28.5	2.6	~45
T-700		50	15	32	3	~60
T-800	52		17	28	3	~55

2.1.3 Stainless steels

Stainless steels are another family of currently favored high performance materials for extremely severe environments because they offer useful combination of high temperature mechanical properties and corrosion/oxidation resistance. The primary character of stainless steels is to withstand corrosion and oxidation, which is enabled by the addition of chromium in excess of 10.5wt%. This stainless character of stainless steels is achieved through the formation of tightly adherent chromium-rich oxide layers on their surfaces. The layer is very thin and has the ability to heal itself very quickly in oxygen environment when damaged. This adherent chromium-rich oxide layer effectively protects and passivates stainless steels in many corrosive environments [13-15].

Since chromium is the most important alloying element in stainless steels, it is necessary to well understand the iron-chromium (Fe-Cr) equilibrium phase diagram, as given in Figure 2-3. Chromium is a strong ferritic-forming element. It stabilizes the body-centered cubic ferrite structure and expands α-ferrite and σ-ferrite fields as chromium content increases. When chromium content is more than 12 wt%, the body-centered cubic ferrite is stable finally and

γ-ferrite field has disappeared. Another important alloying element in stainless steels is nickel. Nickel is an element that stabilizes the face-centered cube structure and expands the γ-ferrite field in iron. The iron-nickel (Fe-Ni) equilibrium phase diagram is shown in Figure 2-4. Austenite is completely stable when nickel content is above 30 wt%. According to these phase diagrams, stainless steels can be conventionally categorized as the five groups: ferritic, martensitic, austenitic, duplex and precipitation hardening stainless steel.

Ferritic stainless steel consists of iron-chromium alloys with a body-centered cubic crystal structure. It contains 13 to 30 wt% chromium and very little carbon content to stabilize the body-centered cubic ferrite structure. Therefore, this type of steel maintains the single-phase microstructure of ferritic under heat treatment.

Martensitic stainless steels have similar chemical compositions to ferritic group. However, the chemical compositions of martensitic stainless steels should within the γ-ferrite field in order to form austenite when heated up. This type of steel contains between 11.5 and 18 wt% chromium, and with up to 1 wt% carbon. The resulted martensitic stainless steels are austenitic at elevated temperatures and harden through transformation to martensite during quenching or cooling down to room temperature [16].

Austenitic stainless steels contain a maximum of 0.15 wt% carbon, a minimum of 16 wt% chromium and sufficient nickel and/or manganese in composition. Owing to the stable effect of nickel and/or manganese on γ-ferrite, austenitic stainless steels retain a face-centered cubic structure at all temperatures from the cryogenic region to the melting point of the metal.

Similar to ferritic group, austenitic stainless steels cannot be strengthened by heat treatment such as quenching to form martensite or by precipitation hardening [13].

Duplex stainless steels consist of roughly equal amounts of two phases at room temperature: austenite and ferrite. They can generally be considered as chromium-molybdenum ferritic stainless steels with sufficient nickel to create a balance of ferrite and austenite at room temperature [13].

Precipitation hardening stainless steels are a group of chromium-nickel steels which have a good corrosion resistance. Due to the addition of precipitation hardening elements such as aluminum, copper, titanium, and so on, they can be precipitation hardened to a higher strength and toughness by a solution and aging heat treatment.

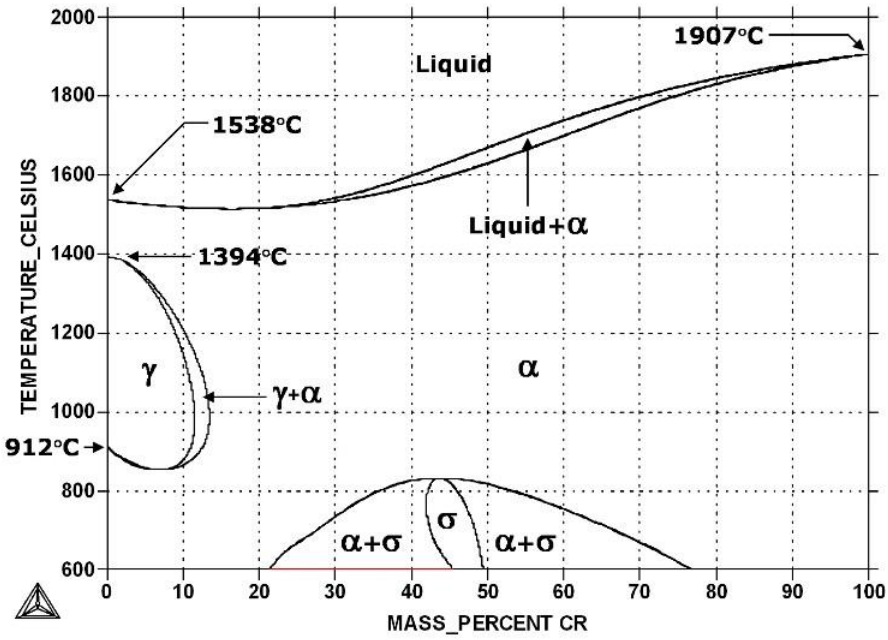

Figure 2-3: Iron-chromium (Fe-Cr) equilibrium phase diagram [13].

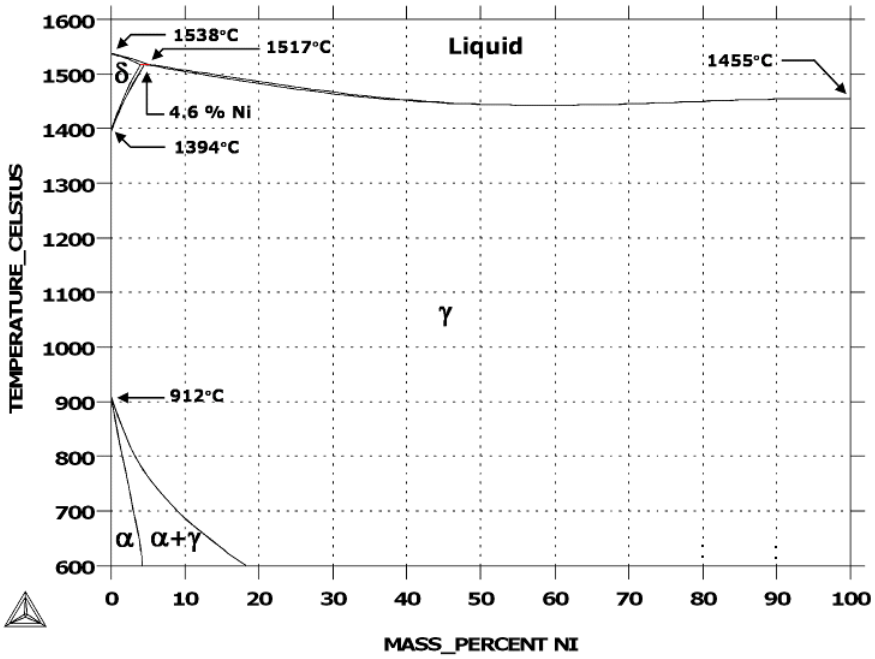

Figure 2-4: Iron-nickel (Fe-Ni) equilibrium phase diagram [13].

2.2 Heat Treatment of High-temperature Alloys

Heat treatment is a series of heating and cooling processes on metals to alter their physical and mechanical properties without changing the product shape. The heat treatment of high temperature alloys can have many purposes and processes, such as annealing to soften the material after cold working, solution annealing to homogenize the structure, heating to temper martensite, stress relieve etc [16].

2.2.1 Annealing

In the annealing process, metallic materials are heated to a designed temperature and then cooled at a set rate. For stainless steels, annealing process is used to produce a refined microstructure and soften the metal. However, it exerts a total reverse influence on some

superalloys. Instead of relieving stress and softening material, superalloys generally exhibit hardening characteristic after annealing treatment. A. OSMA *et al.* [17] investigated the effects of elevated temperature on Stellite 6 alloys. The as-cast Stellite 6 alloys were heat-treated at 1000^{o}C for 30 min and then cooled in air. It was demonstrated that high temperature exposure of Stellite 6 promoted the coarsening of the microstructure and contributed to the increase in bulk hardness [17]. As shown in Figure 2-5 and Figure 2-6, the heat treatment on the alloy at 1000^{o}C resulted in the formation of a characteristic texture structure in dendritic. Also, a high temperature promoted bulk diffusion of tungsten from the dendrites to the interdendritic regions forming carbide phases and/or intermetallic phases (Co_7W_6 and Co_3W) within the interdendritic regions [17]. The formation of textured structure and the precipitation of carbide phase and/or intermetallic phases in heat-treated Stellite 6 altogether contributed to the increase in hardness. Similar research results regarding the effects of annealing treatment on Stellite alloys were confirmed by Ping Huang *et al.* [18]. Bulk hardness in modified Stellite 21 increased and carbide phases precipitated from the eutectic after the annealing at 1050^{o}C for an hour and then air cooled [18]. The high hardness of superalloys is generally dependent on the microstructure and especially on the sizes and amounts of strengthening carbides and intermetallic phases. Annealing treatment promotes the diffusion of carbides and several alloying elements such as tungsten, molybdenum, silicon, etc. and contributes to the formation of hard strengthening phase, hence hardening the alloys.

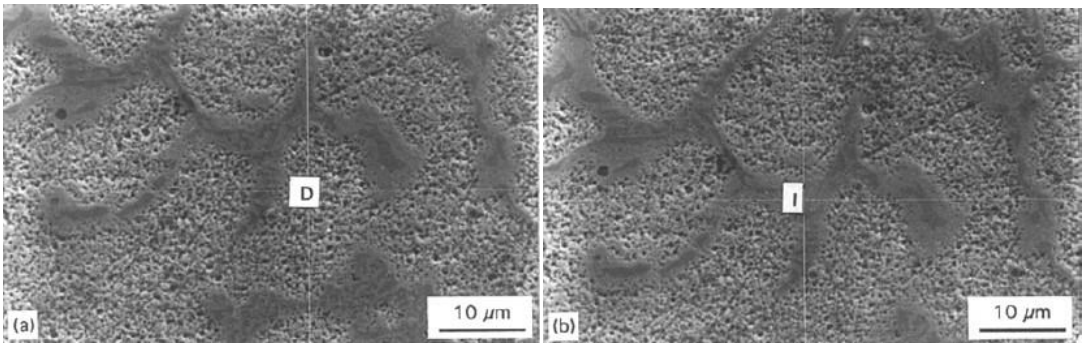

Figure 2-5: SEM micrographs and EDX analyses of as-cast Stellite 6: (a) EDX analysis for dendritic region (D: 61.78 wt%Co, 29.93 wt%Cr, 4.68 wt%W); (b) EDX analysis for interdendritic region (I: 22.68 wt%Co, 70.81 wt%Cr, 4.01 wt%W) [17].

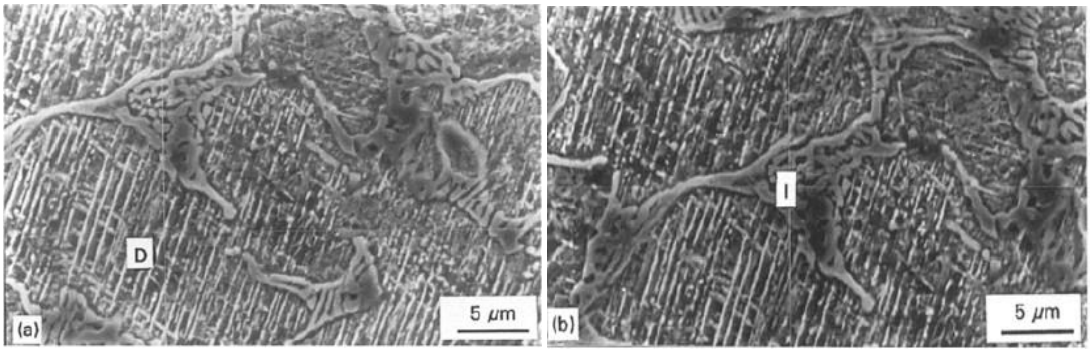

Figure 2-6: SEM micrographs and EDX analyses of as-cast Stellite 6 heated to 1000°C and cooled in air: (a) EDX analysis for dendritic region (D: 62.44 wt%Co, 30.42 wt%Cr, 3.13 wt%W); (b) EDX analysis for interdendritic region (I: 39.65 wt%Co, 50.89 wt%Cr, 6.4 wt%W) [17].

2.2.2 Austenitising

For martensitic stainless steels, austenitising treatment is a very important step before quenching. The alloying elements and carbides dissolve into the austenite matrix and the microstructure then becomes homogeneous. Austenitising temperature and holding time are

two significant parameters in this process. An excessive austenitising temperature and extensive exposure under austenitising temperature result in coarseness of the microstructure, dissolution of carbides and undesirable grain growth. The effects of austenitising temperature on the martensite stainless steel have been studied extensively. Nasery Isfahany *et al.* [19] reported that the maximum strength was acquired for the AISI 420 stainless steel austenitized at 1050^{o}C for 30 to 60 min as shown in Figure 2-7. Garcia de Andres *et al.* [20] demonstrated that the increase of austenitising temperature promoted the carbide dissolution in the matrix and decreased the volume fraction of carbides from 9.9% to 6.6%.

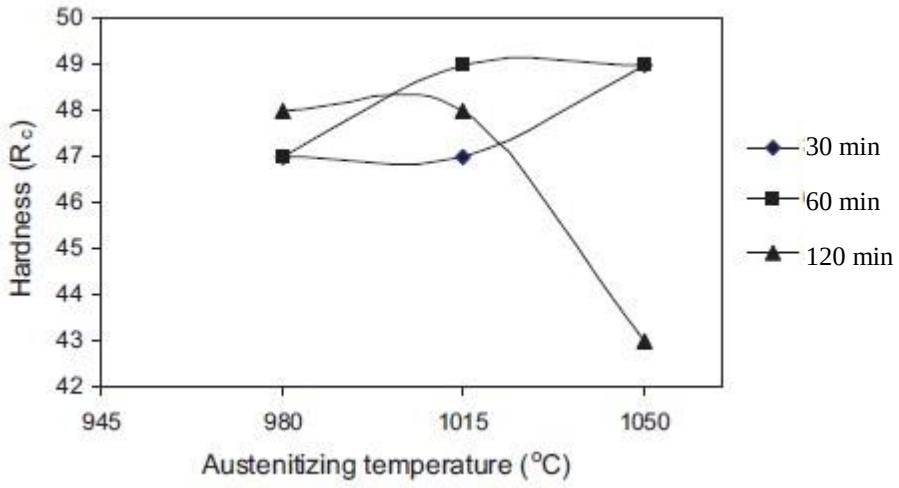

Figure 2-7: Effects of austenitizing time and temperature on hardness of AISI 420 stainless steel [19].

For superalloys, solution treatment before quenching plays the similar role as austenitising treatment for martensitic stainless steels. Carbides and alloying elements dissolve into the austenite matrix during solution treatment. Yao *et al.* [21] investigated the effects of solution treatment temperature on the as-wrought Stellite 706K alloys. It was shown that heat treating

at temperature of 1235^{o}C stabilized the rolled microstructure with fine and large amount of carbides resulting in enhanced wear resistance [21]. However, Yao *et al.* [21] also reported that heat treatment at 1250^{o}C on Stellite 706K caused the dissolution of some carbides and coarsening of carbides, which yielded a lower hardness. The increase of the solution temperature promoted the carbide dissolution and coarsening of the matrix as well as weakened the strengthening effects of carbides.

2.2.3 Quenching

Quenching is a process in which the metal is heated to and held at a specific temperature and then cooled rapidly. It imparts strength and hardness to steels from the martensite transformation. For example, AISI 420 martensitic stainless steel was confirmed to reach the peak hardness approximately 710HV after austenitising at 1120^{o}C and then quenching [20]. The increased hardness and strength of as-quenched steel are attributed to the fact that a high content of martensite has been formed within the microstructure. Due to the hard and brittle crystalline structure, martensite exhibits an excellent combination of mechanical characteristics. However, quenching process can only harden superalloys slightly or in some cases even deteriorated their strength [22, 23]. This adverse phenomenon on superalloys may be explained as superalloys have a distinct hardening/softening mechanism through quenching, instead of the formation of martensite in martensitic stainless steels. Kuzucu *et al.* [22] observed the fcc cobalt-rich matrix transformed to hcp structure in heat-treated Stellite 6 plus 6 wt% Mo alloys; this transformation due to the heat treatment led to slight increase in hardness. Due to the sluggish nature of the transformation, cobalt and cobalt-based superalloys usually retains the fcc structure at room temperature, and hcp formation is only

triggered by mechanical stresses or time at a temperature. The rapid cooling enables cobalt-based superalloys to retain the hcp cobalt structure and increase the hardness. Also, the cooling medium was found to influence the amount of hcp structure and hardness. The cooling in liquid nitrogen of Stellite 6 caused an increase in the amount of hcp structure and a more homogeneous distribution of carbides in the inter-dendritic as well as an increase in hardness than quenching in water [22]. However, for Tribaloy alloys, it was found that their strength was deteriorated by quenching process. It is reported that high-temperature treatment decreased the macro hardness of T-400 from 55HRC to 50HRC [23]. Similar conclusion was drawn by Liu *et al.* [23] that the high temperature heat treatment homogenized the microstructure of T-400C and promoted the cobalt hcp-fcc transformation, and therefore caused slight decrease in macro hardness.

2.2.4 Tempering, aging and precipitation hardening

After quenching treatment, martensitic steels are very hard and brittle. They have to be tempered in order to reduce brittleness, increase ductility and obtain sufficient toughness. This process involves two steps: the steel is first held at a temperature below the austenite transformation range, and then cooled at a set rate. In tempering, carbon is precipitated from the supersaturated state. Since carbon diffuses 10^6 times as fast as iron, chromium, or other carbide formers, heating to even low temperatures under 400^oC allows it enough mobility to diffuse and precipitate as carbides [16]. Generally, the growth of carbides releases strains and softens the metal. However, hard precipitation hardening carbides are formed within the matrix, which causes hardening or strengthening if adding aluminum, titanium, molybdenum and other precipitation hardening elements into martensitic steels. For example, the strength of

precipitation hardening 13-8 Mo stainless steels is accomplished from the precipitation of intermetallic compounds such as Ni_3Al in ductile low-carbon martensitic matrices [13]. Similar hardening phenomenon was observed in Tribaloy alloys. It is reported that after aging at 800^{o}C for 48 hr, the volume fraction of hard intermetallic phase in T-200 alloy increased largely, and hence contributed to the improvement in both hardness and wear resistance [23].

2.2.5 Surface hardening

Surface hardening treatment is an extension of traditional heat treatment techniques. It hardens the material's surface by a variety of methods, including flaming hardening, induction heating, carburizing, nitriding and carbonitriding. These treatment processes are employed for various purposes such as improving wear, fatigue, corrosion, and oxidation resistance [13]. In regard to stainless steels, surface treatment has been proven to improve their wear, corrosion resistance and mechanical properties effectively [24]. Xi *et al.* [25] reported that plasma nitriding at 350^{o}C increased significantly the surface hardness and wear resistance of AISI 420 steel, as shown in Figure 2-8 and Table 2-3. Liu *et al*. [26] found that the surface of 17-4PH martensitic precipitation hardening stainless steel was enhanced by plasma nitrocarburizing; the Vickers hardness test revealed that plasma nitrocarburizing increased the hardness of the treated surface layer to HV1186, which is 3 times higher than that of untreated surface [26]. In addition to plasma nitriding, other surface modification methods such as ion implantation have also been proven improving the wear resistance of stainless steels pronouncedly. Alonso *et al.* [27] reported that high-dose ion implantation with carbon has not only improved the wear and friction properties of AISI 440C steel but also altered the wear mechanism of 440C stainless steel from adhesive wear to a beneficial mild abrasive oxidative wear. Similar

phenomenon of wear resistance improvement and wear mechanism transition were confirmed by Onate *et al* [28] in the study of AISI 420 stainless steel. The formation of a dispersion of fine precipitates enhanced the wear resistance of AISI 420, and the formation of an adherent oxide layer on the surfaces resulted in the transition of wear mechanism from a severe abrasive plus adhesive type to a mild oxidative wear [28].

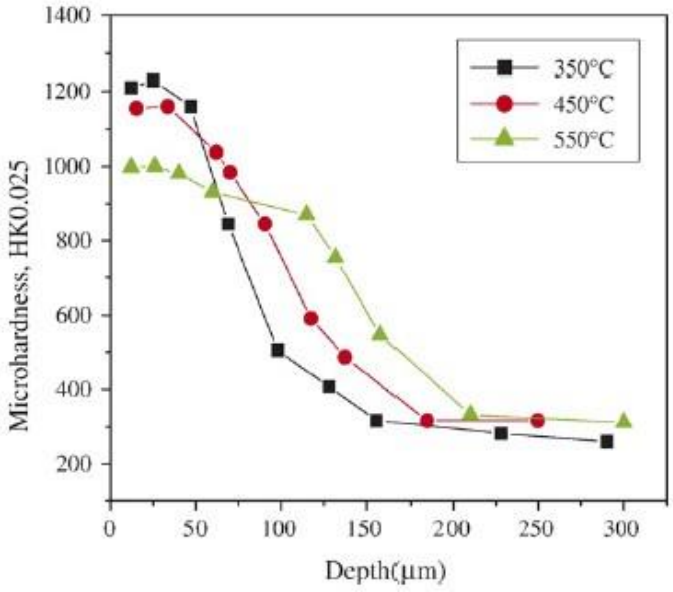

Figure 2-8: Effect of plasma nitriding temperature on microhardness of AISI 420 stainless steel [25].

Table 2-3: Wear weight loss and wear scar width of AISI 420 test samples at different plasma nitriding temperatures [25]

	Untreated sample	Nitrided at 350^{o}C	Nitrided at 550^{o}C
Weight loss (mg)	4.33	0.13	0.21
Wear scar width (mm)	0.55	0.18	0.19

2.3 Sliding Wear of High-temperature Alloys

2.3.1 Mechanism of sliding wear

Sliding wear occurs when one solid surface moves relatively to another. The wear behavior of materials is influenced by several diverse factors. It depends on not only both two contact materials' properties but also the geometric features of the contact surface as well as variables of wear process such as load, temperature, sliding velocity and environment.

When sliding wear occurs at room temperature and the frictional heat between contact surfaces is not high, oxide films break down as long as two metal contact against each other. Under this condition, cold welding of the two surfaces occurs; sliding movement will result in fracture of some small pieces from original interface and finally cause substantial metal transfer from one surface to the other thus gross deformation of the surface materials.

Based on the wear mechanism above, Archard [29] proposed a model relating the wear volume loss with applied normal load, sliding distance and material hardness. Archard's model is commonly used to analyze the wear behavior of materials with the assumption of asperity welding and subsequent shear as follows [29]:

$$V = k\frac{L \times s}{H} \tag{2-1}$$

where V is volume of worn material removed, L is applied normal load, s is total sliding distance, H is hardness of the softer in a pair of materials and k is the dimensionless wear coefficient less than 1. The wear rate is defined as cumulative lost volume V per sliding unit, as expressed below:

$$wear\ rate = \frac{V}{s} = k\frac{L}{H} \tag{2-2}$$

The linear relationship between wear volume loss and $L \times s/H$ has been verified by experimental data in different wear conditions [30-31]. Figure 2-9 is the diagram of wear volume dependence of sliding distance plotted by Bressan *et al.* [31] based on the pin-on-disc experimental results of 17-4PH steel. The hardness of the disc was HRC 43 and pins had different hardness, as indicated in the figure. The wear loss was directly proportional to the sliding distance and decreased as the hardness increased.

The proportional relationship between wear rate and hardness is more clearly shown in Figure 2-10. The trend of the wear rate curves with the hardness of the softer material in the wear pair is approximately constant and linear. The results are all in accordance with the prediction from Archard's equation [29].

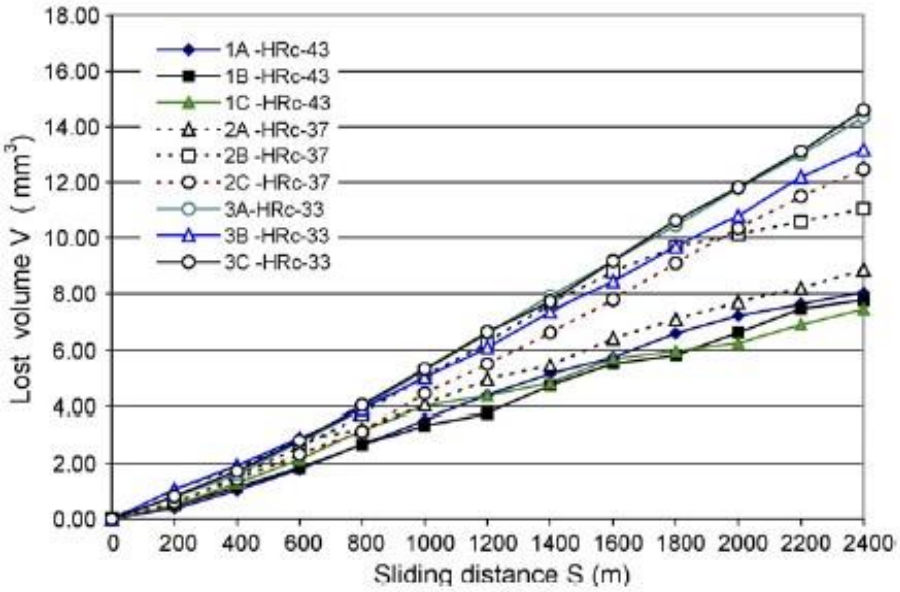

Figure 2-9: Wear lost volume versus sliding distance in 17-4PH pin-on-disc tests under applied load of 30N [31].

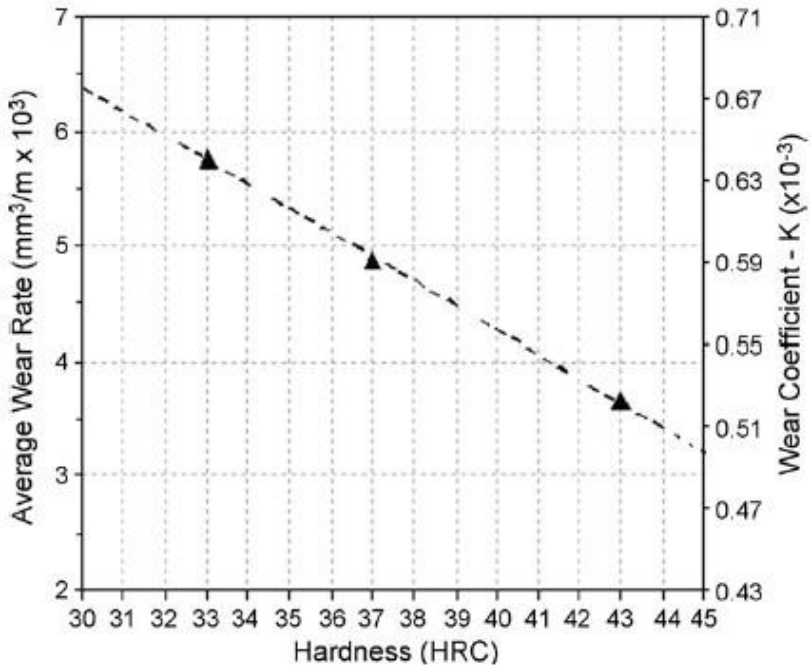

Figure 2-10: Average wear rate versus hardness of the softer material in the wear pair of 17-4PH pin-on-disc tests under applied load of 30N [31].

However, Archard's theory fails to predict the abrupt decrease in wear rate under high temperature sliding wear between two metallic materials [32-36]. Such opinion has been verified by Lancaster *et al.* in the research regarding the influence of temperature on the wear behavior of 60/40 brass against tool steel [32]. As illustrated in Figure 2-11, when temperature is below 300^{o}C, the wear rate increased as the temperature increased. Again, it should be noted that Archard's theory works well when severe wear occurs, which is before the abrupt decrease of wear rate occurring. Softening of the material with temperature is accounted for the increase in wear rate with increasing temperature below 300^{o}C, which is also in accordance with the prediction of Archard's equation, but wear mechanism is altered when temperature is above 300^{o}C. In Figure 2-11, it is obvious that the wear rate decreased abruptly when temperature was around 300^{o}C, causing a mild wear regime. This relatively low wear

rate regime is known attributed to the formation of protective oxide layers. Temperature influences the kinetics of oxidation, and hence affects the nature of wear. The wear rate is low when ‘glazes’ are present because the ‘oxide glazes’ are very smooth. The wear debris consists of very fine oxide particles that can be re-compacted into the ‘glazes’ surface [33]. The formation of oxide glazes’ is the product of high surface temperature. Thus, either high temperature environment or frictional heat will result in the formation of ‘oxide glazes’, subsequently, altering the wear mechanism from severe wear into mild wear and reducing the wear rate.

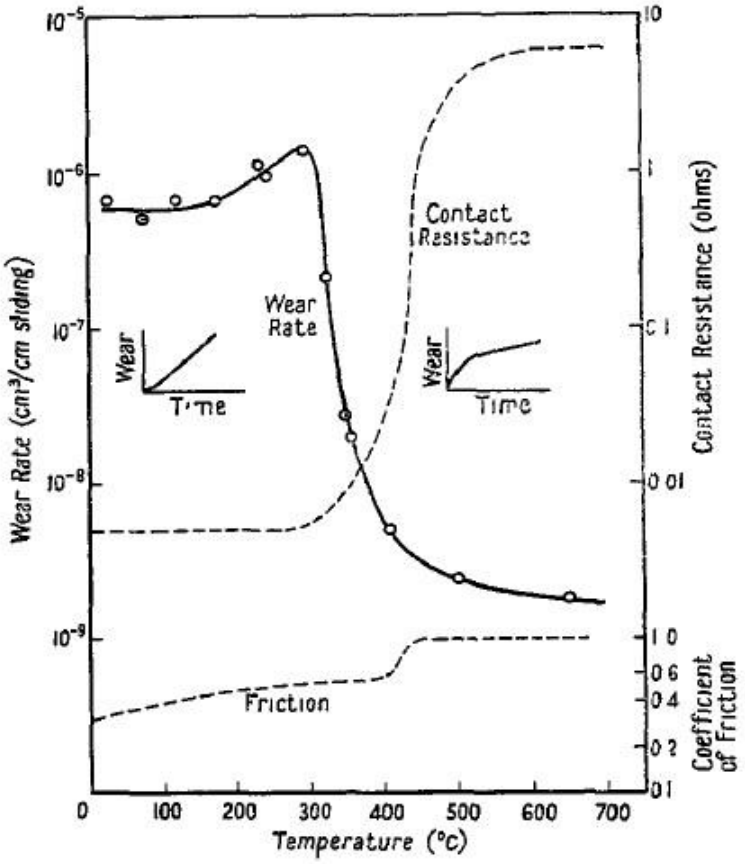

Figure 2-11: Wear rate versus temperature for 60/40 brass against tool steel [32].

2.3.2 Previous research in room-temperature wear

The wear behavior of various metals has been studied extensively. The microstructure effects on the sliding wear behavior of Stellite 6 were explored by Frenk *et al.* [37]. The microstructure of Stellite 6 alloy was modified by different processing conditions. Under a severe metallic wear regime, the microstructure had little influence on the wear rate. The differences in wear rate from a finer microstructure to a coarser one were noticed, although the specimens all had the same chemical composition. They also noted that the initial hardness of material was independent of its wear properties under the severe metallic wear regime, which is in disagreement with the Archard's type of wear relationship, *i.e.* wear rate inversely proportional to hardness. However, contradictive conclusion was drawn in the study of sliding wear behavior of Stellite 4 by Yu *et al* [38]. Sliding wear tests were conducted on both as-cast and HIPed Stellite 4 alloys in their study. The microstructure of HIPed alloys was not only finer, but also had discrete carbides, instead of the interconnected three-dimensional eutectic net in cast alloys [38]. Their wear test results demonstrated that the cast alloy with a coarse microstructure and distinct carbide morphology exhibited a better wear resistance and a different wear mechanism as compared with HIP alloy.

Wear resistance of superalloy can also be influenced by changing the content of alloying elements such as tungsten, molybdenum, silicon, yttrium, etc. In room temperature wear, superalloys usually derive their superior wear resistance from the hard phases. For Stellite alloy, tungsten and molybdenum are two vital alloying elements in the matrix. They participate in the formation of carbides as well as provide added strength to the matrix. Several studies arrived at a conclusion that molybdenum in replace of tungsten or increase

molybdenum content in Stellite alloys improved the wear resistance of the alloys [21, 39]. They suggested that molybdenum had a larger atom size and stronger carbon-forming ability than tungsten and hence increased the volume faction of carbides in the microstructure, which is attributed to the increase in wear resistance [21, 39].

In Tribaloy alloys, the solid solution is strengthened by chromium and molybdenum. Chromium mainly contributes to the corrosion resistance while molybdenum is used to impart high temperature strength to the matrix. Similar to Stellite alloys, Tribaloy alloys are also strengthened by the precipitation of hard phases in the cobalt solid solution matrix. The volume fraction of Laves phase is dependent on chemical compositions greatly. Xu *et al.* [40] reported the decrease of silicon and molybdenum reduced the volume fraction of hard Laves phase in Tribaloy alloys. If silicon and molybdenum content are reduced greatly, the microstructure of Tribaloy alloys is altered significantly. As shown in Figure 2-12, the volume fraction of primary Laves phase in T-400C alloy is slightly less than that in T-400 alloy due to the reduction of Mo content, but a tremendous decrease of the Laves phase amount occurs in T-401 that has much lower Si and Mo contents, compared with T-400 and T-400C. The pin-on-disc sliding wear test showed that the wear resistance of T-401 was apparently low compared with T-400. T-400C had lower wear resistance than T-400, but the difference was relatively small. It was believed that the wear resistance reduction in both T-400C and T-401 were dues to the decrease of the volume fraction of Laves phase in their microstructures.

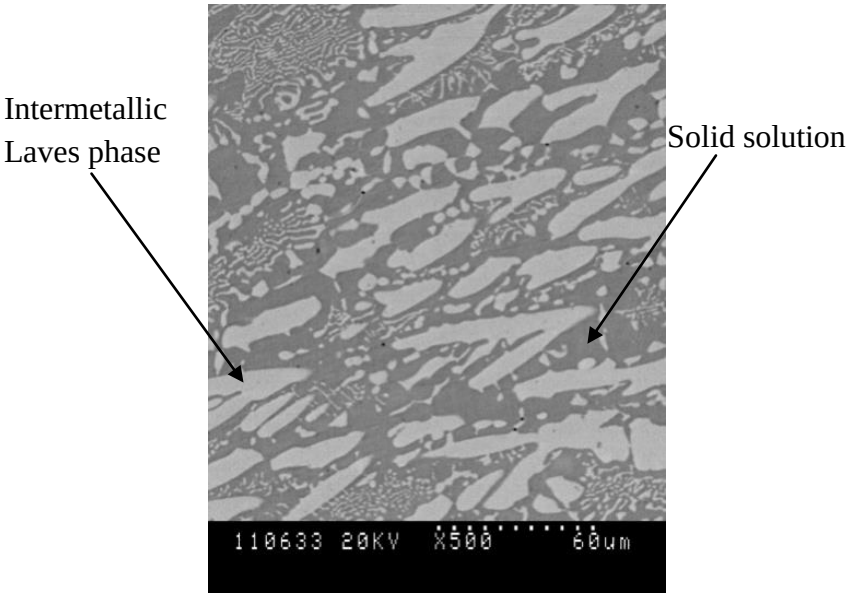
Intermetallic
Laves phase
Solid solution
110633 20KV X500 60um

(a)

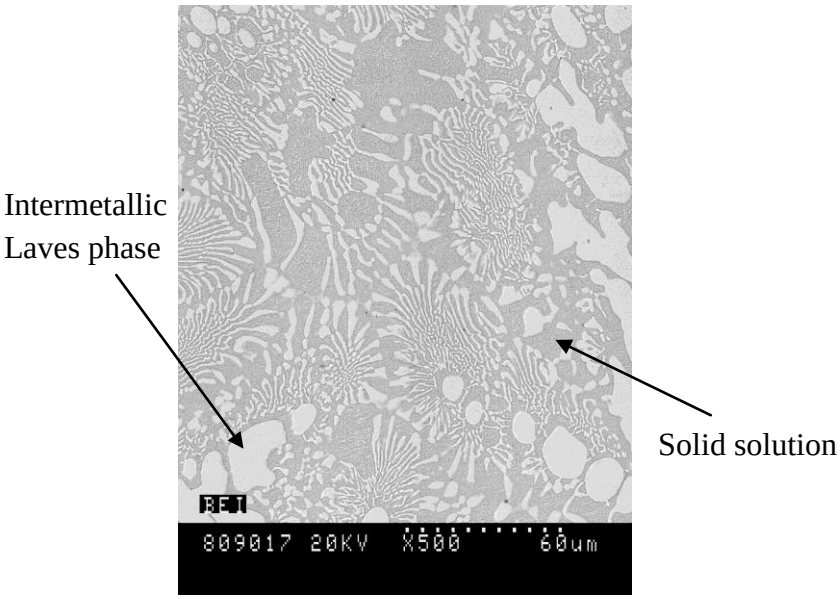
Intermetallic
Laves phase
Solid solution
809017 20KV X500 60um

(b)

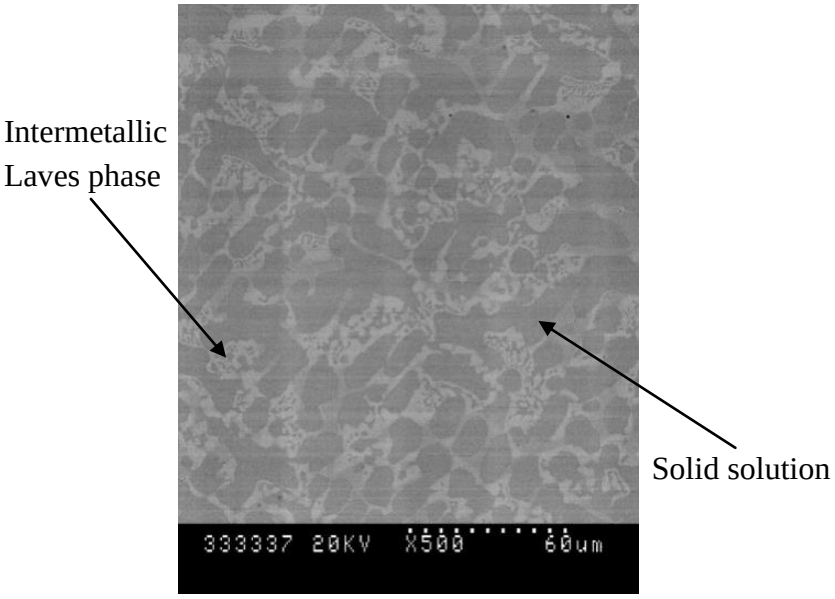

(c)

Figure 2-12: SEM microstructures of Co-based Tribaloy alloys: (a) T400 (8.5 wt%Cr, 28.5 wt%Mo and 2.6 wt%Si); (b) T-400C (14 wt%Cr, 26 wt%Mo and 2.6 wt%Si); (c) T-401 (17 wt%Cr, 22 wt%Mo and 1.2 wt%Si) [40].

Iron is another important element that influences the volume fraction of primary Laves phase largely. Mason *et al.* [41] added 5 to 15 wt% iron into T-700 to study the influences of the iron addition on the microstructure and properties of Tribaloy alloys. After addition of iron, the volume fraction of Laves phase was reduced and general morphology of the Laves phase was changed [41]. The modification of the microstructure led to the improvement in strength and a reduction in hardness. Similar phenomenon observed on T-400 alloy and T-800 alloy was reported by Halstead *et al.* [42]. The addition of iron reduced the volume fraction of the primary Laves phase from 42% to 17% in T-400 and 70% to 26% in T-800 up to additions of 15 wt% Fe [42]. However, the test results suggested the oxidation and corrosion resistance and fracture toughness are independent of the iron content in Tribaloy alloys.

Similar to superalloys, hard phases such as martensitic phase, carbides, precipitation hardening intermetallic compounds, etc. play significant roles for improving wear resistance of steels. Effect of martensite volume fraction on hardness and wear rate in dual-phase steels was investigated by Abouei *et al* [43]. As shown in Figure 2-13, increasing volume fraction of martensite reduced wear rate for dual phase steels. This phenomenon can be explained as the increasing of the volume fraction of martensite hardened the steels and decreased the possibility of crack formation during delamination [43].

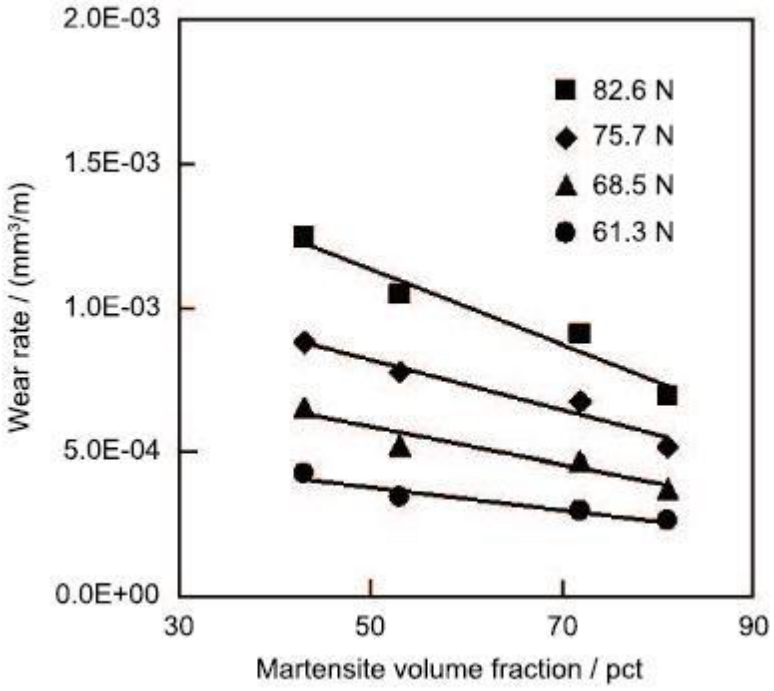

Figure 2-13: Variation of wear rate with martensite volume fraction in DP Steels [43].

2.3.3 Previous research in high-temperature wear

At elevated temperature, the good wear resistance of high temperature alloys is attributed to the excellent mechanical properties and the interfacial bonding strength of the oxide film. Improving the oxide scale adherence is very important for increasing the high temperature

wear resistance of high temperature alloys.

The effects of silicon on the wear behavior of Stellite 6 alloys at elevated temperature were investigated by Celik *et al.* [44]. As shown in Figure 2-14, the silicon with 2.2, 3.1 and 4.2 wt%, respectively, added to Stellite 6 increased the wear resistant at low temperatures (below 100^{o}C) but decreased at high temperatures (above 400^{o}C). At an intermediate temperature period from 100^{o}C to 400^{o}C, the specimen with 2.2 wt% silicon addition exhibited the highest wear resistance. However, an excess addition of silicon to 4.2 wt% resulted in the loss of wear resistance. Also, it is found the wear resistance of the alloy decreased with increasing temperature.

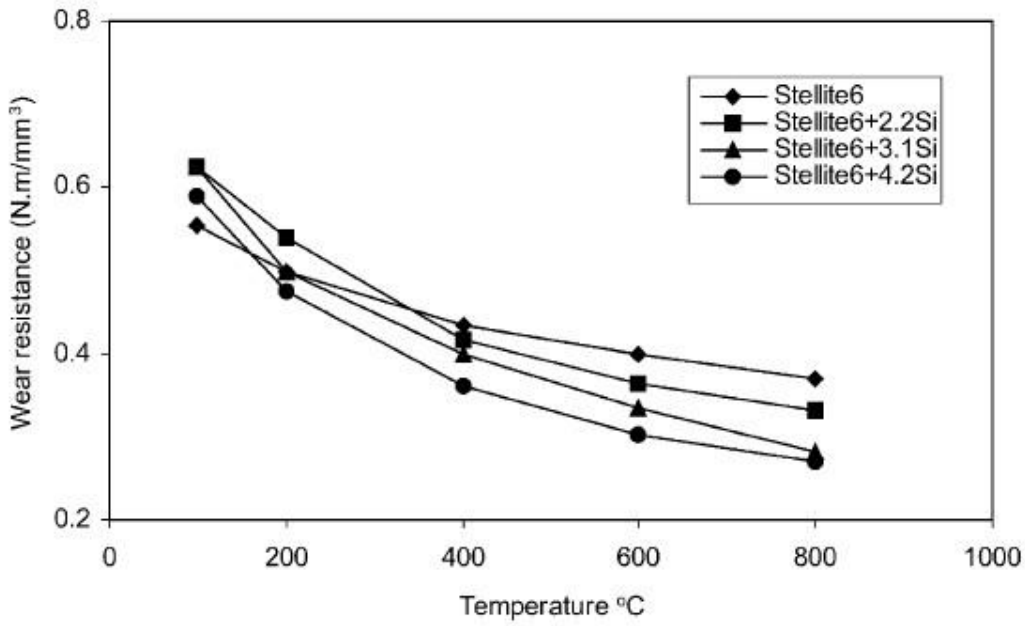

Figure 2-14: Influence of silicon additive on Wear resistance of Stellite 6 at elevated temperatures [44].

The effects of yttrium addition have been studied for several Stellite alloys. Radu *et al.* [45] found that yttrium additive in Stellite 21 improved the mechanical properties and adherence of the oxide scale. It was found the presence of yttrium at 0.5% level enhanced the high-temperature wear performance of Stellite 21 markedly, especially at temperatures above 500^{o}C [45]. Such improvement may largely benefit from the superior mechanical properties of the oxide scale containing Y_2O_3 phase [45]. Moreover, the diffusion of yttrium into grain boundaries favored inward diffusion of oxygen ions therefore inhibited the oxide growth [46].

Similar experiments were conducted on Stellite 6 and Stellite 712 [47, 48]. As shown in Figure 2-15, Wang *et al.* reported addition of 2 wt% yttrium in Stellite 6 markedly increased the hardness and resistance to wear through refining the microstructure and forming Co_2Y phase [47]. However, excess amount of yttrium additive in Stellite 6 alloy diminished in hardness and wear resistance due to the formation of brittle and easily-break phase. Similar experimental results shown in Stellite 712 test, excess of yttrium affected the high temperature wear resistance of Stellite 712 negatively [48]. The mechanical properties and microstructure of Stellite 712 alloy were not influenced markedly by the yttrium addition. The 0.5%Y containing Stellite 712 presented the best wear resistant property at elevated temperatures.

Not only working effectively in Stellite alloys, addition of yttrium was also proved to have beneficial effects on oxidation resistance of Tribaloy alloys, for example, T-800 [49]. It was observed that the alloying additions of yttrium and aluminum modified the microstructure of T-800 by reducing the size of the Laves phase, providing more phase boundaries. Moreover, addition of yttrium would enhance the oxidation resistance of the alloy at 800^{o}C to 1000^{o}C. The beneficial effect of yttrium addition on improving oxidation resistance would become

more pronounced at 1000^{o}C [49]. Also, the addition of yttrium was found to promote the preferable formation of chromium oxides then reduced the oxidation rate greatly. The oxidation rate would be further decreased if adding yttrium plus aluminum due to the development of a protective Al_2O_3 scale [49].

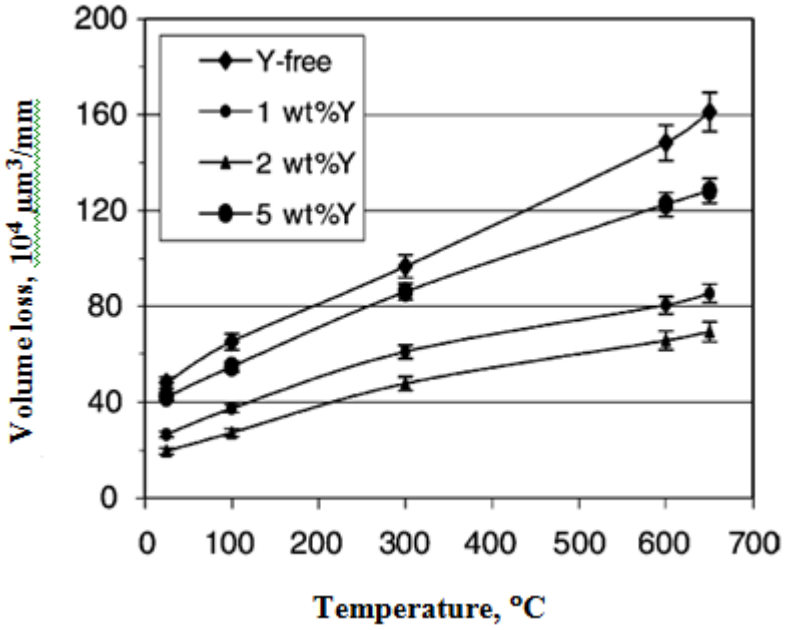

Figure 2-15: Influence of yttrium additive on wear behavior of Stellite 6 at elevated temperature [47].

3 Methodologies and Experiments

3.1 Specimen Preparation

3.1.1 Chemical composition

As introduced in the previous chapter, superalloys and stainless steels are the main categories of materials for high-temperature corrosion and wear resistance applications. In this research, two superalloys, Stellite 22 (Stellite alloy) and T-400C (Tribaloy alloy), and two stainless steels, AISI 420 steel and AISI 440C, were selected for study of a heat treatment on the hardness and wear resistance of superalloys and stainless steels. The nominal chemical compositions of these alloys are presented in Table 3-1 and Table 3-2.

Table 3-1: Chemical composition of superalloys

Material	Process	Co	Cr	Mo	C	Fe	Ni	Si	Mn
Stellite22	Sand Cast	Bal	27	11	0.25	3	2.75	1	1
T-400C	Sand Cast	Bal	14	26				2.6	

Table 3-2: Chemical composition of stainless steels

Material	Process	C	Mn	Si	Cr	P	S	Others
SS420	Wrought	0.25	1.00	1.00	12.0-14.0	0.04	0.03	
SS440C	Wrought	1.00	1.00	1.00	16.0-18.0	0.04	0.03	0.75Mo

For the superalloy group, both Stellite 22 and T-400C were newly developed at Kennametal Stellite Inc. The former is a modified version of conventional Stellite 21, containing very low

carbon content. Compared with Stellite 21, molybdenum content is doubled in Stellite 22, which induces the formation of intermetallic compounds. The later is a modified version of conventional T-400, containing high silicon and molybdenum contents thus a large amount of Laves phase. The difference between these two alloys is the large increase of chromium content in T-400C in order to enhance oxidation resistance at high temperatures.

As concerns the stainless steels, AISI 420 is a medium-carbon stainless steel and AISI 440C is a high-carbon stainless steel, also containing higher chromium content and a small amount of molybdenum. Both alloys are martensitic stainless steels that are widely used for turbine blades and valve parts due to their high corrosion resistance, excellent shock behavior and high plasticity [25]. The higher carbon content provides AISI 440C with higher hardened strength or hardness, while the more chromium and minor molybdenum enhance the corrosion resistance of AISI 440C.

3.1.2 Heat treatment

The specimens of these alloys were provided by Kennametal Stellite Inc. The Stellite 22 and T-400C specimens were in sand cast state while AISI 420 and AISI 440C specimens were in wrought state. Half of the as-received specimens experienced a heat treatment before microstructural analysis, hardness and wear test. The heat treatment was performed in an Oxy-Geo Industries High Temperature Vacuum Furnace, as shown in Figure 3-1, with a temperature range up to 1200^{o}C. The heat treatment cycle is given in the Figure 3-2. This heat treatment cycle was designed so in order to create a high temperature environment similar to the sintering process of slurry coating used for superalloys and stainless steels at Kennametal

Stellite Inc. The specimens were initially heated to 482^{o}C and held at this temperature for one-hour degassing, then continuously heated up to the sintering temperature of 1193^{o}C and held at this temperature for 0.5 hr. During the cooling the specimens were held at 749^{o}C for 4 hr, and then cooled down with the furnace temperature.

Figure 3-1: Oxy-Geo Industries High Temperature Vacuum Furnace.

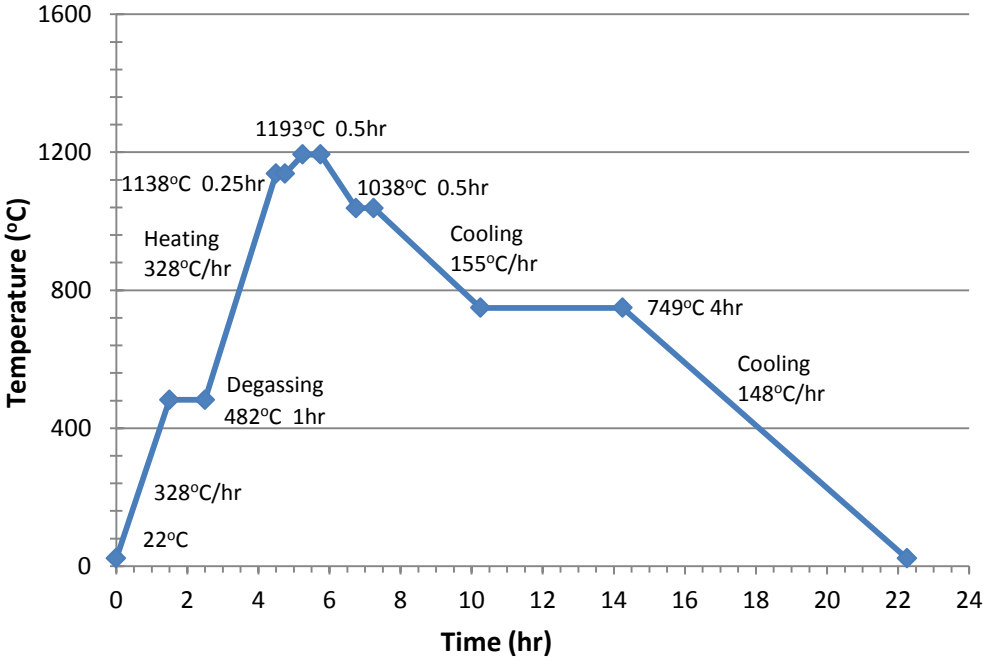

Figure 3-2: Heat treatment cycle.

3.2 Metallographic Analysis

3.2.1 Surface preparation

The microstructure of a material controls directly its performance and properties; the chemical composition and fabrication process as well as heat treatment affect largely the microstructure of a material. Therefore, in order to investigate any changes in microstructure of the four alloys after the heat treatment, all the specimens (with or without heat treatment) were examined using Scanning Electron Microscope (SEM) with an EDAX energy dispersive X-ray (EDX) spectroscopy system. The surface of each specimen (both as-received and heat-treated) was prepared for microstructural analysis. The metallographic preparation steps include cutting, mounting, rough grinding, intermediate polishing, final polishing and etching. The detailed preparation procedures are described below.

In the cutting operation process, attention should be paid to avoid the damage of the specimen and the alteration of the microstructure caused by a poor cutting condition. The quality of the cut depends on various factors such as the choice of cut-off blade, lubricant, cooling conditions and the hardness of the material being cut. In this study, the specimens were sectioned precisely on the Struers Secotom-10 cut-off machine, shown in Figure 3-3. Since the specimens are all high strength alloys, the spindle speed of 1800 rpm and Al_2O_3 abrasive cut-off blades were chosen to fulfill the need. The metallographic specimens cut from the main body of the alloys were approximately in dimensions of 15 × 10 × 10 mm. The cut specimens were cleaned thoroughly with water flushing and methanol solvent swabbing to remove grease, coolant and residue from the cut-off blades.

Figure 3-3: Struers Secotom-10 cut-off machine.

Then, samples were taken to the second stage of specimen preparation: the mounting stage. After cleaning the specimens were mounted by encapsulating into epoxy resin using a Struers LaboPress-3 mounting machine, shown in Figure 3-4. During the mounting process, a load of

20 kN was applied on the specimen at 180^{o}C for a time period of 6 min and the specimen was then cooled down within 3 min.

Figure 3-4: Struers LaboPress-3 mounting press.

Each specimen was first rough-ground automatically by a Buehler Ecomet polishing/grinding machine, shown in Figure 3-5, with water as coolant to bring the frictional heat away during grinding. A 180 standard grit size of silicon carbide abrasive paper was used to remove the surface layer of the specimen. The rough grinding was continued till producing a flat and free of burrs surface. The contact pressure of 20 MPa and the spindle speed of 200 rpm were the operation parameters used in the rough grinding process.

After rough grinding, Buehler Ecomet polishing/grinding machine was used again in the next polishing process. The objective of this operation was to produce a scratch-free and mirror-like surface without any visible defects. The polishing procedure included two stages: intermediate polishing and final polishing. During the intermediate polishing process, the specimens were polished with sequentially finer silicon carbide abrasive papers from #180 to

#1200 for each successive step. Scratches from the previous coarser abrasive paper were removed by each polishing step. It produced a specularly reflecting and bright mirrorlike surface when the polishing went to the #1200 abrasive paper step.

Figure 3-5: Buehler Ecomet polishing/grinding machine.

The final polishing operation was to eliminate the surface damage. Struers MD Rondo Trident cloth with suspension of 3 um and that of 1 um was used in the diamond polishing for 5 min and 3 min respectively. Buehler Metadi Fluid Extender was use as coolant and water was off all the time during the polishing process. After the diamond polishing, the specimens were polished with 1 um Struers MD Chem cloth and Mastermet Colloidal Silica Polishing Suspension for 5 min. Distill water was continuously sprayed on the polishing pad as coolant to reduce the frictional heat generated in the polishing process. Each grinding and polishing step was followed by thoroughly cleaning the surface using water flushing and an ultrasonic

bath in order to remove the debris produced from the previous step and prevent the surface from scratching. The suspensions for final polishing are presented in Figure 3-6.

Figure 3-6: Suspensions for final polishing.

Etching was made on each specimen surface in order to visualize the main structure characteristics of the alloys. The reagent of etching varied with the alloy category and chemical composition. The reagent for Stellite 22 and T-400C specimens was a standard reagent for cobalt-based alloys with the chemical composition of 15 ml HNO_3 + 15 ml acetic acid + 60 ml HCl + 15 ml distill water. The reagent solution was aged for 1 hr before use. The reagent for AISI 420 steel and AISI 440C specimens was a Viella's reagent. The chemical composition of Viella's reagent was 5 ml HCl, 2 gram picric acid and 100 ml ethyl alcohol. After etching in each correspondence reagent, all the specimens were cleaned gently with water, methanol, and finally dried by compressed air.

3.2.2 Microstructural examination

The facilities used for microstructural analysis in this research is a Tescan Vega-II XMU scanning electron microscope, shown in Figure 3-7,.equipped with an Oxford X-ray detection system (INCA EDS) for elemental analysis and quantitative mapping.

Figure 3-7: Tescan Vega-II XMU scanning electron microscope.

Each polished and etched specimen was examined under the Tescan Vega-II XMU scanning electron microscope; the images of the microstructures were captured at a low magnification and at a high magnification. Each phase in the microstructures was analyzed with the Oxford X-ray detection system that can provide the chemical constituents in a specific area. The EDX spectrum for the chemical constituents can be obtained, along with the element content table.

The SEM/EDX facilities were also utilized to analyze the worn surfaces of the specimens from the pin-on-disc wear test. Both surface morphology and chemical composition of the wear

tracks were examined to explore the wear mechanism of each alloy. In particular, the worn surfaces from the high-temperature wear test were analyzed to investigate temperature effect on the tribological behavior of these alloys with or without heat treatment.

3.3 Hardness Test

3.3.1 Experimental preparation

Hardness is a measure of a material's resistance to localized plastic deformation. This important characteristic mechanical property is considered firmly associated with other mechanical properties such as ductility, toughness, strength etc. It is generally accepted that the harder a material, the more resistant to wear the material is. The heat treatment may alter the microstructures of the alloys being studied thus affect their hardness property. Moreover, it is well known that the hardness of a metal decreases as temperature climbs up to a high level. The hardness change at high temperatures may influence the wear resistance of the material. Therefore hardness measurement and understanding of the alloys are essential in this study.

The equipment used for hardness measurement in this research is a Microhardness Tester Unit, Model SMT-X7 Dual Indenter, shown in Figure 3-8. It is equipped with a microscope and with a Clemex video camera so that the microscopy image is able to be transferred into a computer. With a microscope equipped, each individual phase in a microstructure can be identified and selected to measure. For hardness measurement at elevated temperatures, a Hot-Stage Assembly with the temperature of 700°C, shown in Figure 3-9, is attached to the Microhardness Tester Unit to heat up the testing specimen to a desired temperature. The Hot-Stage Assembly is also equipped with a controller unit to maintain the temperature

throughout the test time.

Figure 3-8: Microhardness Tester Unit, Model SMT-X7 Dual Indenter.

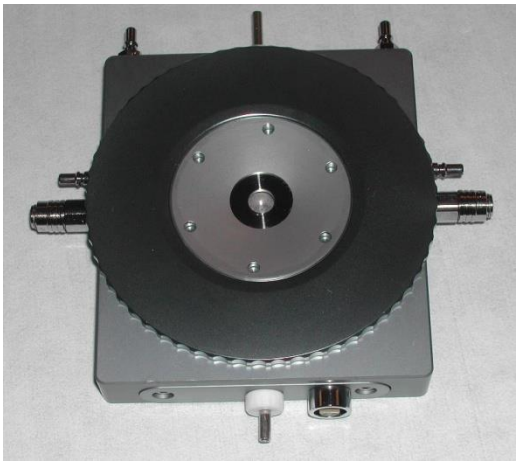

Figure 3-9: Hot-Stage Assembly.

3.3.2 Test procedures

The specimen for the hardness test had dimensions of 6.5 mm in diameter and 1.5 ~ 2 mm in

thickness in order to sit into the hot-stage furnace, but for room temperature test, the specimen can be in any dimensions. For each specimen, the surface was ground with grit papers from #180 to #600 and polished with abrasive cloth plus 1 μm alumina powders. Both bulk hardness and individual phase hardness of each specimen were measured. The indentation test was conducted on each specimen at room temperature, 250°C, 450°C and 600°C. A low indentation load of 25 gf was selected for individual phase hardness test, which allowed the indentation to be made on a selected phase, because if the load was too high, the indentation may cover an area with other phases involved. A high load of 300 gf was used for bulk hardness test in order to cover the overall microstructure. The load selections for each indentation are summarized in Table 3-3 below.

Table 3-3: Load selections for each indentation in hardness test

Material	Bulk hardness test load (gf)	Strengthening phase hardness test load (gf)	Solid solution hardness test load (gf)
As-cast T-400C	300	100	100
Heat-treated T-400C	300	100	100
As-cast Stellite 22	300	25	50
Heat-treated Stellite 22	300	100	50
As-wrought AISI 420	100	N/A	N/A
Heat-treated AISI 420	100	N/A	N/A
As-wrought AISI 440C	100	N/A	N/A
Heat-treated AISI 440C	100	N/A	N/A

Five indentations were made at each temperature for each specimen and two specimens were tested for each alloy. The hardness value for each test case was an average of the ten test results. In order to avoid the influence of material pre-deformation under previous indentations on the hardness result, there should be a space between two indentations at least larger than three indentation diagonal lengths.

3.4 Wear Test

3.4.1 Test apparatus

The wear resistances of the as-received and heat-treated alloy specimens were evaluated under the pin-on-disc test, according to the testing procedure of ASTM G99-05(2010) Standard Test Method for Wear Testing with a pin-on-disc apparatus and a surface profiler measuring system. The pin-on-disc apparatus was a Nanovea Pin-On-Disc Tribometer, as shown in Figure 3-10, the disc was referred to as the ‘specimen’ and the pin was to as the ‘standard counterpart’. The pin-on-disc tribometer system consists of a pin rigidly held with an arm lever device, a revolving disk held by chuck with a driven spindle, a computer controller and a high temperature heating/holding system. The pin used in the study was a ball made of 94% WC and 6% Co with the hardness of HV1534. The ball had a radius of 2.5 mm with a spherical tip while the disc specimen had a flat surface and was approximately 5 mm in thickness. During the test, the pin was forced perpendicularly against the flat disc specimen by a precise weight. Equipped with a speed integrated feedback/calibration system, the motor drove the bottom disc specimens rotating at a desire speed. As a result, the pin created a circular wear track on the rotating specimen surface. A computer control unit monitored and recorded the frictional

force during the test and the associate software calculated and plotted the friction coefficient in real time. For high temperature wear test, a furnace was added to the system, as shown in Figure 3-11, to keep the specimen in a specific temperature environment. The pin goes through the top cover of the furnace to contact with the rotating disc specimen during the test. The furnace can operate up to 500^{o}C and is controlled by a high temperature heating/holding system. The system uses temperature sensors and calibration software for maintaining the temperature through time. However, the high temperature module is not an oxygen-isolated system; therefore oxidation of metallic materials is definitely inevitable in the high-temperature wear test.

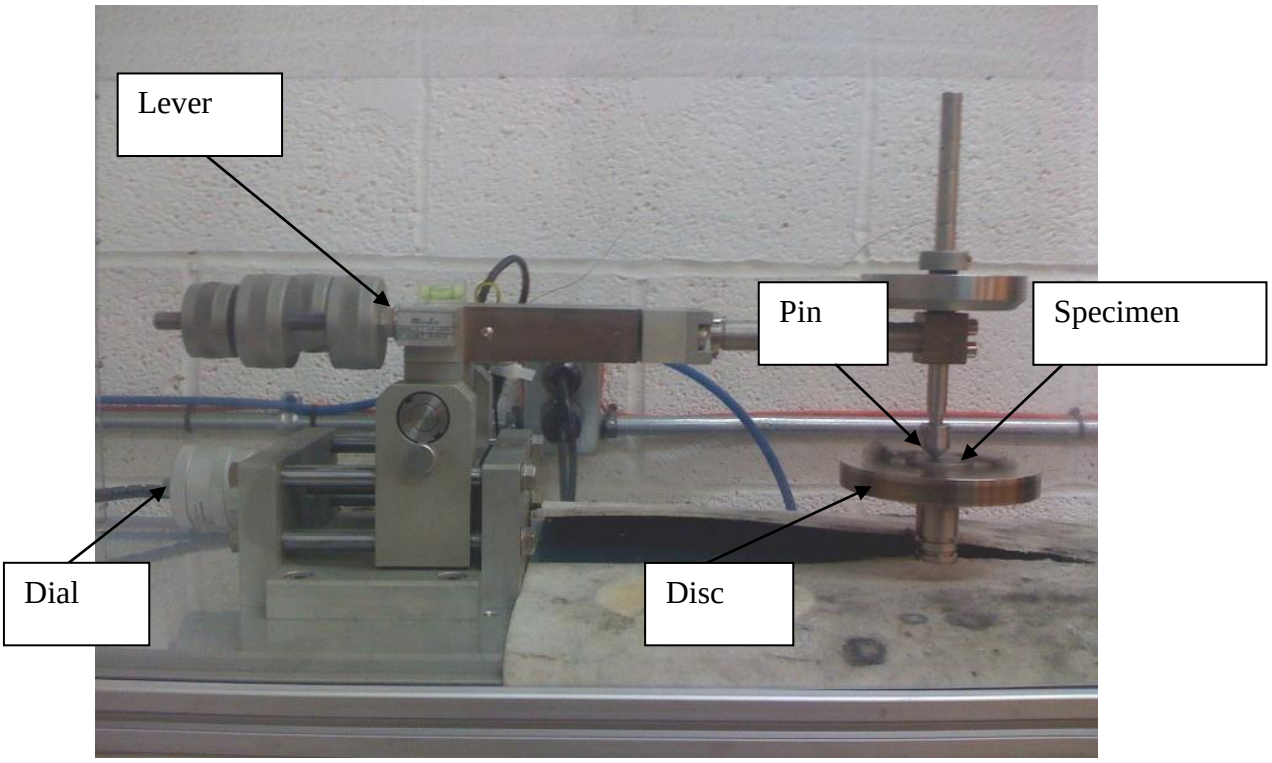

Figure 3-10: Pin-on-Disc Tribometer System.

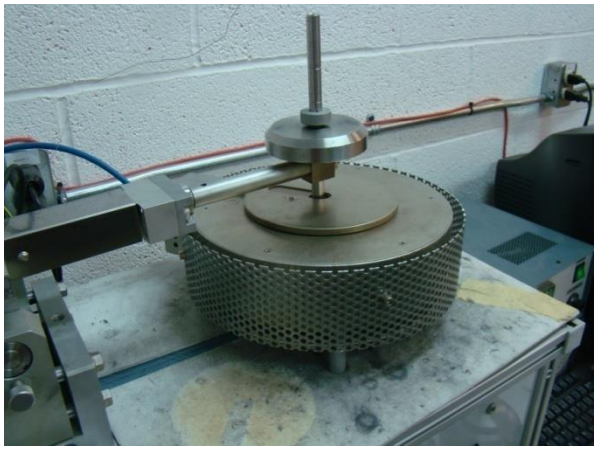

Figure 3-11: Pin-on-Disc Tribometer System equipped with a heating furnace.

3.4.2 Test parameters

The wear test at room temperature and at elevated temperatures was performed on both the as-received and heat-treated alloy specimens. The specimens were prepared with thickness approximately in 10 mm. Each specimen was ground with silicon carbide abrasive papers from #180 to #600 in order to obtain a flat surface and also to remove the oxide layer. After the surface polished, the specimen was cleaned thoroughly using water flushing and an ultrasonic bath and finally dried by compressed air.

Immediately prior to the wear test, disc specimens were cleaned again by swabbing with methanol solvent and the ball pin was cleaned by acetone to remove dirty and foreign matters. The tests were conducted in a dry-lubricating condition. During the test, the ball pin was pressed against the disc specimen surface with the compressive load (L) of 10 N. The position of the pin was set away from the center of the spindle to create a 6 mm diameter (D) circular wear track on the rotating specimen during the test. The rotational speed of the specimen (N) was set to be 350 rpm and the test duration (t) was 2.5 hr. For each as-received and heat-treated

alloy, wear test was conducted at 20°C, 250°C and 450°C, respectively. Disc specimens were warm up to the test temperature before the wear test was started. The total sliding distance (s) resulted from the above parameters for each test was computed according to the Equation (3-1).

$$s = D \times \pi \times N \times t = 6mm/r \times \pi \times 350r/min \times 2.5hr = 989.6m \quad (3\text{-}1)$$

In the study, at least three identical tests were performed for each test condition of each alloy in as received state or in heat-treated state to verify the experimental results. Table 3-4 is a summary of test setup and parameters.

Table 3-4: Pin-on-disc wear test parameters

Test specimen:	State	As-received & heat-treated
	Cleaning	Methanol
Pin:	Geometry:	Ball
	Material:	94% Tungsten carbide and 6% cobalt
	Size	6 mm in diameter
	Cleaning:	Acetone
Testing parameters:	Normal Load (L)	10 N
	Rotational speed of disc (N)	350 rpm
	Test duration (t)	2.5 hr
	Test environment (T)	20°C, 250°C, 450°C
	Diameter of wear track (D)	6 mm
	Sliding distance (s)	~1000 m

3.4.3 Wear loss evaluation

After the wear test, the wear resistance of each specimen was studied in the two aspects: wear quantification and wear behavior analysis. For wear quantification, the wear loss of each specimen was evaluated by measuring the volume of the wear track left in the worn surface. Prior to the wear track measurement, both the worn specimen and pin were cleaned softly with warm tap water to remove the debris produced during the wear test and then dried by compressing air. The photographic wear tracks on a specimen surface are shown in Figure 3-12 as an example. According to the ASTM G99-05(2010) Standard, the wear measurement was reported as the volume loss in cubic millimetres for the worn material. By comparing worn severity level of the pin and alloy specimens, one may see that there was no significant pin wear. The wear loss of the specimen material was estimated by calculating the volume of the wear track. A DEKTAK 150 Surface Profile Measuring System, shown in Figure 3-13, was utilized to simulate the section profile of each wear track. This system is a profilemeter for measuring step heights or trench depths on a surface using contact stylus profilometry techniques. In the measuring process, a very low force stylus was dragged across the cross-section of the wear track. The system used the stylus sensor to collect surface data and then transfer the data into the computer. In the computer, surface data was processed and finally a two-dimensional cross-section profile, as shown in Figure 3-14, was mapped. Based on the cross-section profile, the volume of the wear track can be calculated easily. In the study, the volume of the wear track (V, mm^3) was calculated using Equation (3-2):

$$V = A \times C = A \times \pi D \tag{3-2}$$

The volume of the wear track (V, mm^3) was calculated as cross-sectional area (A, mm^2) multiplied by the periphery length of the wear track (πD, mm^2). The cross-sectional area (A)

was calculated automatically with the associate software built in the DEKTAK 150 Surface Profile Measuring System, according to the two-dimensional profile mapping data. Six locations along each wear track were measured to calculate the cross-section area (*A*). The average wear loss and the derivation were determined based on the six measurements.

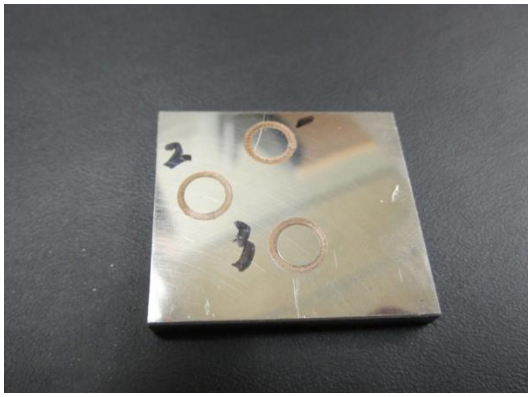

Figure 3-12: Photographic wear tracks on a worn specimen surface.

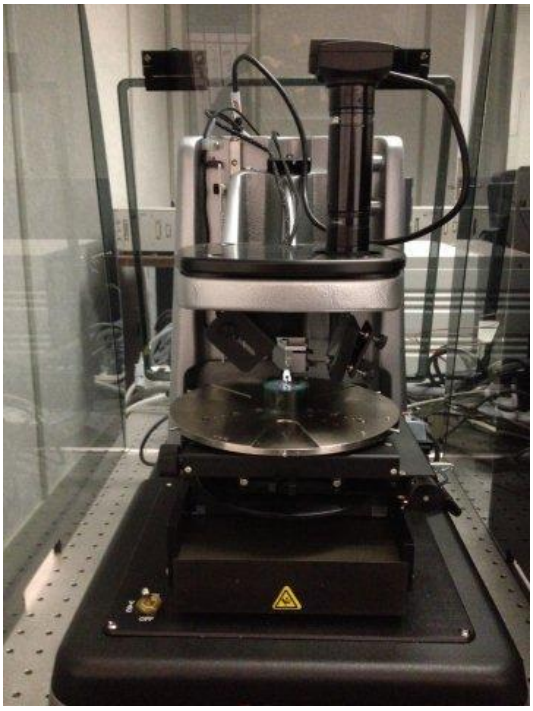

Figure 3-13: DEKTAK 150 Surface Profile Measuring System.

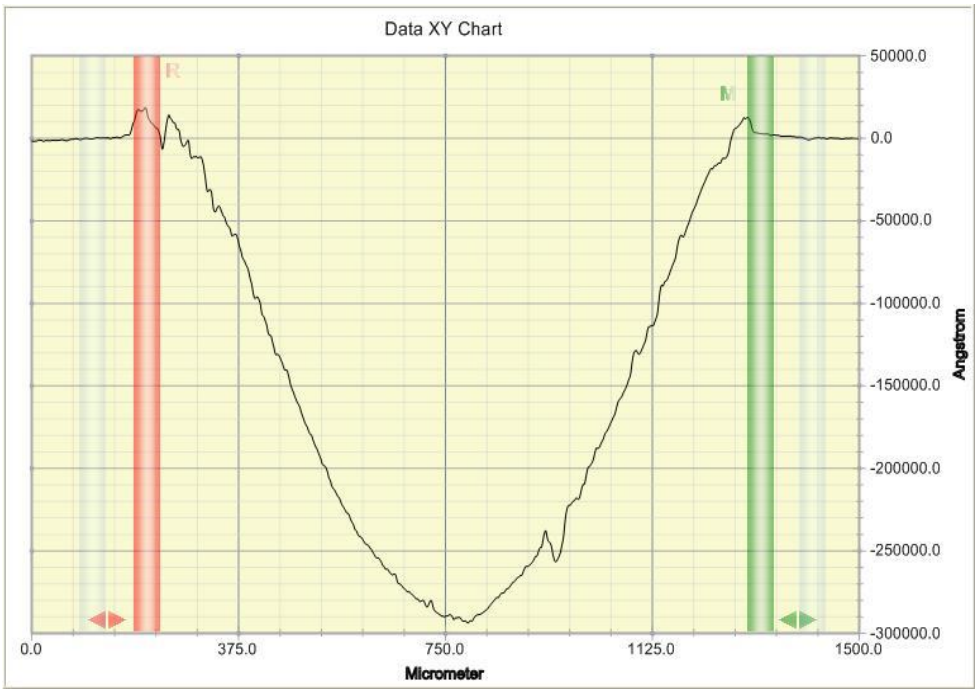

Figure 3-14: Two-dimensional wear track cross-section profile.

In addition to wear loss, the tribological behavior of the tested alloys was further studied through worn surface morphology investigation. The worn surface morphology of each specimen was characterized by the Tescan Vega-II XMU scanning electron microscope. The wear mechanisms of the alloys were explored, with the focus on the influence of the heat treatment on the tribological behavior of the alloys.

4 Microstructural Characterization

4.1 SEM Images and EDX Spectra

Microstructural characterization of each specimen was conducted using SEM/EDX. The obtained SEM images of microstructure, along with the EDX results of each phase in the microstructure, for as-received and heat-treated Stellite 22, T-400C, AISI 420 and AISI 440C are presented in Figure 4-1 to Figure 4-18. The EDX technique provides more accurate analysis for phases present in a microstructure. However, the instrument used in this research has a limitation in detection of carbon; it cannot provide an accurate content of carbon; therefore the element content tables presented below contain only the metallic elements for each phase. The detailed analyses of microstructure for each specimen are given below.

4.2 Stellite 22

Stellite alloys have a microstructure typically consisting of complex hard carbides (mostly chromium-rich carbides) and brittle intermetallic compounds (commonly Co_3Mo and $CoMo_6$ in high-molybdenum Stellite alloys) dispersed in a tough cobalt solid solution matrix mainly containing chromium and tungsten or chromium and molybdenum. The volume fraction of carbides in the microstructure of a Stellite alloy is proportional to its carbon content. Stellite 22 is a low-carbon cobalt-based superalloy, also containing chromium and molybdenum, as seen in Table 3-1. Due to the very low carbon content, this alloy contains a very small volume fraction of carbides. However, it contains a large amount of Co_3Mo and $CoMo_6$ intermetallic compounds owing to the high molybdenum content.

4.2.1 As-cast specimen

The SEM images of microstructure for as-cast Stellite 22 are presented in Figure 4-1; the EDX results associated with each phase in the microstructure are provided in Figure 4-2. According to the SEM images, this alloy has a microstructure consisting of two phases, they are primary Co solid solution and eutectic mixture including Cr-rich carbides, Co_3Mo and $CoMo_6$ intermetallic compounds, and Co solid solution as well, as labeled in Figure 4-1(b). Molybdenum in Stellite alloys serves mainly to provide additional strength to the matrix, but when present in large quantities, it participates and promotes the formation of two intermetallic compounds of Co_3Mo and $CoMo_6$. The presence of these phases are further confirmed with the EDX results in Figure 4-2. The maximum errors of EDX results are presented in the bracket.

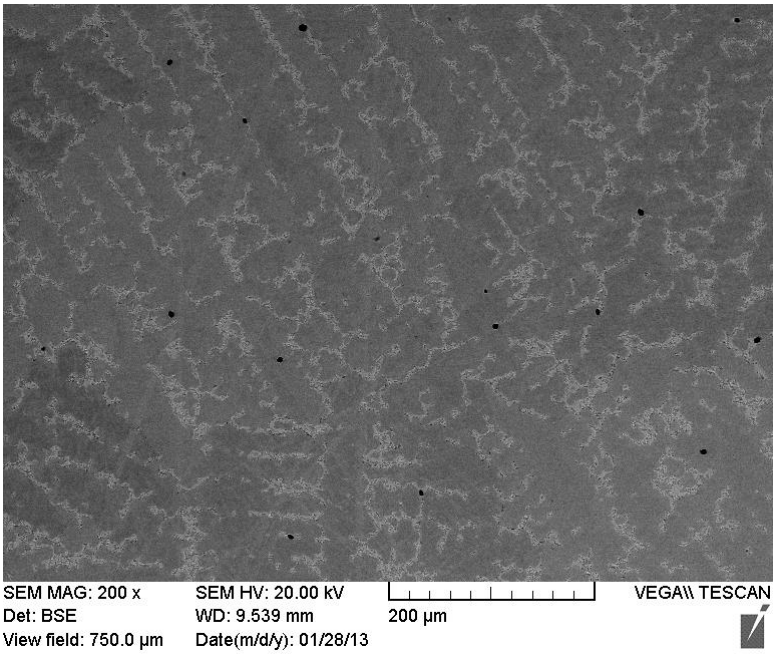

(a)

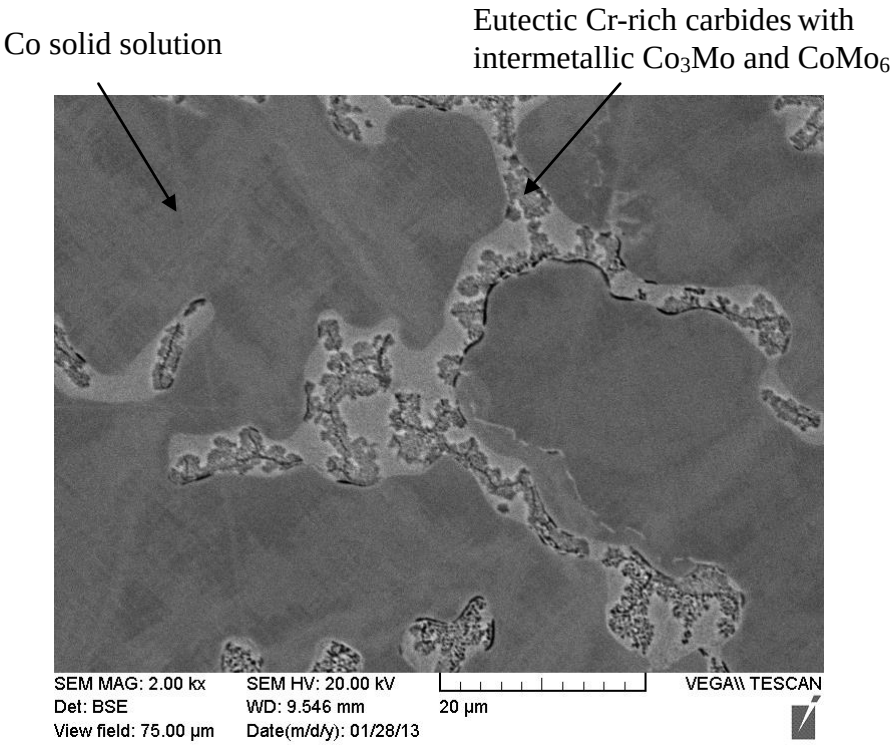

(b)

Figure 4-1: SEM images of microstructure of as-cast Stellite 22: (a) at lower magnification and (b) at higher magnification.

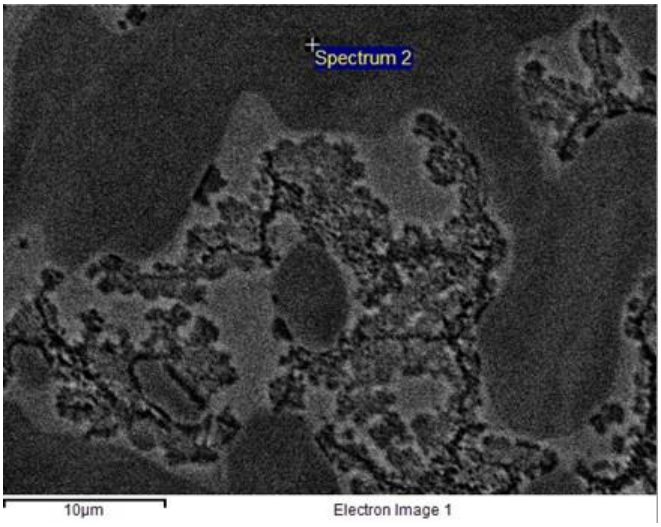

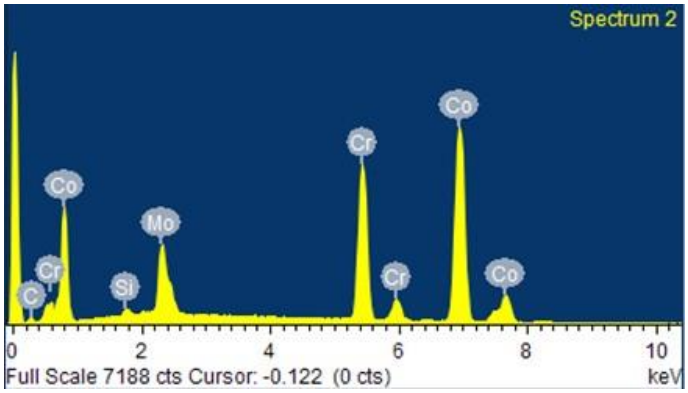

Element	Weight%	Atomic%
Si K	0.47 (11.36%)	1.00 (13.19%)
Cr K	26.24 (0.13%)	30.10 (0.67%)
Co K	59.90 (0.33%)	60.57 (0.22%)
Mo L	13.39 (7.73%)	8.32 (7.09%)
Total	100.00	100.00

(a)

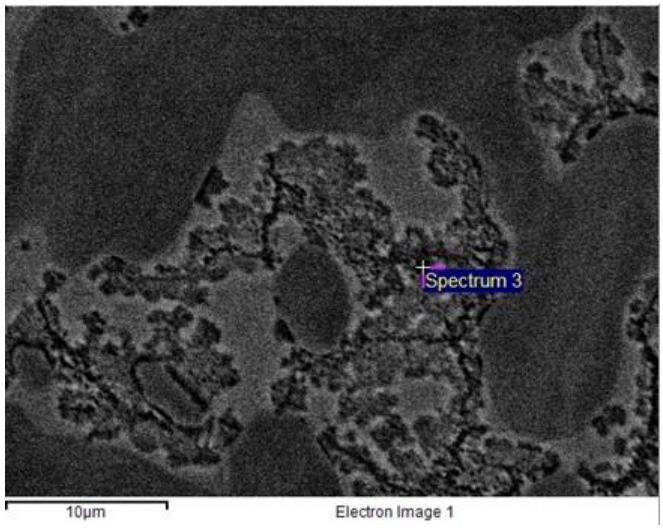

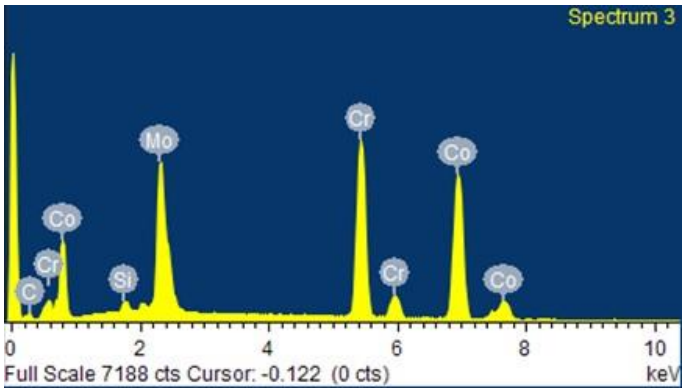

Element	Weight%	Atomic%
Si K	0.72 (13.26%)	1.60 (12.73%)
Cr K	29.81 (8.93%)	35.70 (8.72%)
Co K	43.36 (3.58%)	45.76 (3.42%)
Mo L	26.11 (4.76%)	16.94 (5.03%)
Total	100.00	100.00

(b)

Figure 4-2: EDX spectra of as-cast Stellite 22: (a) primary Co solid solution; (b) eutectic Cr-rich carbides, Co_3Mo and $CoMo_6$ intermetallic compounds.

4.2.2 Heat-treated specimen

The SEM image of microstructure and EDX spectra results of heat-treated Stellite 22 are presented in Figure 4-3 and Figure 4-4, respectively. It is shown that there is no significant difference in microstructure between the as-cast specimen and heat-treated one. However, the heat-treated specimen exhibits slight increase in the volume fraction of the eutectic mixture, if comparing the microstructure in Figure 4-1(a) with that in Figure 4-3(a). Also it is observed the boundaries of intermetallic compounds and Cr-rich carbides become more distinct after heat treatment. The EDX results in Figure 4-4(c) show very high Cr content in the eutectic mixture, which implies that there is also $Cr_{23}C_6$ precipitation in the alloy during the heat treatment. From the EDX results in Figure 4-4(a), it seems no change in chemical composition of primary Co solid solution, which indicates that the $Cr_{23}C_6$ precipitates only occurred in the eutectic mixture.

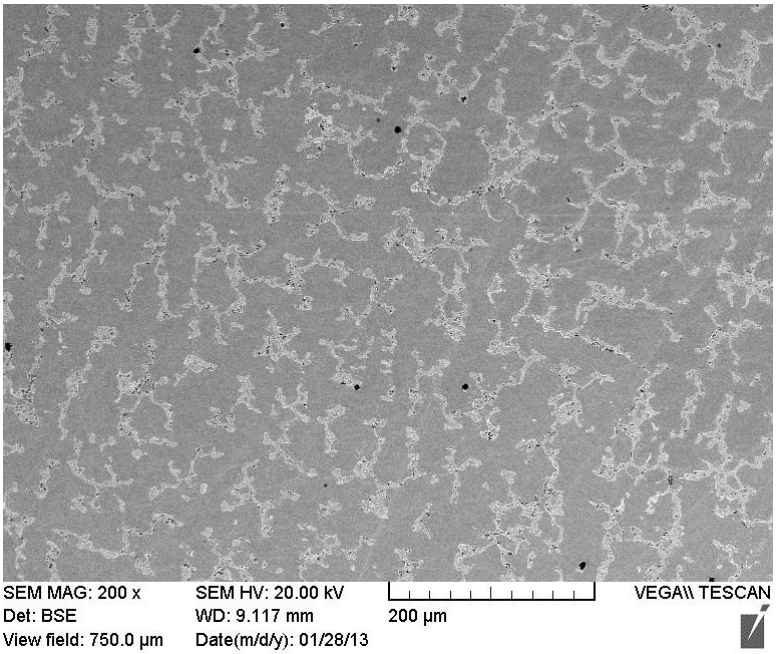

(a)

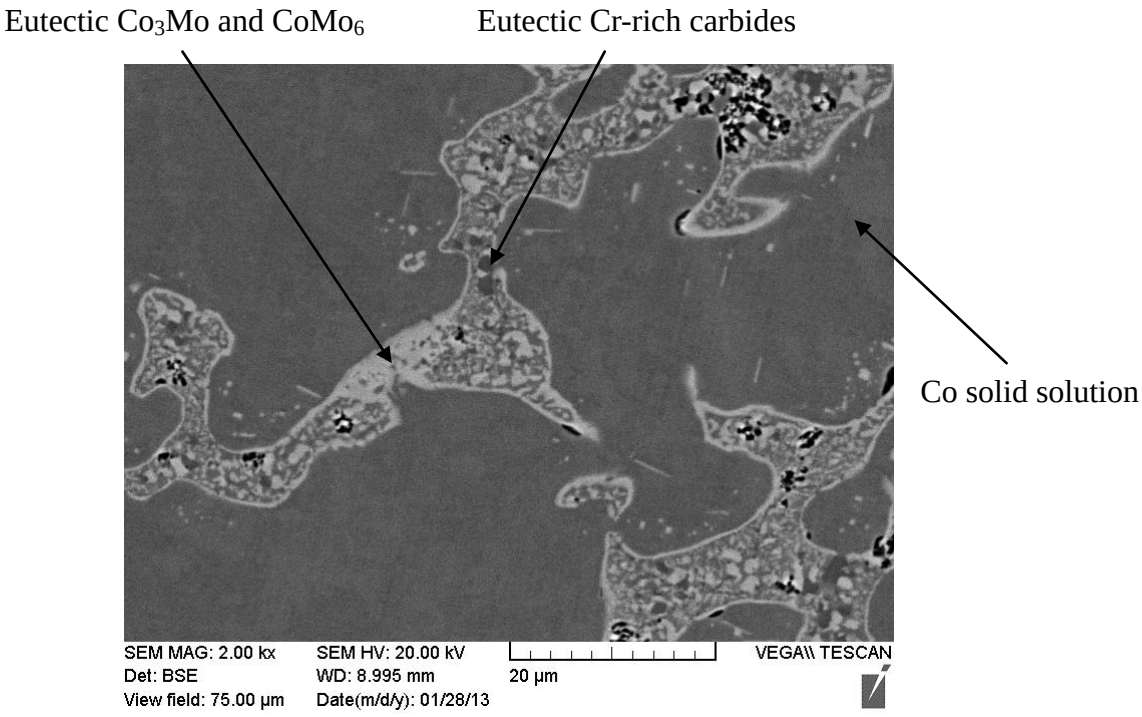

(b)

Figure 4-3: SEM images of microstructure of heat-treated Stellite 22: (a) at lower magnification and (b) at higher magnification.

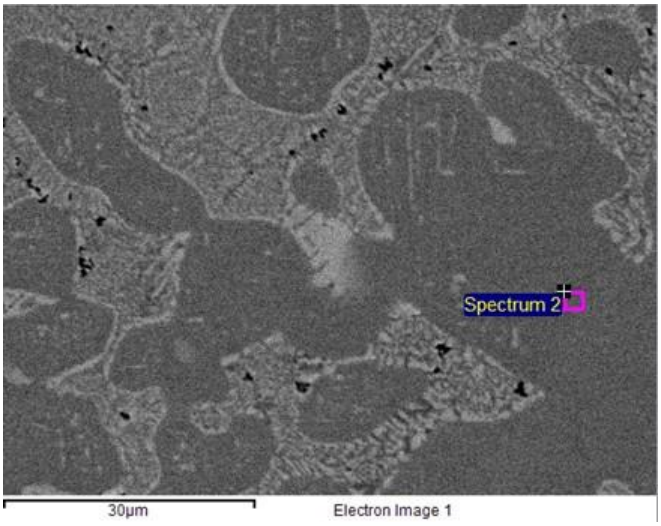

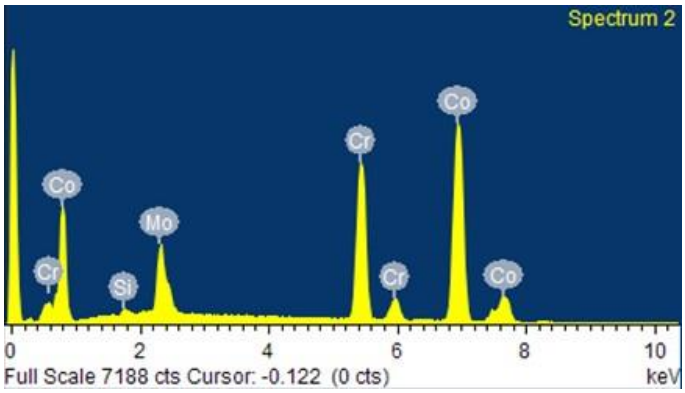

Element	Weight%	Atomic%
Si K	0.49 (2.27%)	1.04 (1.05%)
Cr K	26.37 (0.66%)	30.15 (0.79%)
Co K	60.53 (0.64%)	61.00 (0.28%)
Mo L	12.61 (1.66%)	7.81 (2.66%)
Total	100.00	100.00

(a)

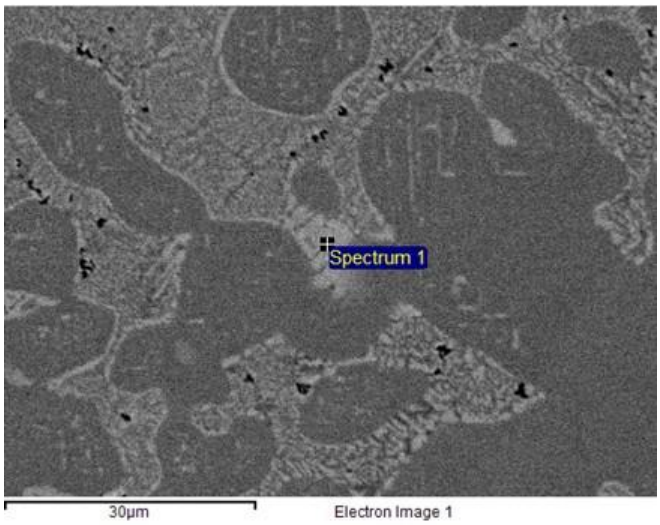

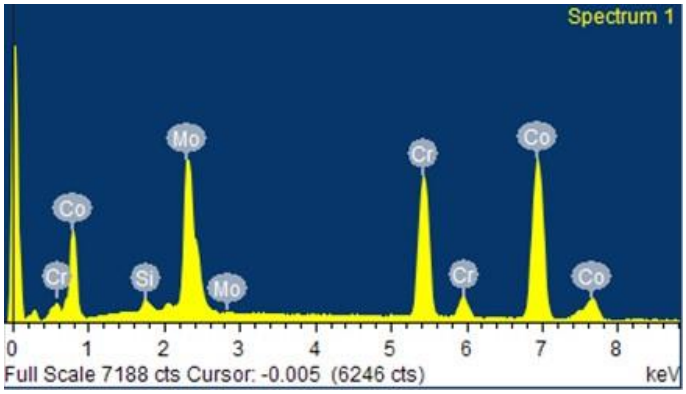

Element	Weight%	Atomic%
Si K	0.87 (3.78%)	1.96 (3.54%)
Cr K	24.37 (4.43%)	29.49 (3.97%)
Co K	47.54 (2.01%)	50.71 (1.97%)
Mo L	27.22 (0.73%)	17.84 (0.66%)
Total	100.00	100.00

(b)

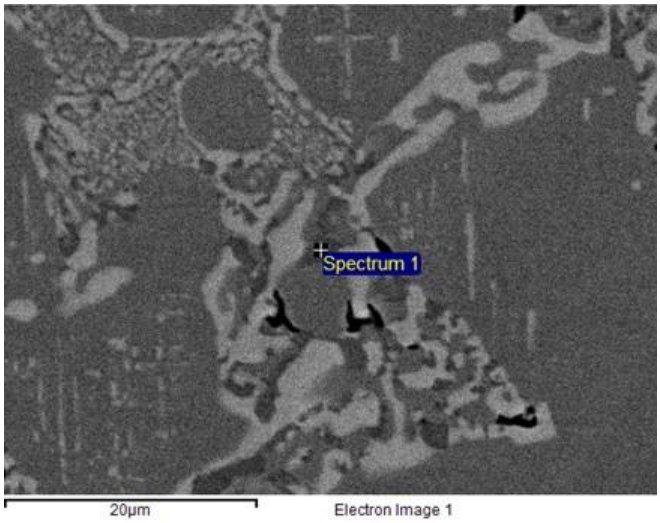

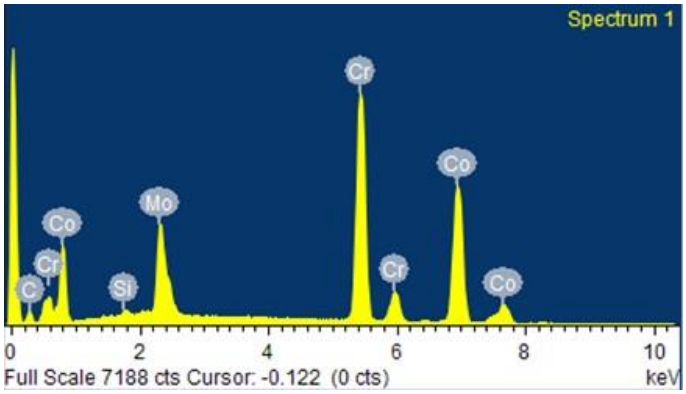

Element	Weight%	Atomic%
Si K	0.35 (2.58%)	0.75 (2.36%)
Cr K	39.71 (2.90%)	45.37 (0.91%)
Co K	43.29 (10.10%)	43.59 (8.52%)
Mo L	16.64 (16.16%)	10.30 (18.80%)
Total	100.00	100.00

(c)

Figure 4-4: EDX spectra of heat-treated Stellite 22: (a) primary Co solid solution; (b) eutectic intermetallic Co_3Mo and $CoMo_6$ and (c) eutectic Cr-rich carbides.

4.3 T-400C

Tribaloy alloys present a microstructure typically consisting of a large volume fraction of hard intermetallic Laves phase dispersed in a much softer solid solution matrix. The hard primary Laves phase is a ternary Laves phase of the C-14 ($MgZn_2$) type and its compositions are approximately Co_3Mo_2Si or CoMoSi. These alloys are usually hypereutectic with 30 - 70 vol% Laves phase. It is the presence of this large volume fraction of Laves phase that enables these materials to achieve their good wear resistance, which differ from Stellite alloys that gain their wear resistance mainly from a dispersion of carbides. The carbon content in Tribaloy alloys is kept low to prevent carbides forming in preference to Laves phase.

4.3.1 As-cast specimen

The SEM images of microstructure of as-cast T-400C specimen are given in Figure 4-5; the EDX results associated with each phase in the microstructure are given in Figure 4-6. T-400C presents the primary dendritic intermetallic Laves phase in a Co solid solution matrix. The matrix is a lamellar structural eutectic mixed with cobalt solid solution and secondary Laves phases. The volume fraction of the Laves phase in this specimen was estimated about 38.9% with the associated software of SEM image analysis; the mapping image is shown in Figure 4-7 with the areas of Laves phase in yellow and Co solid solution in blue. The EDX spectrum in Figure 4-6(a) shows very high Mo content and high Si and Co contents that represent the Laves phase (Co_3Mo_2Si or CoMoSi); the EDX spectrum in Figure 4-6(b) exhibits very high Co content and high Cr content as well as medium Mo content that represent the Co solid solution. Cr is a very significant alloying element for γ matrix but not the constituent element for primary Laves phase so it is mostly in the Co solid solution. Mo is another alloying

element therefore it can also be found in the solid solution to provide added strength to the matrix, in addition to the main role in formation of Laves phase.

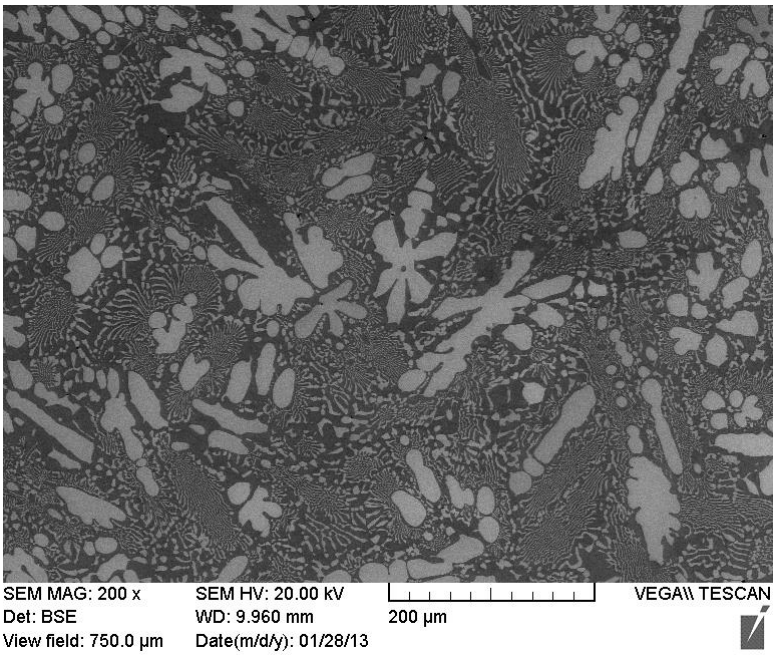

(a)

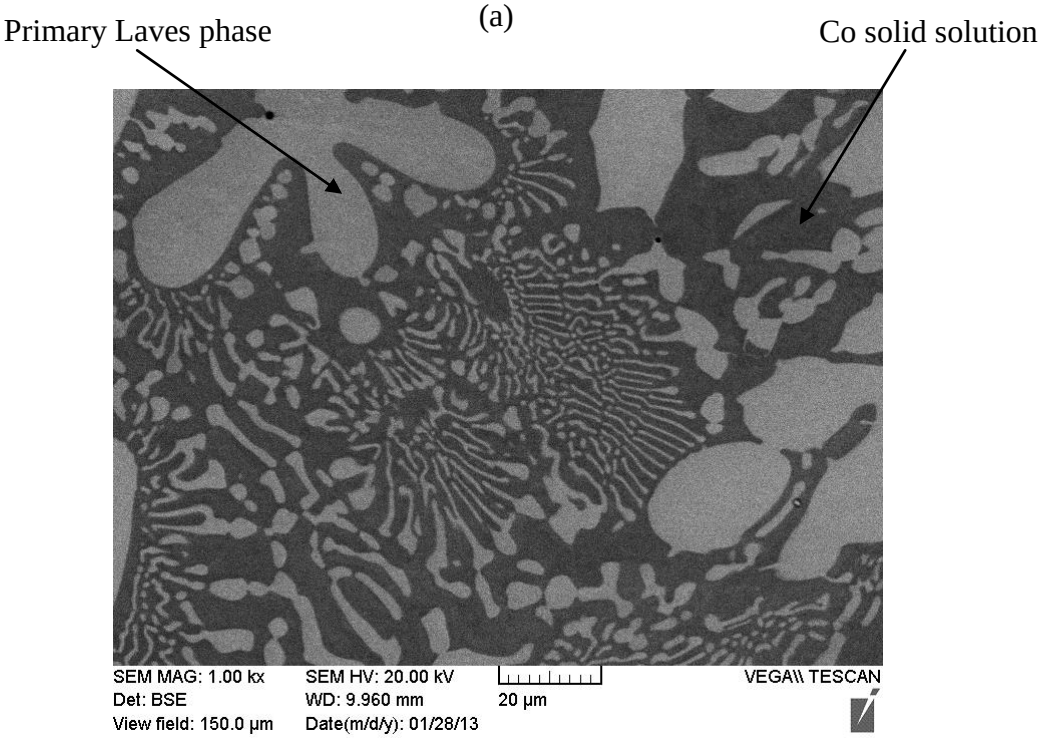

(b)

Figure 4-5: SEM images of microstructure of as-cast T-400C: (a) at lower magnification and (b) at higher magnification.

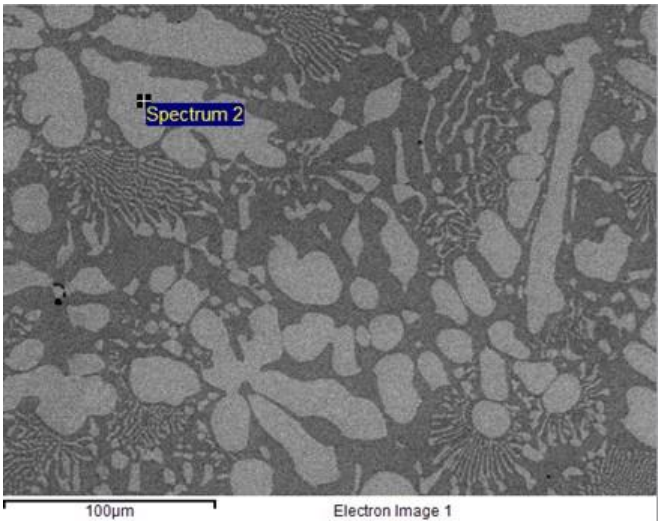

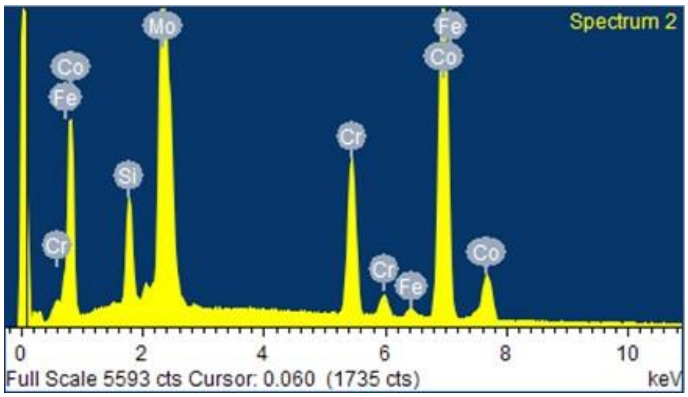

Element	Weight%	Atomic%
Si K	3.56 (3.23%)	8.21 (4.11%)
Cr K	12.14 (0.22%)	15.07 (0.77%)
Fe K	1.05 (28.57%)	1.21 (27.93%)
Co K	46.24 (3.41%)	50.61 (1.90%)
Mo L	37.02 (0.87%)	24.90 (1.06%)
Total	100.00	100.00

(a)

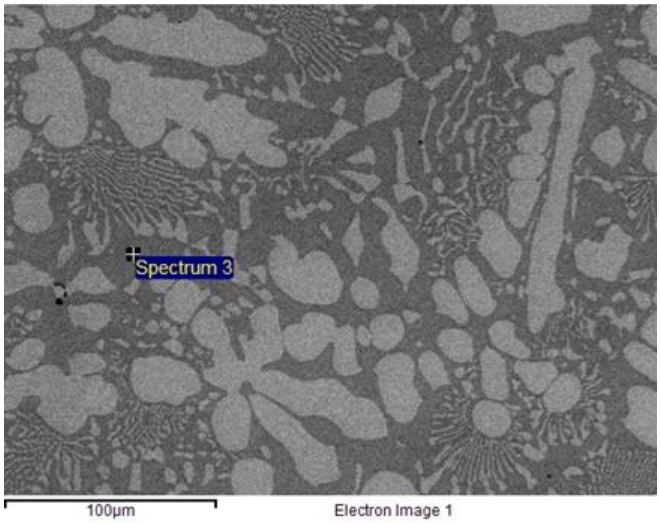

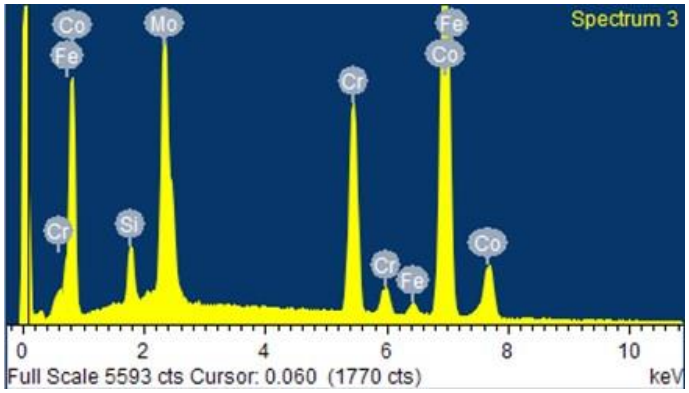

Element	Weight%	Atomic%
Si K	2.21 (19.49%)	4.86 (17.56%)
Cr K	16.16 (0.82%)	19.16 (1.10%)
Fe K	1.42 (13.24%)	1.56 (12.98%)
Co K	56.86 (2.69%)	59.42 (0.68%)
Mo L	23.35 (5.01%)	15.00 (6.79%)
Total	100.00	100.00

(b)

Figure 4-6: EDX spectra of as-cast T-400C: (a) Laves phase and (b) Co solid solution.

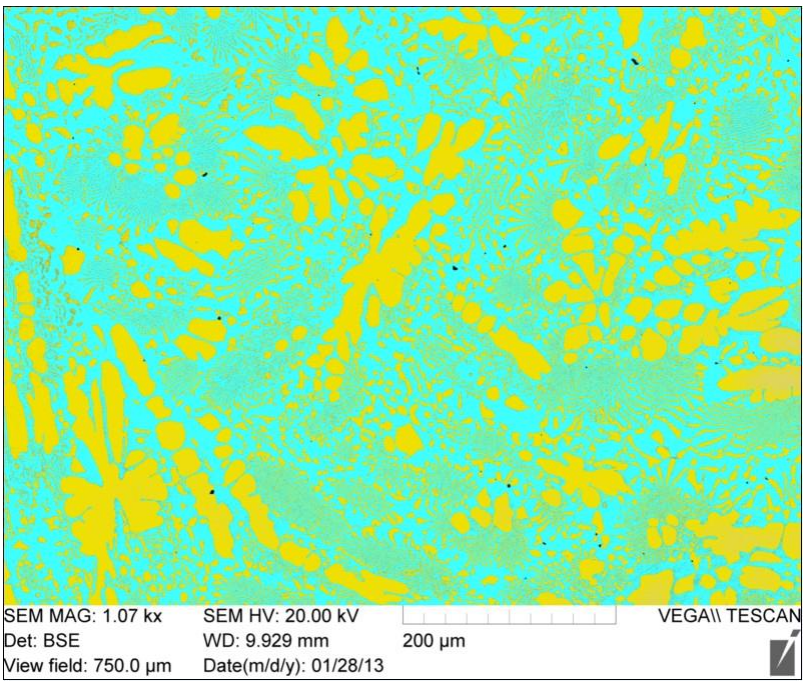

As-cast T-400C	Color	Volume Fraction (%)	Objective Area (mm^2)
Laves phase	Yellow	38.9	0.16
Solid solution	Blue	61.1	0.24

Figure 4-7: SEM image mapping for volume fraction estimation of Laves phase in as-cast T-400C.

4.3.2 Heat-treated specimen

The SEM images of microstructure of heat-treated T-400C are presented in Figure 4-8. This microstructure is similar to the microstructure of as-cast T-400C in that it also consists of primary Laves phases and the eutectic of secondary Laves phase and solid solution. However, an obvious difference is also observed that an amount of ternary Laves phase was precipitated

in the solid solution matrix during the heat treatment process, as indicated in Figure 4-8. The EDX spectra of each phase in the heat-treated T-400C specimen are provided in Figure 4-9. The elemental contents of the primary Laves phase and solid solution were not changed by the heat treatment; except that the Mo content in the heat-treated specimen decreased slightly. The ternary Laves phase contains high Mo and Co, also high Si, which are the formers of Co_3Mo_2Si or CoMoSi Laves phase, but it is also noticed that both Mo and Si contents in the ternary Laves phase are lower than those in the primary Laves phase while Co content is higher, as shown in Figure 4-9(c). This implies that the ternary Laves phase is likely Co_3Mo_2Si rather than CoMoSi. The volume fraction analysis of Laves phase also confirmed the precipitated Laves phase. As demonstrated in Figure 4-10, the volume fraction of Laves phase in heat-treated T-400C as increased to 48.9% after the heat treatment process.

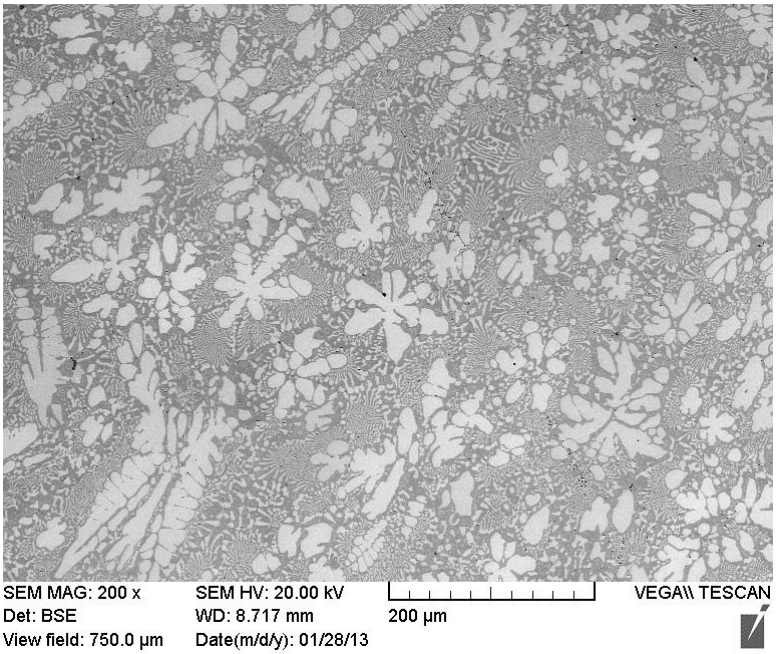

(a)

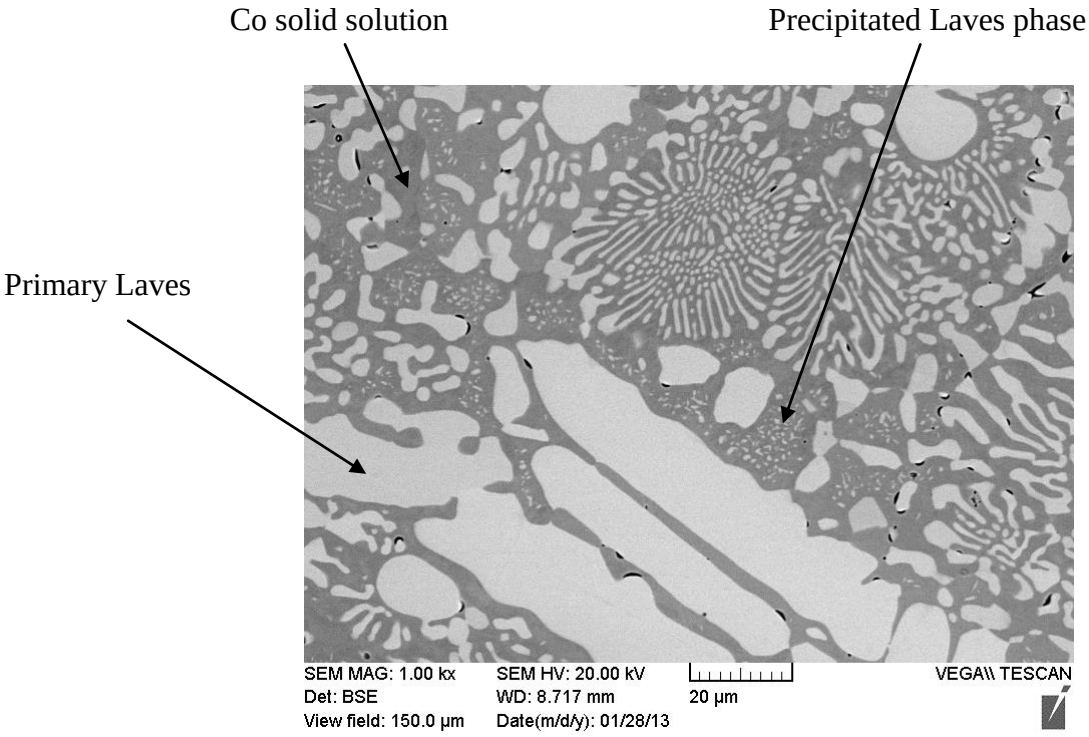

(b)

Figure 4-8: SEM images of microstructure of heat-treated T-400C: (a) at lower magnification and (b) at higher magnification.

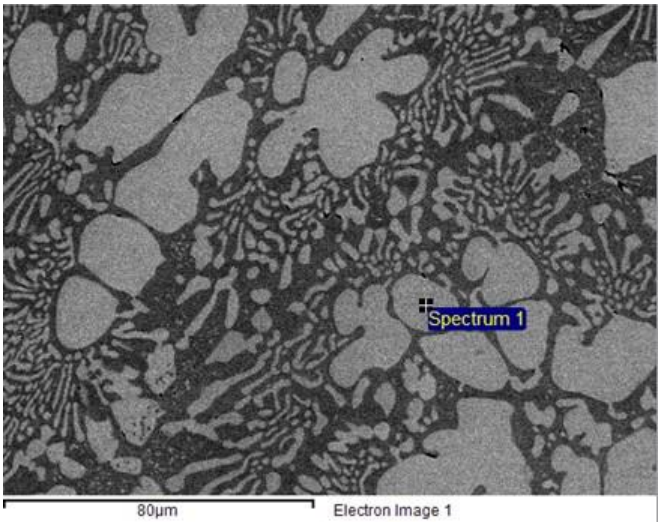

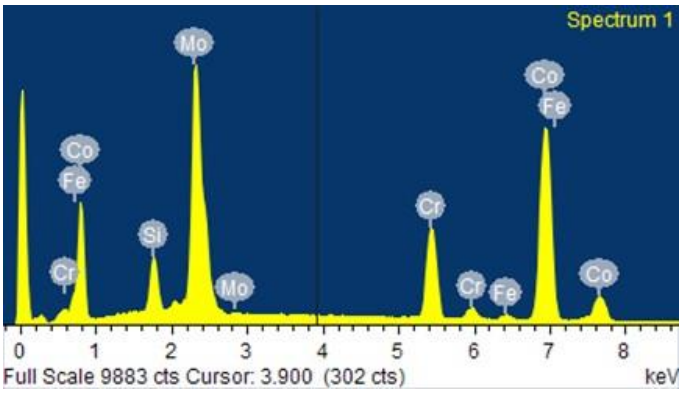

Element	Weight%	Atomic%
Si K	3.43 (1.81%)	7.86 (0.96%)
Cr K	12.66 (5.29%)	15.64 (4.34%)
Fe K	1.03 (6.78%)	1.18 (5.68%)
Co K	47.30 (1.40%)	51.50 (0.58%)
Mo L	35.59 (1.80%)	23.82 (2.59%)
Total	100.00	100.00

(a)

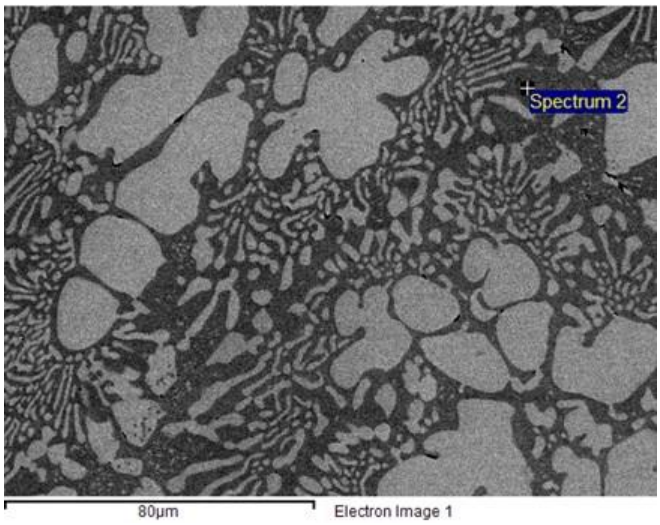

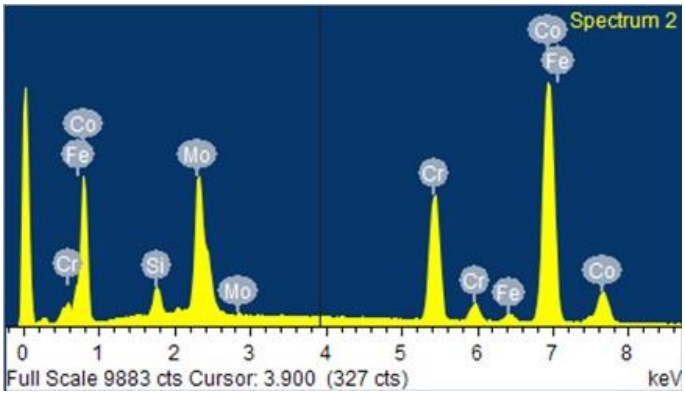

Element	Weight%	Atomic%
Si K	1.88 (31.11%)	4.10 (28.89%)
Cr K	17.10 (0.63%)	20.10 (2.02%)
Fe K	1.53 (3.24%)	1.67 (2.98%)
Co K	58.84 (0.28%)	60.97 (2.92%)
Mo L	20.65 (23.80%)	13.15 (21.70%)
Total	100.00	100.00

(b)

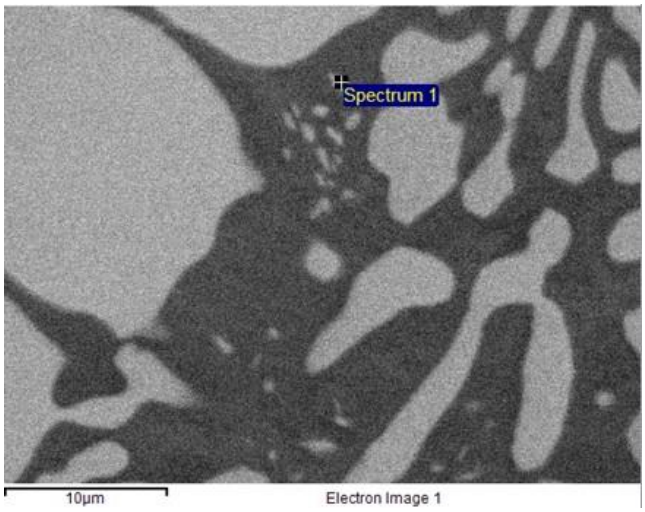

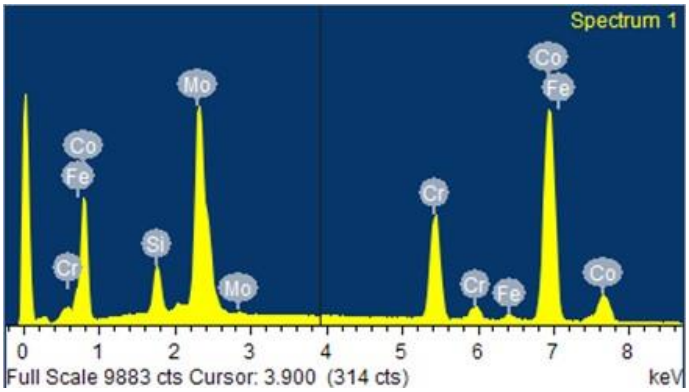

Element	Weight%	Atomic%
Si K	3.00 (15.38%)	6.76 (13.49%)
Cr K	14.10 (4.89%)	17.11 (4.65%)
Fe K	1.08 (1.78%)	1.22 (1.52%)
Co K	51.25 (5.62%)	54.82 (5.43%)
Mo L	30.58 (3.81%)	20.10 (2.98%)
Total	100.00	100.00

(c)

Figure 4-9: EDX spectra of heat-treated T-400C: (a) Laves phase; (b) Co solid solution and (c) precipitated Laves phase.

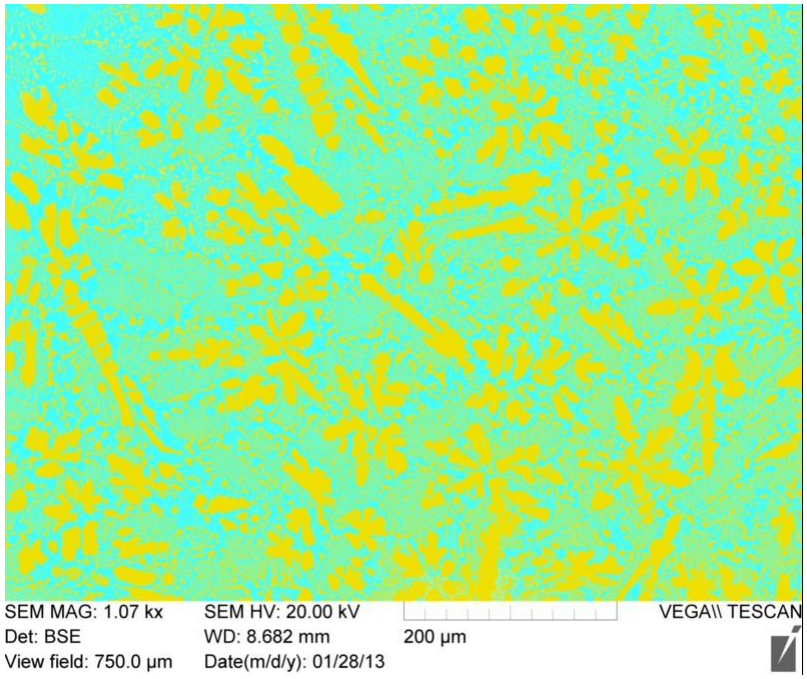

Heat-treated T-400C	Color	Volume Fraction (%)	Objective Area (mm^2)
Laves phase	Yellow	48.9	0.21
Solid solution	Blue	51.1	0.22

Figure 4-10: SEM image mapping for volume fraction estimation of Laves phase in heat-treated T-400C.

4.4 AISI 420

AISI 420 is a medium-carbon martensitic stainless steel; like most non-stainless steels it can be hardened by heat treatment. It contains a minimum of 12 wt% chromium, just sufficient to give corrosion resistance properties. Martensitic stainless steels are optimized for high hardness, and other properties are to some degree compromised. Corrosion resistance is lower than the common austenitic grades, and their useful operating temperature range is limited by

their loss of ductility at sub-zero temperatures and loss of strength by over-tempering at elevated temperatures.

4.4.1 As-wrought specimen

The AISI 420 specimen studied in this research is a wrought product. It has a microstructure consisting of multi-layer stacking ferrite with carbide precipitates, shown in Figure 4-11. The carbides are tiny and uniformly distributed in the ferrite matrix. The EDX results confirmed that the ferrite matrix contains very high level of Fe and medium level of Cr to provide corrosion resistance, as shown in Figure 4-12(a). The EDX spectrum in Figure 4-12(b) shows the carbide precipitates contain high Cr and Fe, which implies the carbides are Cr-rich $Mr_{23}C_6$.

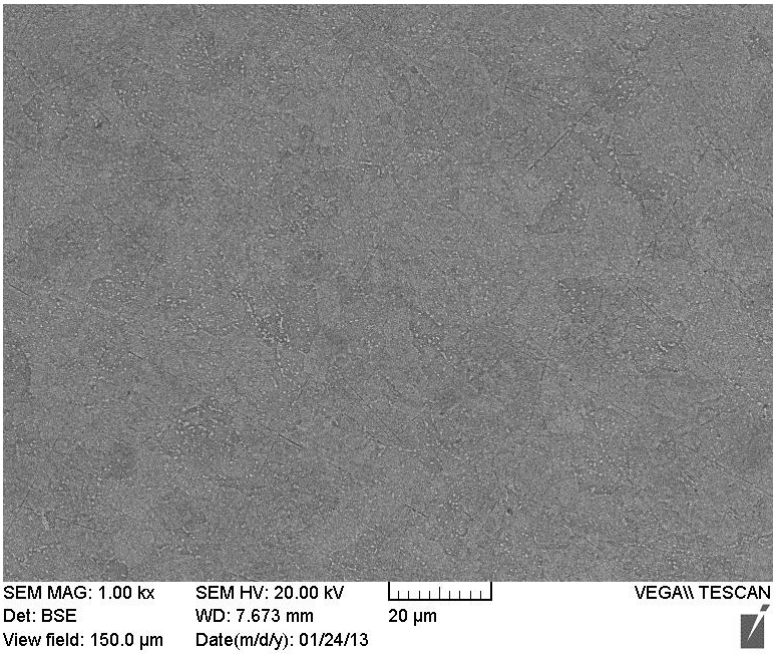

(a)

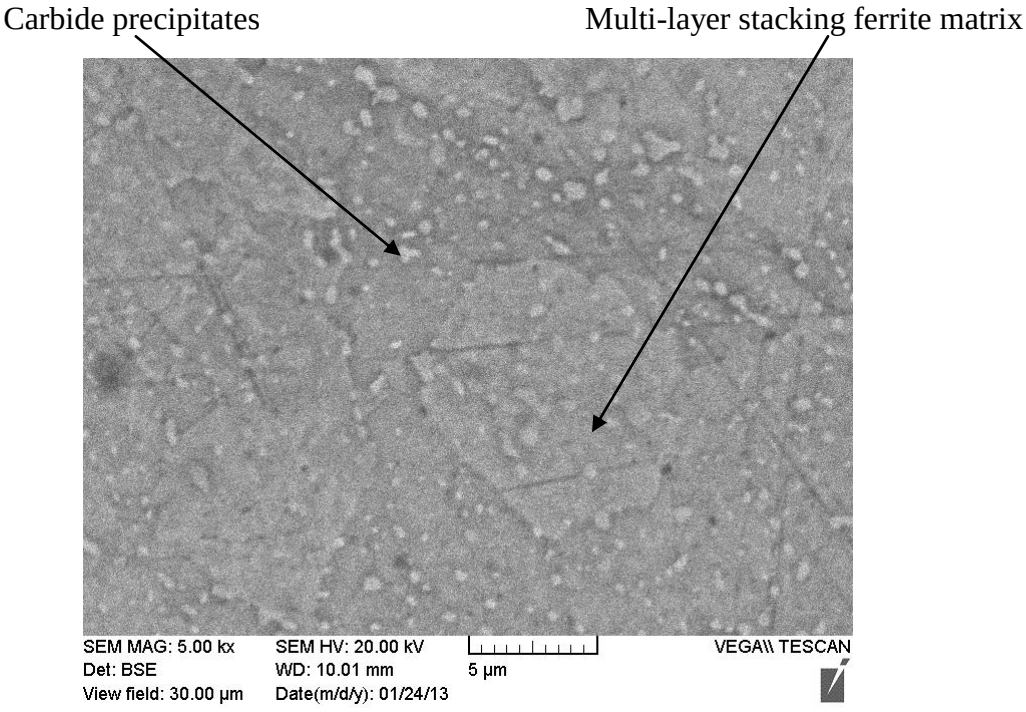

(b)

Figure 4-11: SEM images of microstructure of as-wrought AISI 420: (a) at lower magnification and (b) at higher magnification.

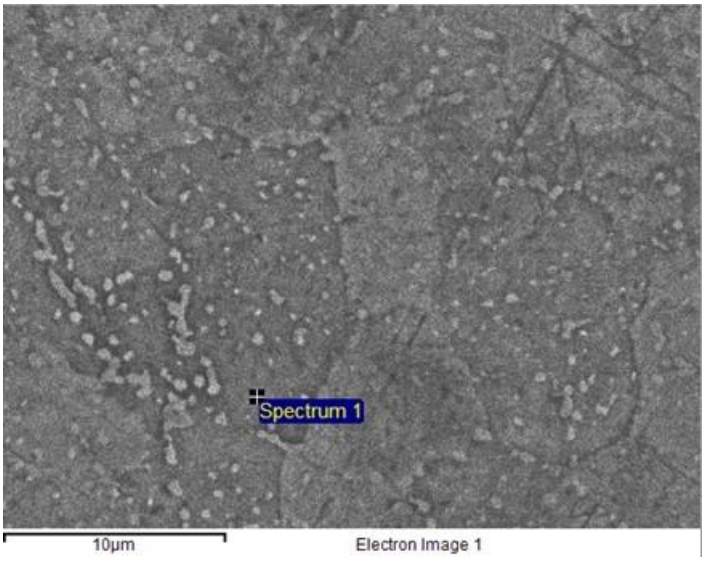

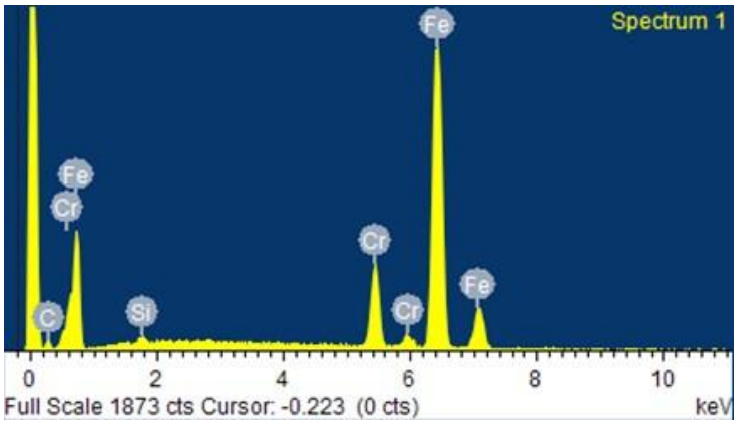

Element	Weight%	Atomic%
Si K	0.57 (6%)	1.13 (6.12%)
Cr K	13.14 (0.23%)	13.93 (0.85%)
Fe K	86.28 (1.23%)	84.94 (0.20%)
Total	100.00	100.00

(a)

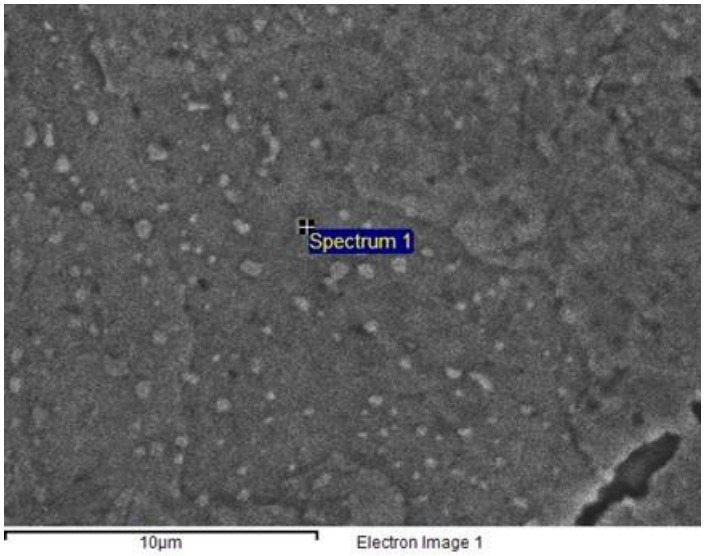

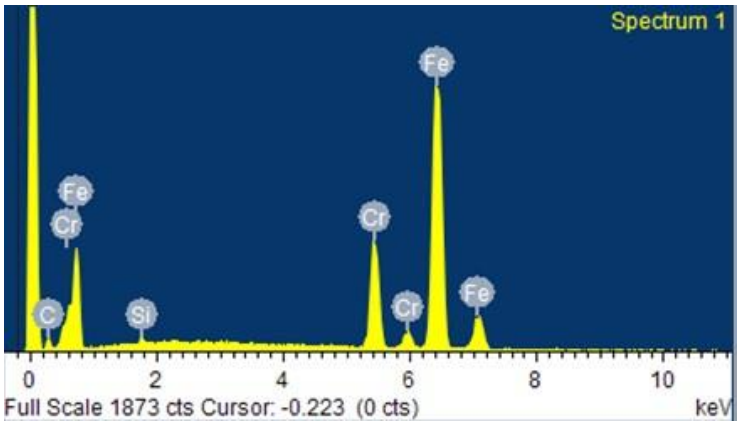

Element	Weight%	Atomic%
Si K	0.49 (6.67%)	0.97 (6.54%)
Cr K	18.69 (2.13%)	19.75 (1.73%)
Fe K	80.81 (0.62%)	79.28 (0.85%)
Total	100.00	100.00

(b)

Figure 4-12: EDX spectra of as-wrought AISI 420: (a) α-ferrite solid solution and (b) carbide precipitates.

4.4.2 Heat-treated specimen

As shown in Figure 4-13, the microstructure of AISI 420 was changed greatly by the heat treatment. The microstructure became a mixture of primary pearlite phase and martensite matrix with a small amount of ferrite. It is the typical product of austenizing steel cooled down at an intermediate rate. In Figure 4-13(a), pearlite phase is in dark color while martensite matrix is in light color. In the high magnification image in Figure 4-13(b), pearlite phase presents a lamellar structure with various orientations and spacings, which may be the consequence of these pearlite structures formed at different temperatures. The carbides dissolved into the pearlite phase and martensite matrix during the cooling in the heat treatment process. Moreover, the grain size was increased through the heat treatment, which can be observed obviously by comparing the image in Figure 4-11(a) with that in Figure 4-13(a). This may be due to the fact that AISI 420 was overheated and held at the higher austenitization temperature for a long time during the heat treatment. The EDX spectra of the pearlite phase and martensite phase are provided in Figure 4-14. It is shown that these two phases have similar elemental contents.

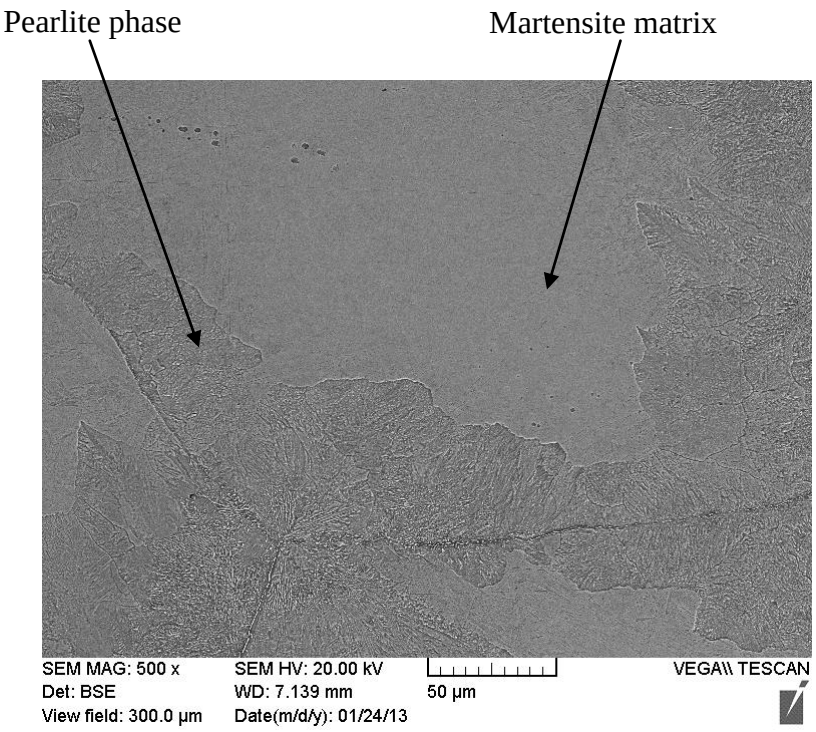

(a)

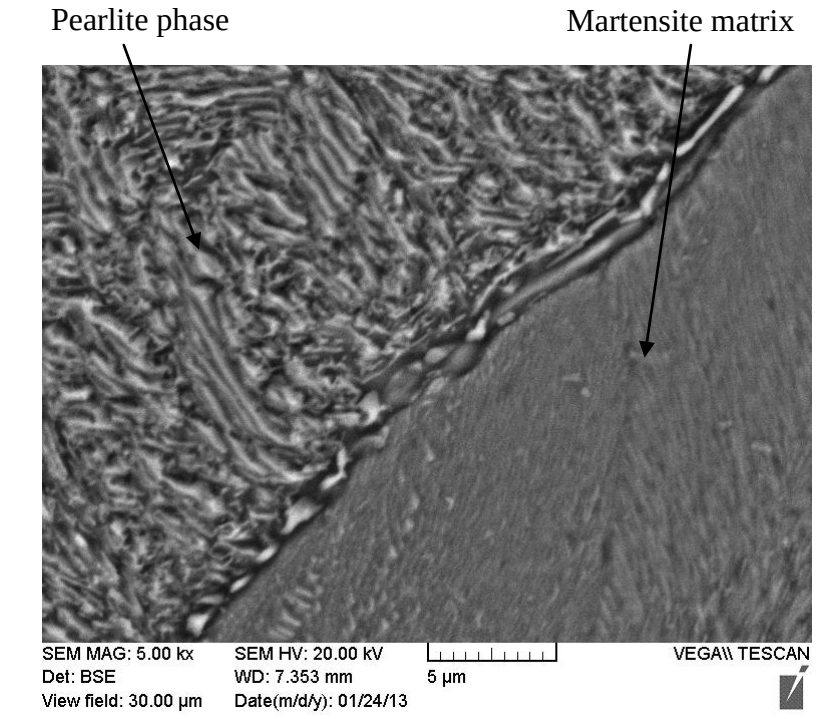

(b)

Figure 4-13: SEM images of microstructure of heat-treated AISI 420: (a) at lower magnification and (b) at higher magnification.

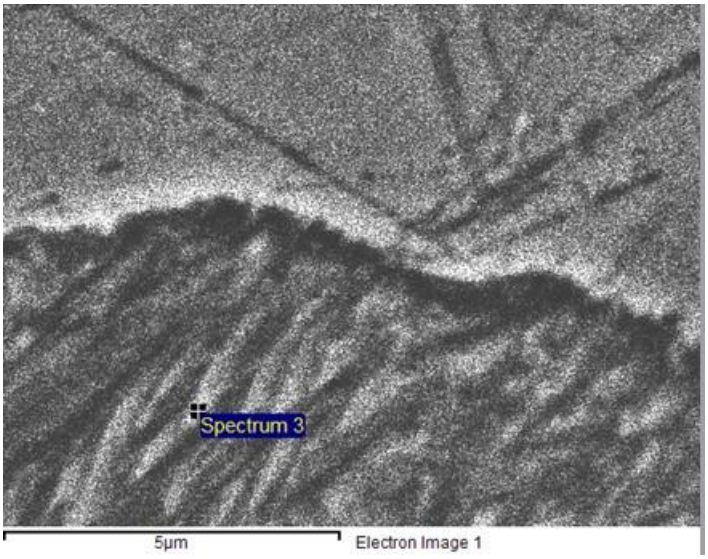

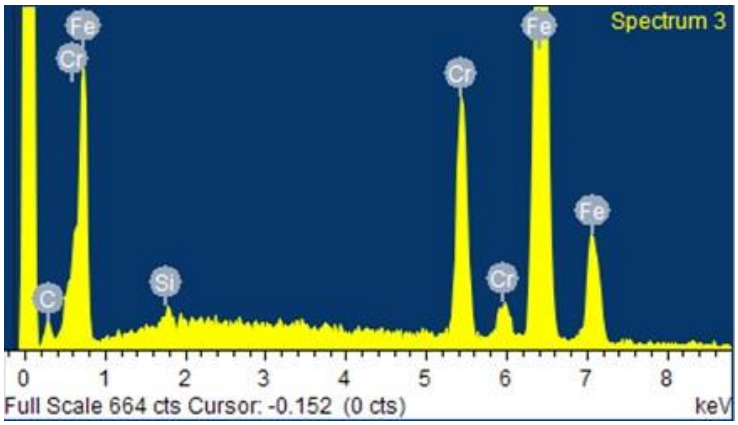

Element	Weight%	Atomic%
Si K	0.47 (8.22%)	0.92 (7.19%)
Cr K	14.23 (1.02%)	15.09 (2.06%)
Fe K	85.30 (1.28%)	83.99 (0.24%)
Total	100.00	100.00

(a)

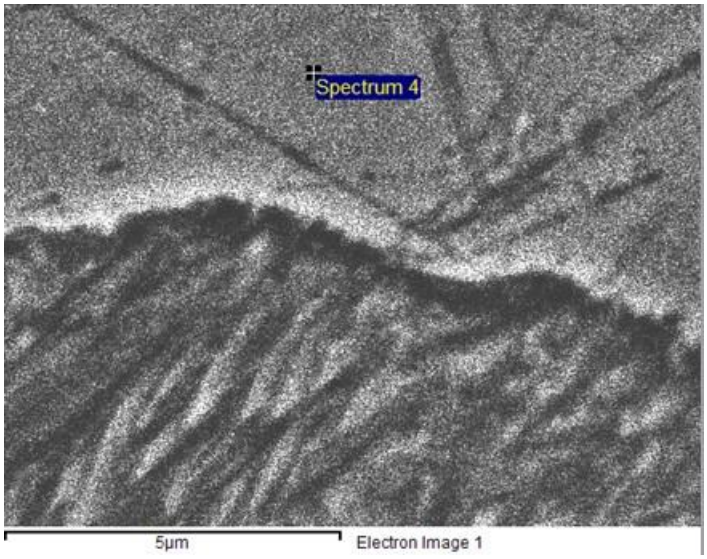

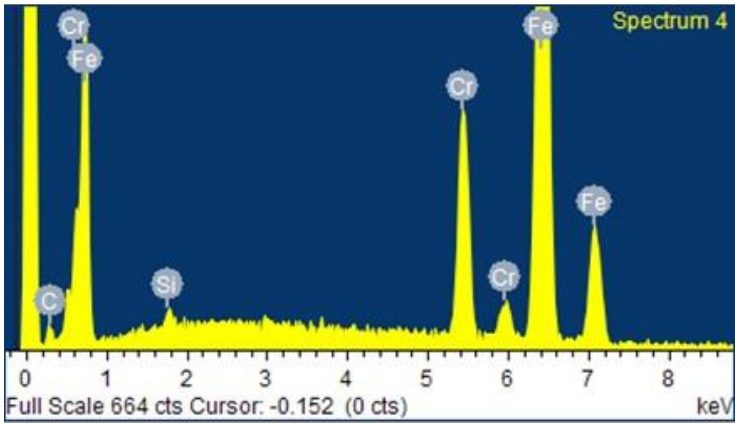

Element	Weight%	Atomic%
Si K	0.55 (6.67%)	1.08 (6.51%)
Cr K	13.77 (5.03%)	14.59 (5.15%)
Fe K	85.69 (0.07%)	84.33 (0.13%)
Total	100.00	100.00

(b)

Figure 4-14: EDX spectra of heat-treated AISI 420: (a) pearlite phase and (b) martensite matrix.

4.5 AISI 440C

AISI 440C is a high-carbon stainless steel, and is a type of modern steel famous for its high corrosion resistant, wear resistance, strength and hardness qualities, among all stainless steels, capable of attaining (after heat treatment) the highest hardness (60 HRC) as a martensitic stainless steel.

4.5.1 As-wrought specimen

The AISI 440C specimen studied in this research is a wrought product. Its microstructure is similar to that of wrought AISI 420 with carbides precipitated within the ferritic structure, as shown in Figure 4-15. However, compared with AISI 420, the size and volume fraction of carbides in AISI 440C are apparently large. This is attributed to the much higher C content and increased Cr content in AISI 440C. Carbide precipitation occurred intergranularly and intragranularly in this alloy during solidification, as shown in Figure 4-15(b). The grain boundaries can be identified clearly from the microstructure in this alloy. The EDX analysis results of each phase are present in Figure 4-16. It is shown that most of the Cr contributes to form M_7C_3 and $M_{23}C_6$ carbides. Cr is also found in the solid solution to provide corrosion resistance for this alloy.

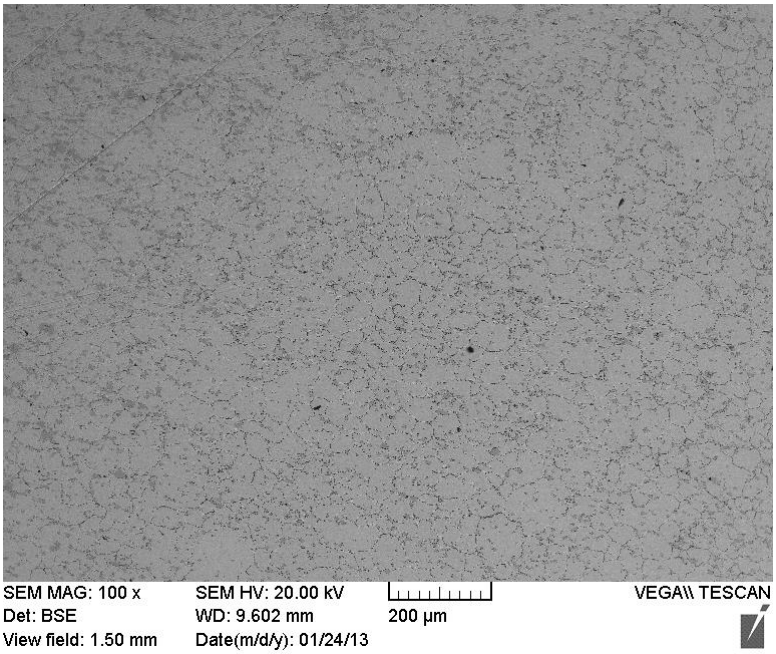

(a)

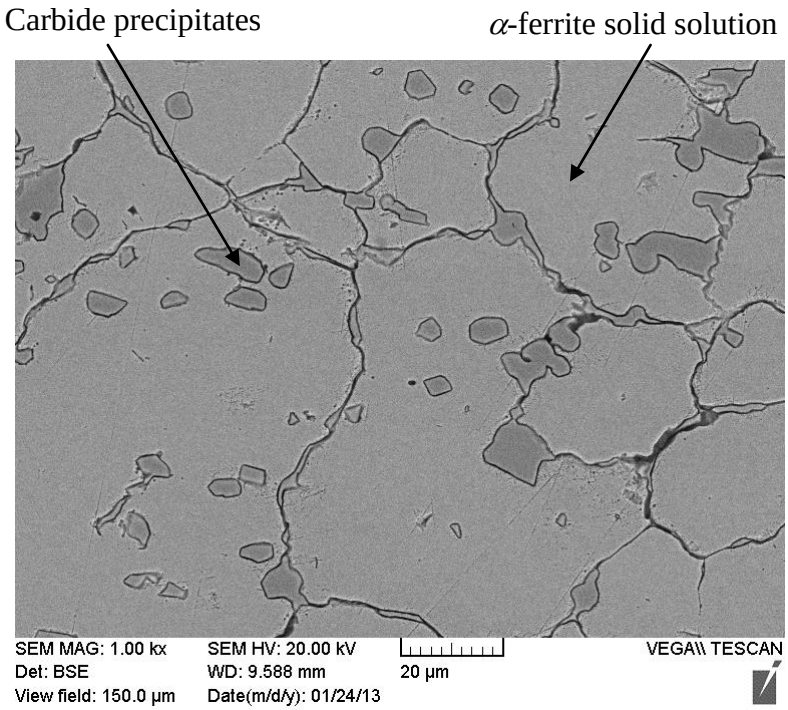

(b)

Figure 4-15: SEM images of microstructure of as-wrought AISI 440C: (a) at lower magnification and (b) at higher magnification.

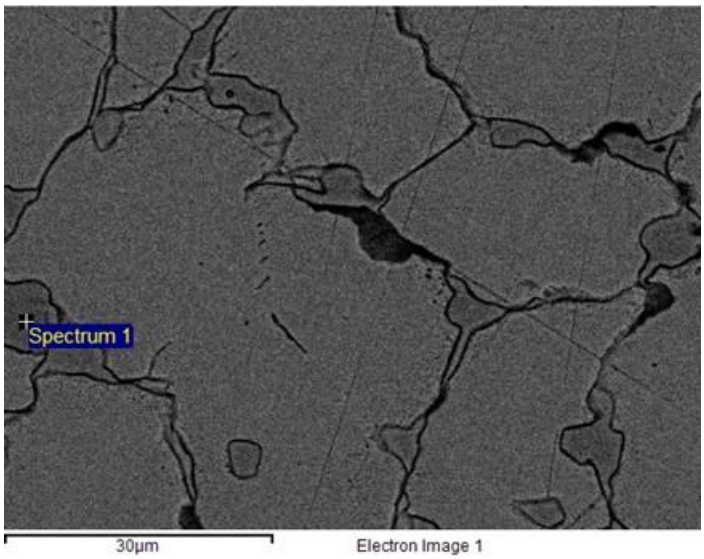

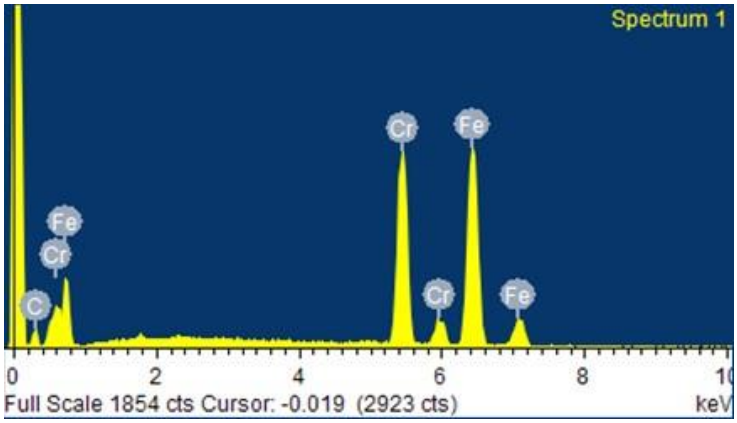

Element	Weight%	Atomic%
Si K	0.00	0.00
Cr K	37.52 (0.71%)	39.27 (1.04%)
Fe K	62.48 (0.74%)	60.73 (0.43%)
Total	100.00	100.00

(a)

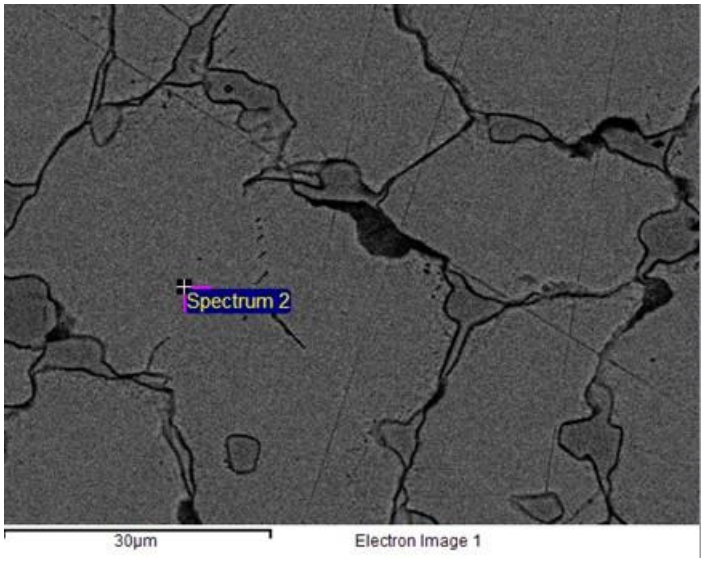

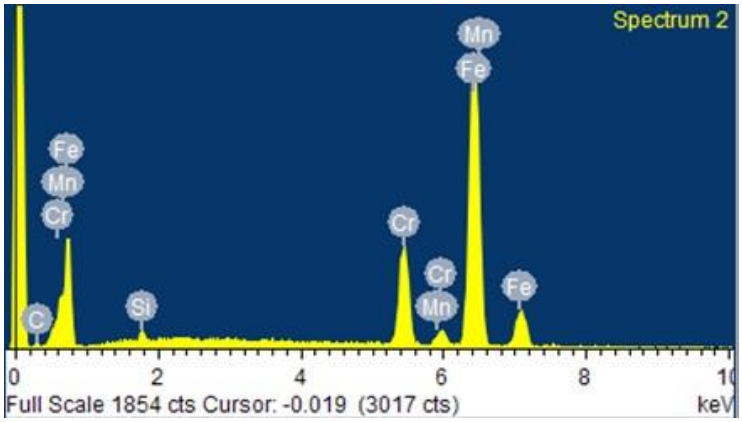

Element	Weight%	Atomic%
Si K	0.90 (6.67%)	1.76 (6.38%)
Cr K	16.48 (2.27%)	17.38 (2.22%)
Fe K	82.62 (1.48%)	80.87 (1.51%)
Total	100.00	100.00

(b)

Figure 4-16: EDX spectra of as-wrought AISI 440C: (a) carbide precipitates and (b) α-ferrite solid solution.

4.5.2 Heat-treated specimen

Different from AISI 420, the microstructure of AISI 440C seems not changed significantly by the heat treatment; the only difference that can be observed is the slight increment in carbide volume fraction of the heat-treated specimen, as seen in Figure 4-17. Owing to the high C content and the high Cr content, Cr-rich M_7C_3 and $M_{23}C_6$ carbides have priority to form, thus there is no sufficient C in the ferrite solid solution to promote the transformation to pearlite phase and martensite phase. The EDX spectra of the carbide phase and solid solution are presented in Figure 4-18. As demonstrated by the spectra, there is no much change in elemental contents between the as-wrought specimen and the heat-treated specimen.

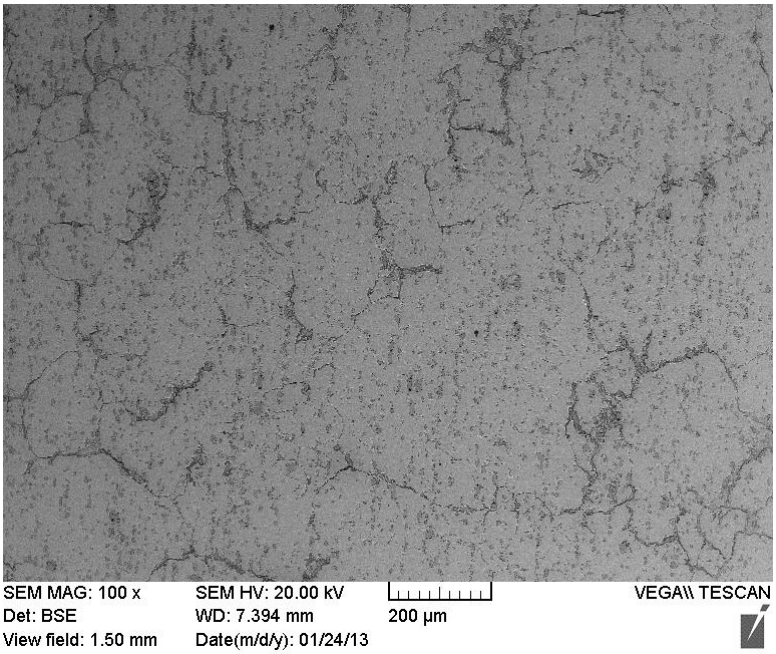

(a)

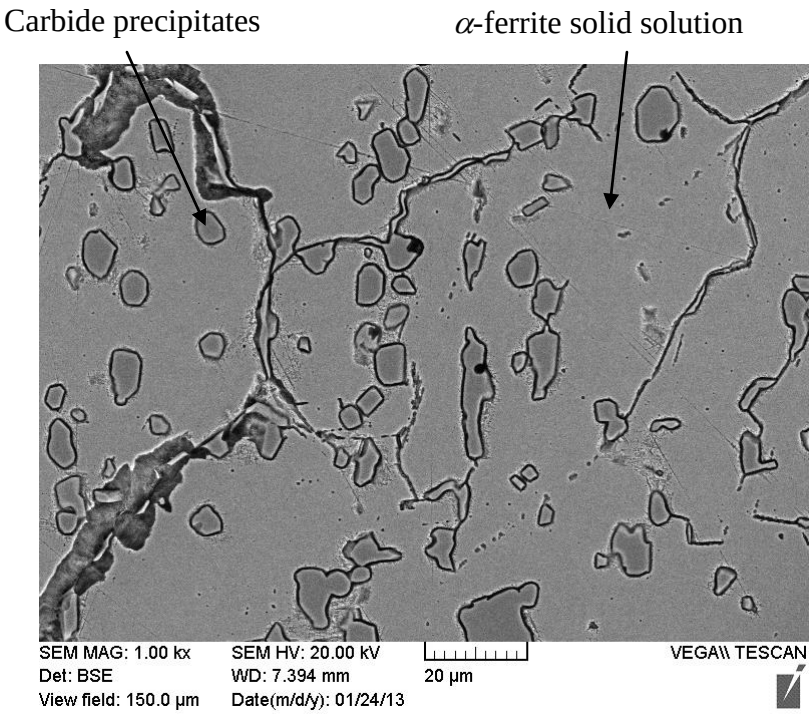

(b)

Figure 4-17: SEM images of microstructure of heat-treated AISI 440C: (a) at lower magnification and (b) at higher magnification.

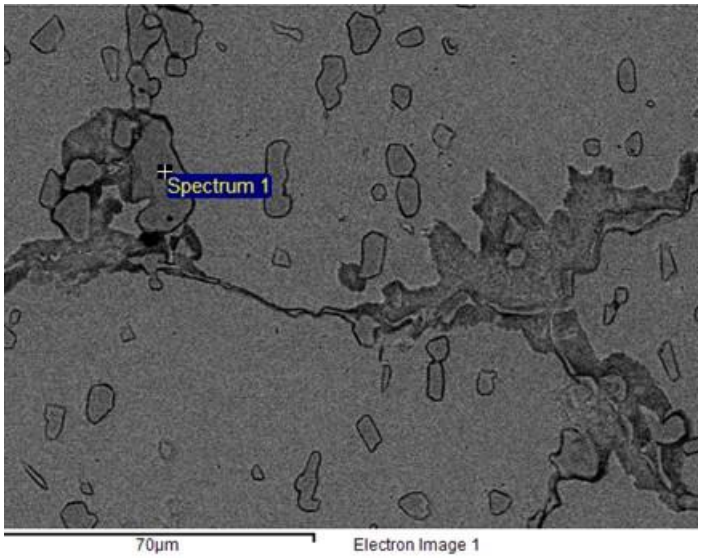

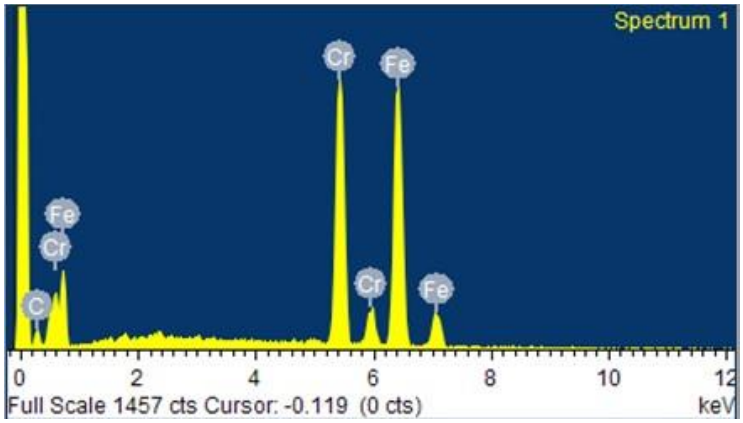

Element	Weight%	Atomic%
Si K	0.00	0.00
Cr K	39.58 (0.88%)	41.36 (1.21%)
Fe K	60.42 (0.93%)	58.64 (0.78%)
Total	100.00	100.00

(a)

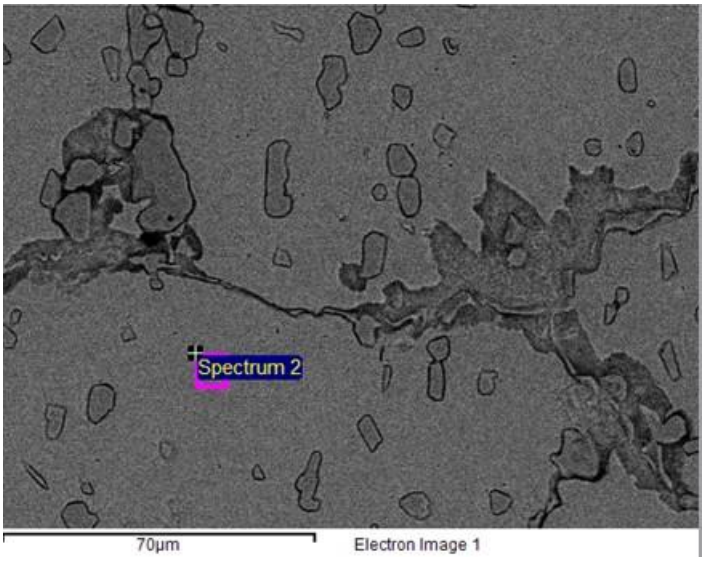

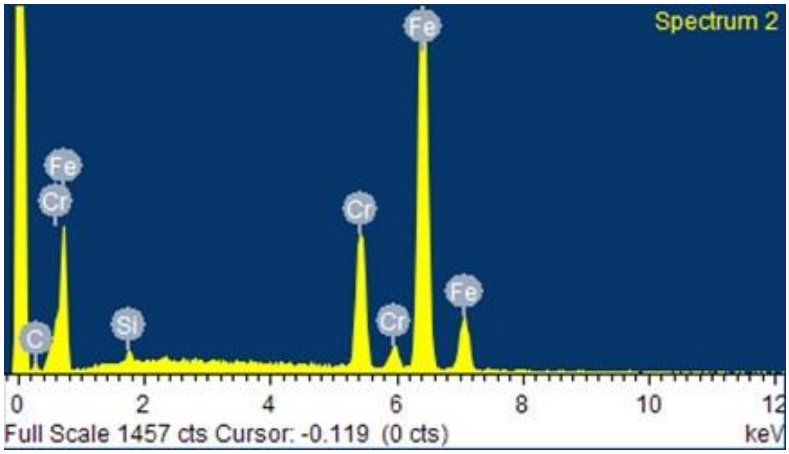

Element	Weight%	Atomic%
Si K	0.77 (3.61%)	1.51 (3.54%)
Cr K	16.86 (1.58%)	17.79 (1.59%)
Fe K	82.37 (3.28%)	80.70 (3.42%)
Total	100.00	100.00

(b)

Figure 4-18: EDX spectra of heat-treated AISI 440C: (a) carbide precipitates and (b) α-ferrite solid solution.

5 Hardness Behavior

5.1 Microhardness Results

As analyzed in the preceding chapter, Stellite 22, T-400C, AISI 420 and AISI 440C are all multi-phase alloys. Therefore, microhardness indentation test was conducted on each phase of these alloys to investigate the hardness change of these phases by the heat treatment and also to study the hardness variation of these phases with temperature. In the meanwhile, the overall hardness of these alloys before and after the heat treatment was also evaluated to reveal the influence of the heat treatment on the overall hardness of these alloys. The overall hardness of these alloys was also determined at different temperatures to obtain the temperature-dependence of hardness.

At least five indentations were made for each test condition, thus the average values of the multiple tests were taken as the final results and reported in this thesis. The maximum error percentages for each average value were calculated and presented along with the hardness results. The indentation mark made on the tested surface was imaged in each test and the Vickers hardness value was computed directly with the associate software of the hardness tester.

5.2 Stellite 22

Stellite 22 has a microstructure consisting of primary solid solution and a eutectic mixture including carbides and intermetallic compounds. Therefore, indentation was made on the solid solution and the eutectic, as well as overall microstructure, respectively. Figure 5-1 provides

the images of indentation mark on individual phases and overall microstructure for as-cast Stellite 22 specimen tested at room temperature as examples. By visual comparison, it is believed that the solid solution is much softer than the eutectic mixture, as the indentation mark made on the solution phase is much bigger than that on the eutectic mixture under the same normal load.

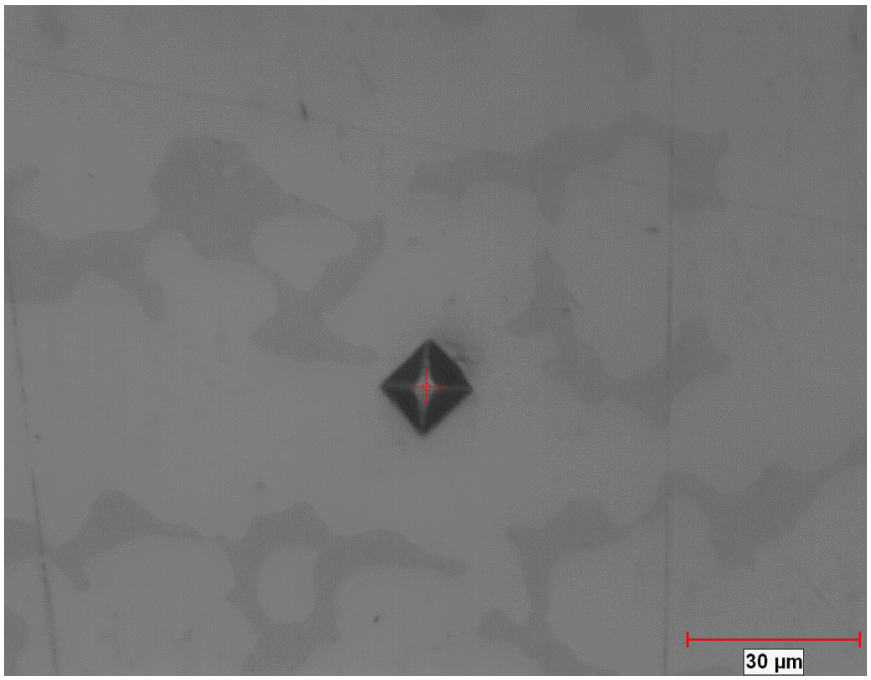

(a)

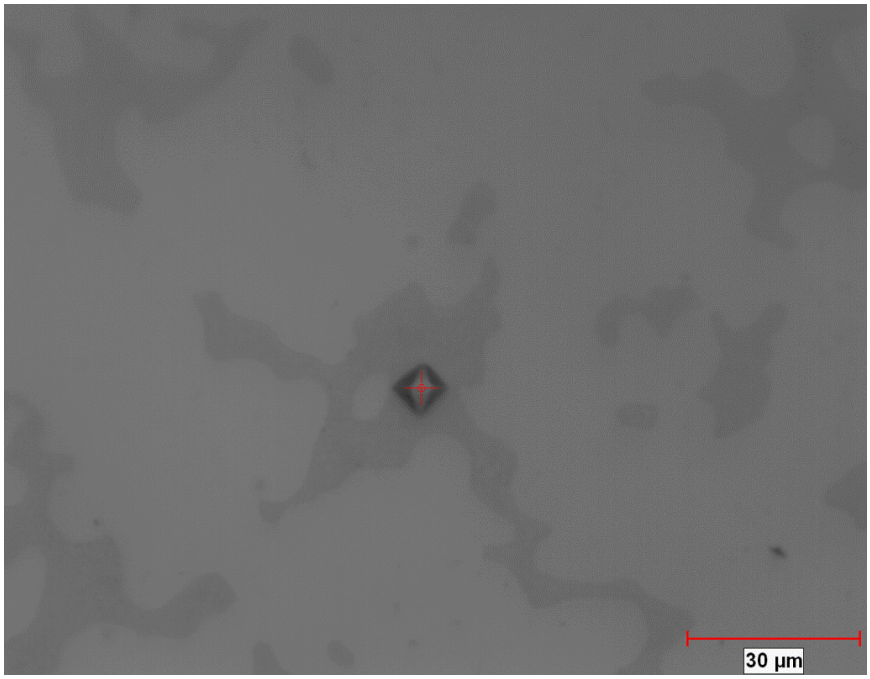

(b)

(c)

Figure 5-1: Indentation marks on as-cast Stellite 22 surface tested at room temperature: (a) solid solution, (b) eutectic mixture and (c) overall microstructure.

5.2.1 As-cast specimen

The average hardness values of solid solution and eutectic mixture as well as overall microstructure for as-cast Stellite 22 at room temperature and at elevated temperatures are presented in Table 5-1, with the maximum error in brackets. It is confirmed that the solid solution is softer than the eutectic mixture which is composed of carbides, intermetallic compounds and solid solution whether at room temperature or at elevated temperatures. This implies that carbides and intermetallic compounds are harder than Co solid solution. The overall hardness of this alloy measured is between the hardness values of solid solution and eutectic mixture, but closer to the former. It can be explained as the proportion of solid solution phase is larger than that of the eutectic phase in this alloy so that the former contributes more than the latter to the overall hardness. As concerned to temperature effects, it is noticed all the hardness values decrease with temperature, which indicates that both the solid solution and eutectic can be softened by temperature.

Table 5-1: Average hardness values (HV) for as-cast Stellite 22

Phase / Temperature	Solid solution	Eutectic mixture	Overall microstructure
25°C	314 (2.56%)	501 (1.65%)	420 (3.59%)
250°C	255 (3.57%)	393 (2.54%)	342 (2.71%)
450°C	242 (3.63%)	328 (2.18%)	326 (3.06%)
600°C	246 (2.95%)	310 (2.38%)	305 (2.38%)

5.2.2 Heat-treated specimen

The average hardness values of solid solution and eutectic mixture as well as overall microstructure for heat-treated Stellite 22 at room temperature and at elevated temperatures are presented in Table 5-2, with the maximum error in brackets. Similar behavior to as-cast Stellite 22 can be found for heat-treated Stellite 22. To demonstrate the heat treatment effects on the hardness of this alloy, the hardness values of the as-cast specimen and heat-treated specimen are plotted together in Figure 5-2.

Table 5-2: Average hardness values (HV) for heat-treated Stellite 22

Phase / Temperature	Solid solution	Eutectic mixture	Overall microstructure
25°C	307 (2.47%)	646 (3.54%)	433 (2.75%)
250°C	271 (3.42%)	542 (3.38%)	375 (3.49%)
450°C	241 (3.69%)	418 (2.44%)	338 (2.53%)
600°C	211 (2.34%)	360 (3.36%)	311 (3.45%)

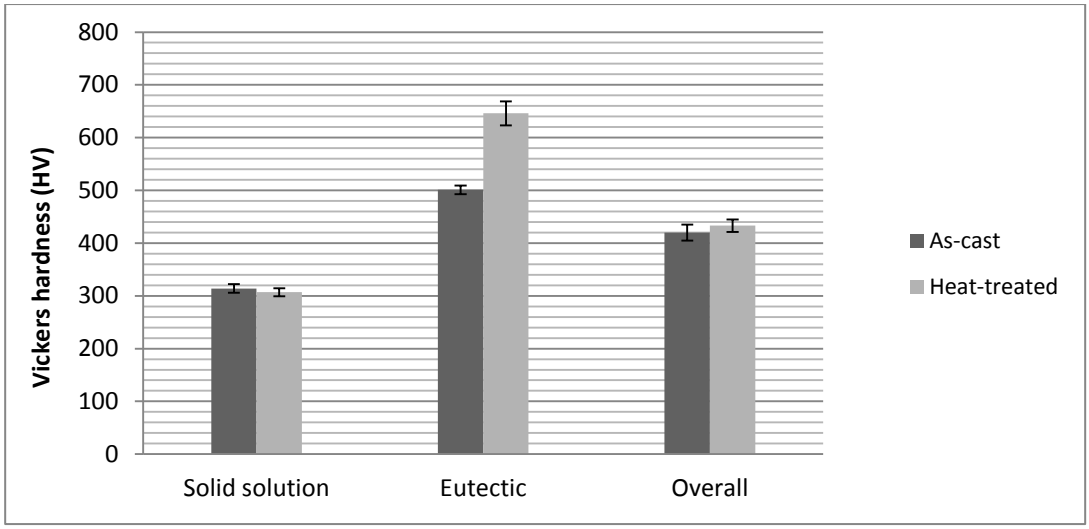

(a)

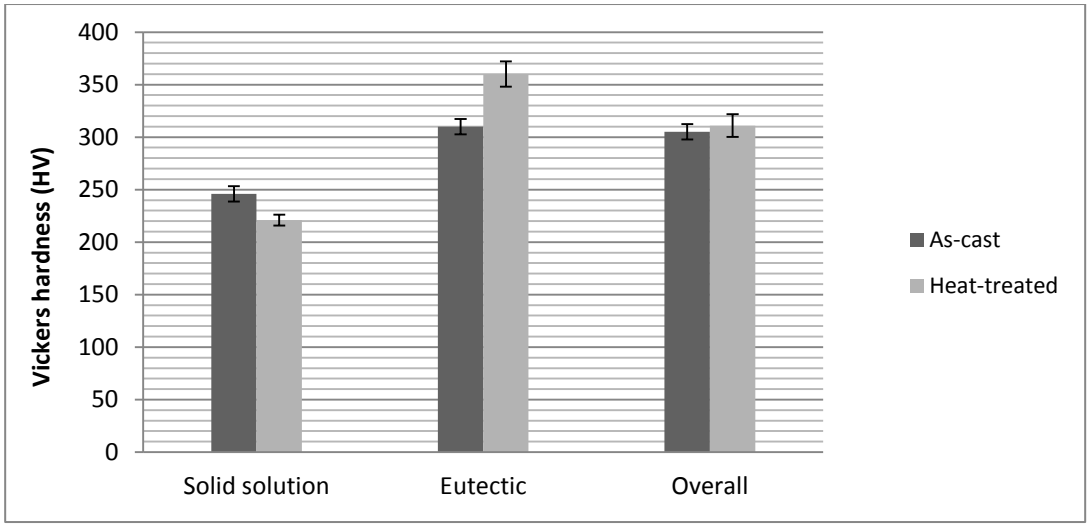

(b)

Figure 5-2: Comparison of hardness between as-cast and heat-treated Stellite 22: (a) at room temperature and (b) at 600°C.

It is found that the hardness of the Co solid solution was reduced by the heat treatment; in particular, at the high temperature of 600°C, the hardness reduction of the solid solution by the heat treatment was more evident. On the contrary, the hardness of the eutectic mixture was

increased after the alloy was heat treated. This was possibly caused by secondary carbide and intermetallic compound precipitates.

5.3 T-400C

T-400C is a two-phase alloy, consisting of primary Laves phase and eutectic Co solid solution with secondary Laves phase. For this alloy, indentation was made on primary Laves phase and Co solid solution, as well as overall microstructure, respectively. The images of indentation mark on individual phases and overall microstructure for as-cast T-400C specimen tested at room temperature are given in Figure 5-3 as examples. Through visually comparing the sizes of the indentation marks, it can be believed that Laves phase is much harder than the Co solid solution.

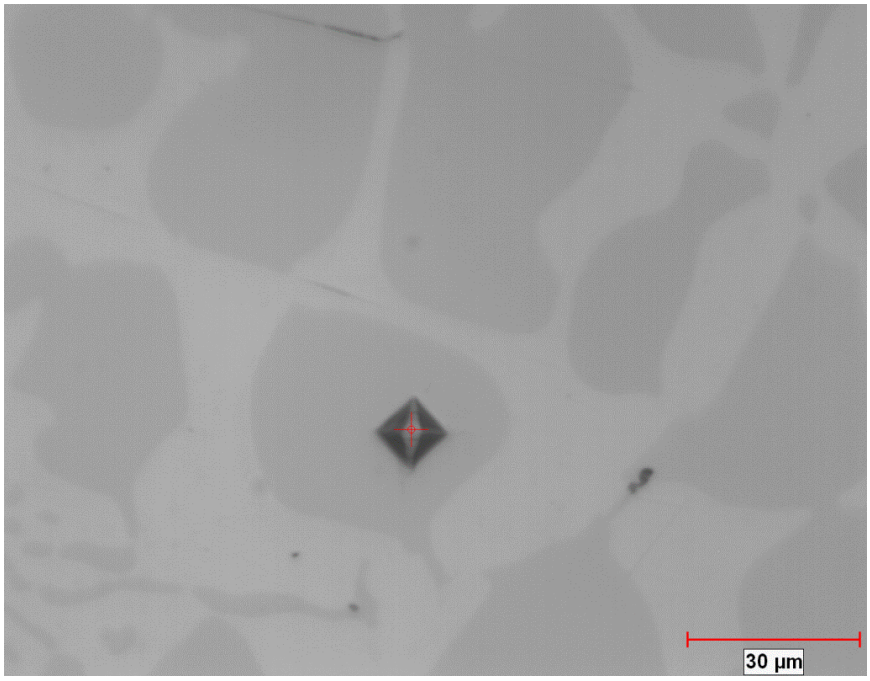

(a)

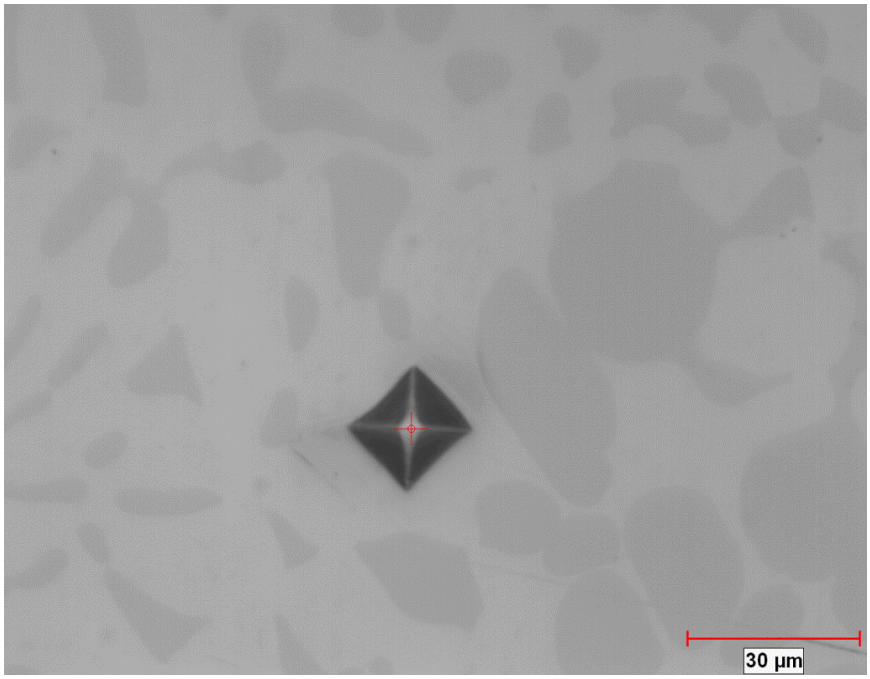

(b)

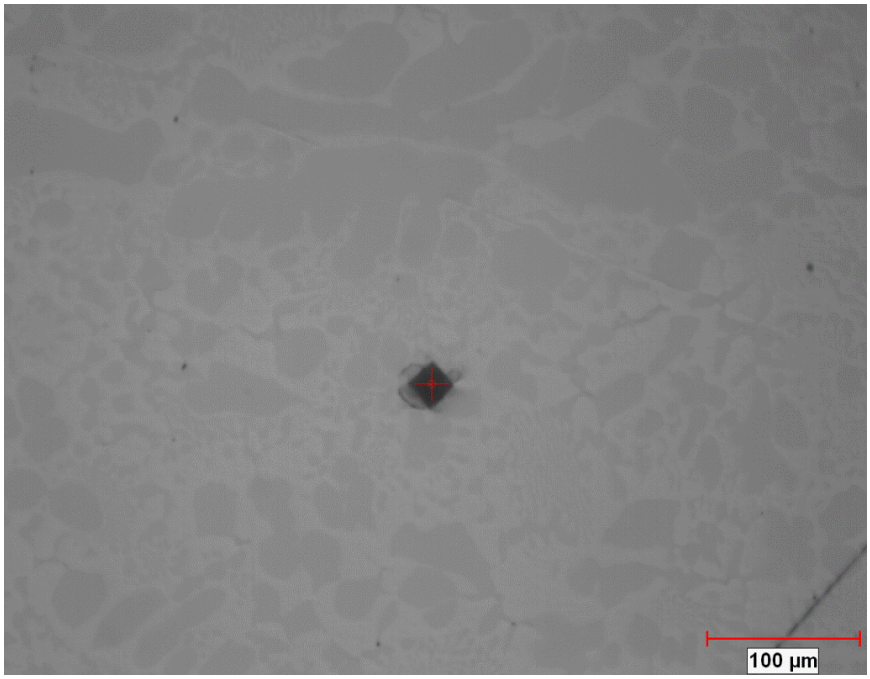

(c)

Figure 5-3: Indentation marks on as-cast T-400C surface tested at room temperature: (a) Laves phase, (b) solid solution and (c) overall microstructure.

5.3.1 As-cast specimen

The average hardness values of individual phases and overall microstructure for as-cast T-400C at room temperature and at elevated temperatures are presented in Table 5-3, with the maximum error in brackets. It is confirmed that Laves phase is much harder than the Co solid solution. The overall hardness of this alloy is greater than that of the solid solution and much lower than that of Laves phase. According to the volume fraction (38.9%) of Laves phase in this alloy, the hardness values of overall microstructure are explainable. Similar to Stellite 22, the hardness of T-400C is also influenced by temperature, as shown in Table 5-3, hardness decreased with temperature for all the phases and thereby for the overall microstructure.

Table 5-3: Average hardness values (HV) for as-cast T-400C

Phase / Temperature	Primary Laves phase	Solid solution	Overall microstructure
25°C	1068 (2.31%)	380 (3.51%)	574 (4.51%)
250°C	1034 (3.46%)	342 (2.53%)	529 (3.04%)
450°C	909 (2.29%)	329 (2.36%)	494 (3.87%)
600°C	878 (2.41%)	324 (2.54%)	477 (4.68%)

5.3.2 Heat-treated specimen

For the heat-treated specimen, the average hardness values of Laves phase and Co solid solution as well as overall at room temperature and at elevated temperatures are given in Table 5-4, with the maximum error in brackets. The heat-treated specimen behaved similarly to as-cast T-400C in hardness variation with phase and temperature. The comparison of hardness

between as-cast T-400C and heat-treated T-400C is illustrated in Figure 5-4. Unlike Stellite 22, the Co solid solution of T-400C was hardened by the heat treatment, which was attributed to the ternary Laves phase precipitates, as known from the microstructural analysis in Chapter 4. However, the hardness of primary Laves phase was almost unchanged after the heat treatment. These resulted in slight increase in the overall hardness of this alloy.

Table 5-4: Average hardness values (HV) for heat-treated T-400C

Phase / Temperature	Primary Laves phase	Solid solution	Overall microstructure
25°C	1048 (2.49%)	485 (1.37%)	587 (2.58%)
250°C	980 (3.69%)	445 (3.47%)	546 (4.38%)
450°C	908 (2.46%)	441 (2.38%)	505 (3.48%)
600°C	889 (3.39%)	429 (2.43%)	495 (3.59%)

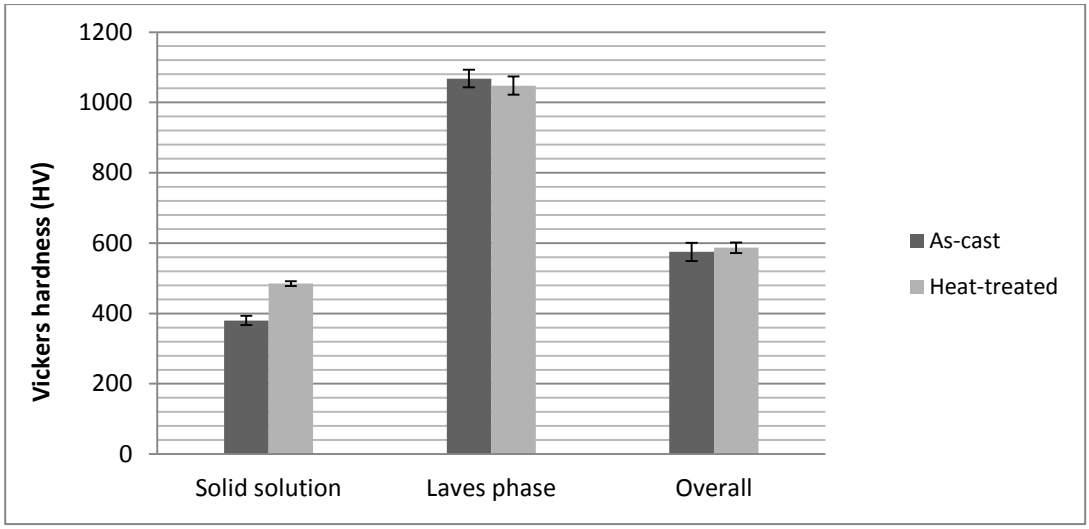

(a)

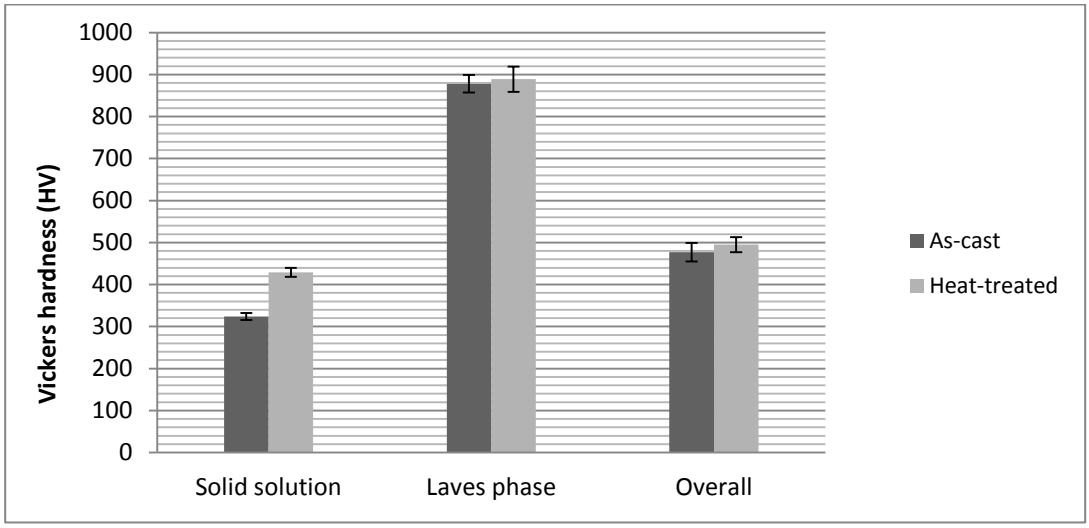

(b)

Figure 5-4: Comparison of hardness between as-cast and heat-treated T-400C: (a) at room temperature and (b) at 600°C.

5.4 AISI 420

AISI 420 is a medium-carbon stainless steel and has a microstructure consisting of ferrite matrix with carbide precipitates, as known from the microstructural analysis previously. For

this alloy, indentation test was intended to perform on ferrite matrix and carbides, respectively. However, since the size of the carbides was too small to allow the indenter covering the single carbide phase, that is, the indenter had to cover some area with the ferrite matrix, which would provide an erroneous result of hardness for the carbides. Therefore, for this alloy, only overall hardness was measured; the indentation mark made on the as-wrought specimen tested at room temperature is shown in Figure 5-5 as an example.

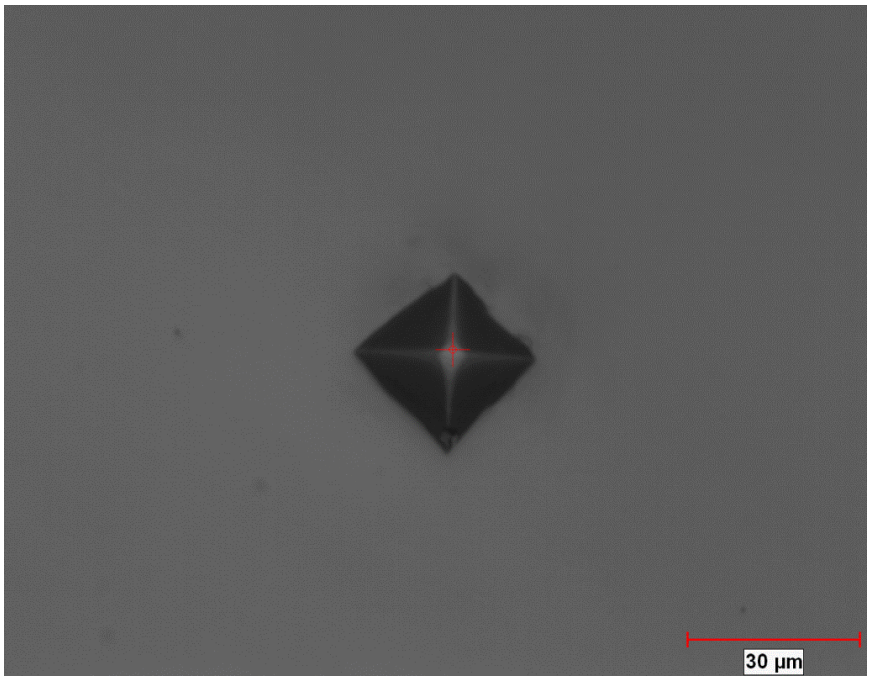

Figure 5-5: Indentation mark on as-wrought AISI 420 surface tested at room temperature.

5.4.1 As-wrought specimen

The average overall hardness values of as-wrought AISI 420 at room temperature and at elevated temperatures are summarized in Table 5-5. Similar to Stellite alloy and Tribaloy alloy, stainless steel can also be softened by temperature. The hardness of AISI 420 decreased with

the increase in temperature.

Table 5-5: Average hardness values (HV) for as-wrought AISI 420

Phase / Temperature	Overall microstructure
25°C	179 (4.73%)
250°C	156 (4.21%)
450°C	137 (4.43%)
600°C	125 (4.74%)

5.4.2 Heat-treated specimen

The average overall hardness values of heat-treated AISI 420 at room temperature and at elevated temperatures are presented in Table 5-6. Similarly, the hardness of heat-treated AISI 420 also decreased with the increase in temperature. Comparing hardness between the as-wrought and heat-treated specimens, as illustrated in Figure 5-6, it is found that the heat treatment enhanced the hardness of this alloy significantly, especially the room-temperature hardness. Referring to the microstructure change of this alloy after the heat treatment, as discussed previously, the ferrite matrix was transformed to pearlite and martensite mixed matrix, with the dissolution of carbides. Pearlite and martensite matrix is definitely harder than ferrite matrix.

Table 5-6: Average hardness values (HV) for heat-treated AISI 420

Temperature \ Phase	Overall microstructure
25°C	349 (3.56%)
250°C	298 (3.22%)
450°C	261 (2.29%)
600°C	213 (2.98%)

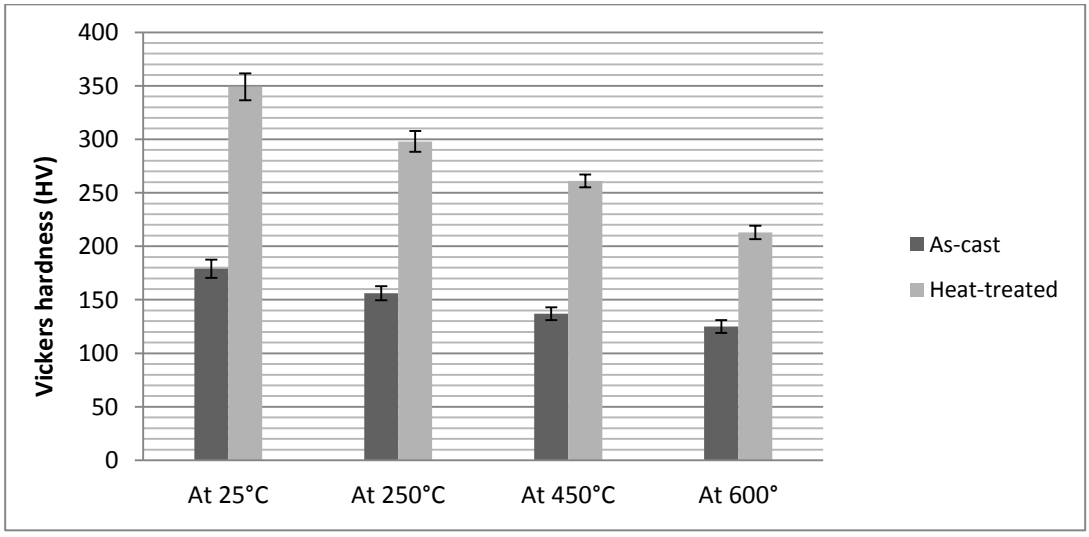

Figure 5-6: Comparison of hardness between as-wrought and heat-treated AISI 420.

5.5 AISI 440C

Similar to AISI 420, but also different, AISI 440C is a high-carbon stainless steel. Its microstructure consists of ferrite matrix with more carbide precipitates than AISI 420, as discussed previously. Again, indentation test was tried to perform on ferrite matrix and carbides, respectively for this alloy, but due to the limited size of the carbides, the indentation

could not be made on the single carbide phase, that is, the indenter had to cover some area with the ferrite matrix. As a result, for this alloy, only overall hardness was measured; the indentation mark made on the as-wrought specimen tested at room temperature is shown in Figure 5-7 as an example.

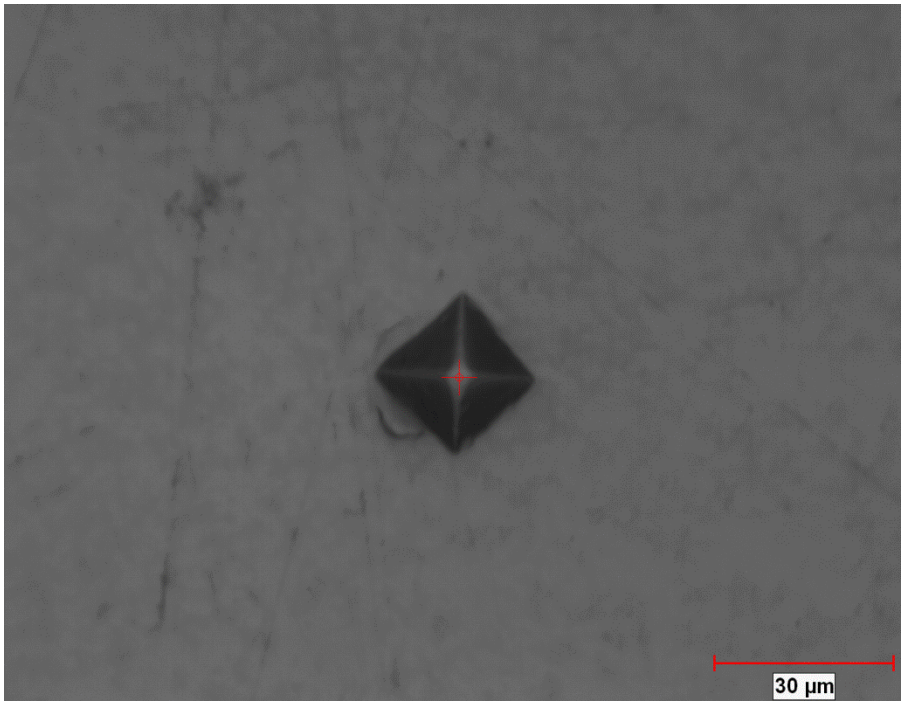

Figure 5-7: Indentation mark on as-wrought AISI 440C surface tested at room temperature.

5.5.1 As-wrought specimen

The average overall hardness values of as-wrought AISI 440C at room temperature and at elevated temperatures are provided in Table 5-7. Owing to the higher carbon content thus larger volume fraction of carbides, the overall hardness of as-wrought AISI 440C is higher than that of as-wrought AISI 420, comparing the hardness data in Table 5-5 with those in Table 5-7. The hardness of AISI 440C also decreased with the increase in temperature.

Table 5-7: Average hardness values (HV) for as-wrought AISI 440C

Phase / Temperature	Overall microstructure
25°C	196 (4.23%)
250°C	170 (4.65%)
450°C	157 (2.22%)
600°C	145 (4.29%)

5.5.2 Heat-treated specimen

The average overall hardness values of heat-treated AISI 440C at room temperature and at elevated temperatures are presented in Table 5-8. The same variation trend of hardness with temperature was observed on this specimen, compared with the as-wrought specimen. However, regarding the heat treatment effect, as illustrated in Figure 5-6, unlike AISI 420, although the heat treatment did increase the hardness of AISI 440C, its effect did not so significant as on AISI 420. This also relates to the microstructure. As observed in the microstructure, after the heat treatment, there was no significant change for AISI 440C, which differed from AISI 420. Heat-treated AISI 440C still consists of ferrite matrix with carbide precipitates; the only change is a little increase in carbide amount and carbide size, which may influence the hardness slightly.

Table 5-8: Average hardness values (HV) for heat-treated AISI 440C

Temperature \ Phase	Overall microstructure
25°C	199 (4.97%)
250°C	179 (2.43%)
450°C	162 (4.54%)
600°C	155 (3.43%)

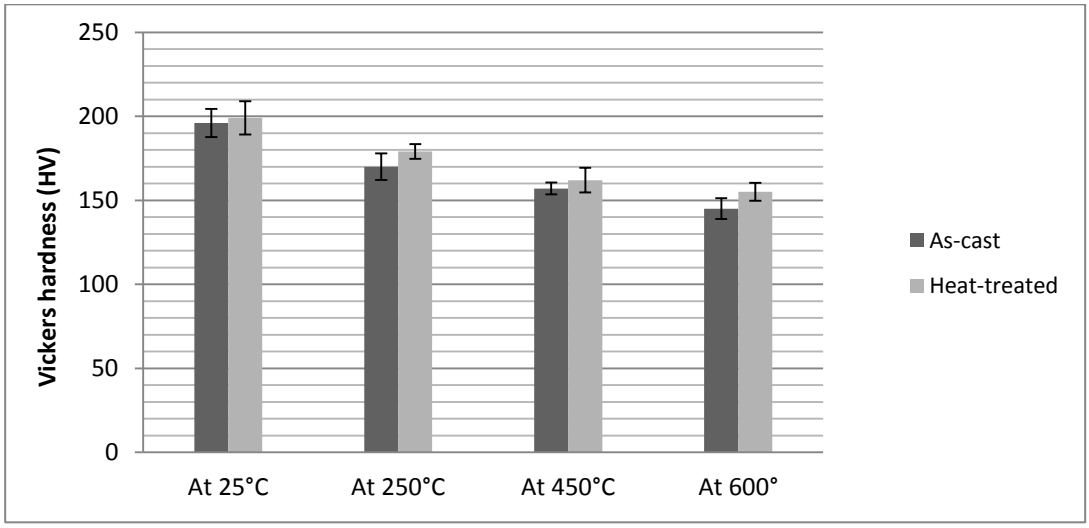

Figure 5-8: Comparison of hardness between as-wrought and heat-treated AISI 440C.

6 Wear Resistance

6.1 Wear Loss

As described previously, each as-received and heat-treated specimen of Stellite 22, T-400C, AISI 420 and AISI 440C experienced pin-on-disc wear tests at room temperature, 250°C and 450°C. The wear tracks resulted from the sliding wear were measured using the DEKTAK 150 Surface Profile Measuring System. Six locations along each wear track were measured to obtain the cross-section area; the average wear loss (wear track volume) and the derivation were determined based on the six measurements. The calculated wear loss values for each tested specimen are summarized below.

6.1.1 Stellite 22

The average wear losses of as-cast Stellite 22 and heat-treated Stellite 22 specimens are illustrated in Figure 6-1, with the maximum error calculations given in Table 6-1. It is shown that both the as-cast and heat-treated specimens behaved differently at room temperature wear and at high temperature wear. They were more resistant to wear at room temperature than at elevated temperatures. The least wear resistance occurred at 250^{o}C. But at the high temperature of 450°C, the wear resistance of this alloy was increased, compared with that at 250°C. This phenomenon was also observed on a similar Stellite alloy (Stellite 21) by other researchers [50]. Regarding the heat treatment effect, it seems not beneficial for the wear resistance of Stellite 22.

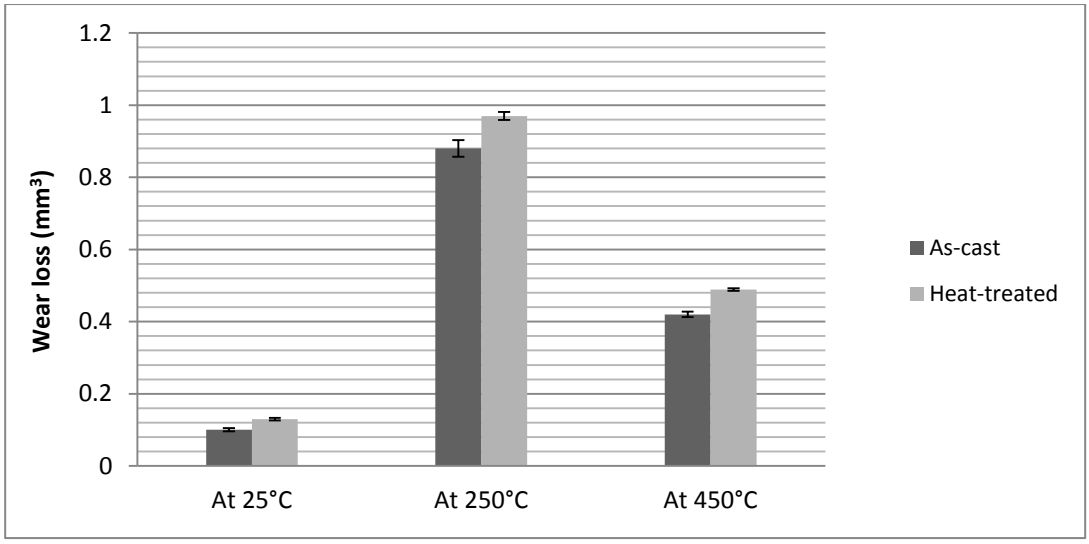

Figure 6-1: Wear loss of Stellite 22 under pin-on-disc wear test.

Table 6-1: Maximum error calculations of wear loss for Stellite 22

Temperature / Specimen	25°C	250°C	450°C
As-cast	4.10%	6.31%	3.26%
Heat-treated	6.44%	2.98%	6.25%

6.1.2 T-400C

The average wear losses of as-cast T-400C and heat-treated T-400C are illustrated in Figure 6-2, with the maximum error calculations given in Table 6-2. It is observed that the heat treatment had slight beneficial effect on the wear resistance of this alloy. In addition, similar to Stellite 22, both as-cast and heat-treated T-400C exhibited much better wear resistance at room temperature than at elevated temperatures. However, the wear resistance of T-400C was higher at 450^{o}C than at 250^{o}C, as illustrated in Figure 6-2.

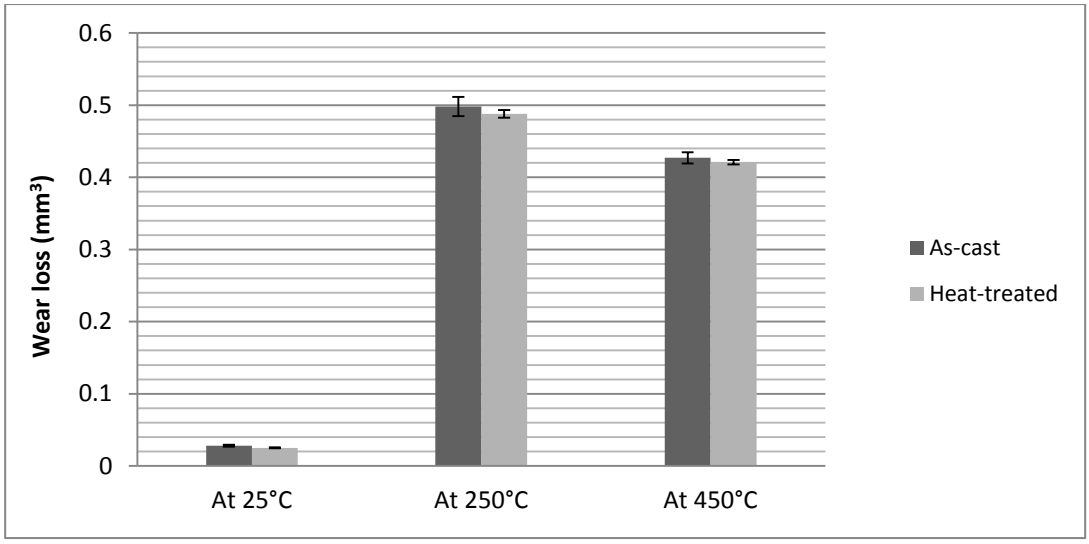

Figure 6-2: Wear loss of T-400C under pin-on-disc wear test.

Table 6-2: Maximum error calculations of wear loss for T-400C

Temperature / Specimen	25°C	250°C	450°C
As-cast	4.43%	2.66%	1.81%
Heat-treated	2.63%	1.11%	0.73%

6.1.3 AISI 420

The average wear losses of as-wrought and heat-treated AISI 420 specimens are presented in Figure 6-3, with the maximum error calculations given in Table 6-3. AISI 420 exhibited quite different behavior from Stellite 22 and T-400C, as seen in Figure 6-3. The wear resistance of this alloy increased with temperature; especially the heat-treated specimen exhibited much lower wear resistance at room temperature than at elevated temperatures. Furthermore, the heat treatment had a detrimental effect on the wear resistance of AISI 420 at room temperature,

but it improved the wear resistance at high temperatures

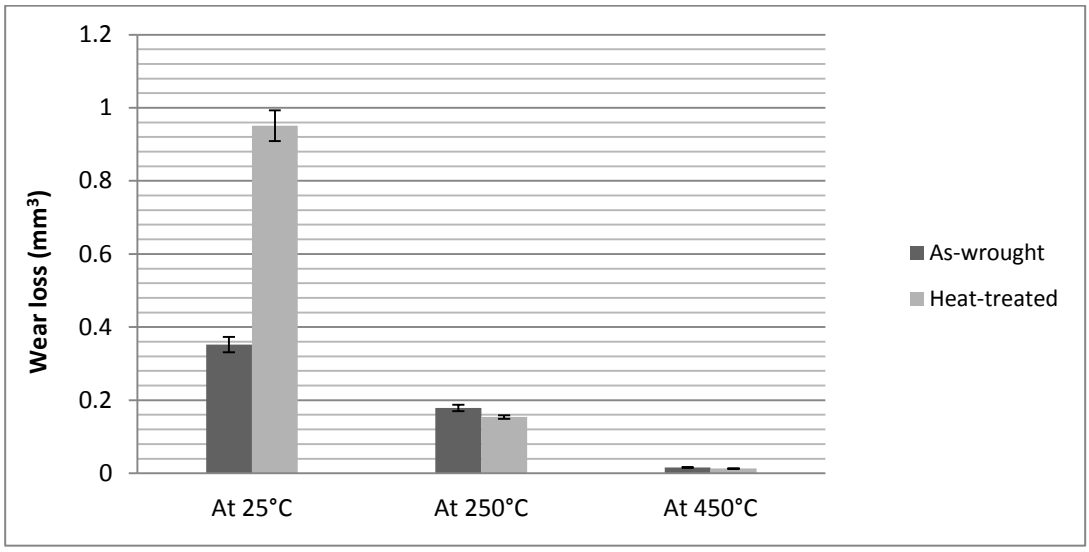

Figure 6-3: Wear loss of AISI 420 under pin-on-disc wear test.

Table 6-3: Maximum error calculations of wear loss for AISI 420

Temperature / Specimen	25°C	250°C	450°C
As-wrought	5.97%	4.98%	3.46%
Heat-treated	4.43%	3.02%	2.94%

6.1.4 AISI 440C

The average wear losses of as-wrought and heat-treated AISI 440C specimens are presented in Figure 6-4, with the maximum error calculations given in Table 6-3. Similar to AISI 420, this alloy exhibited better resistance to wear at the high temperature of 450°C. However, at 250^{o}C the wear loss was increased, as seen in Figure 6-4. The heat treatment enhanced the wear resistance of this alloy at room temperature and at high temperatures.

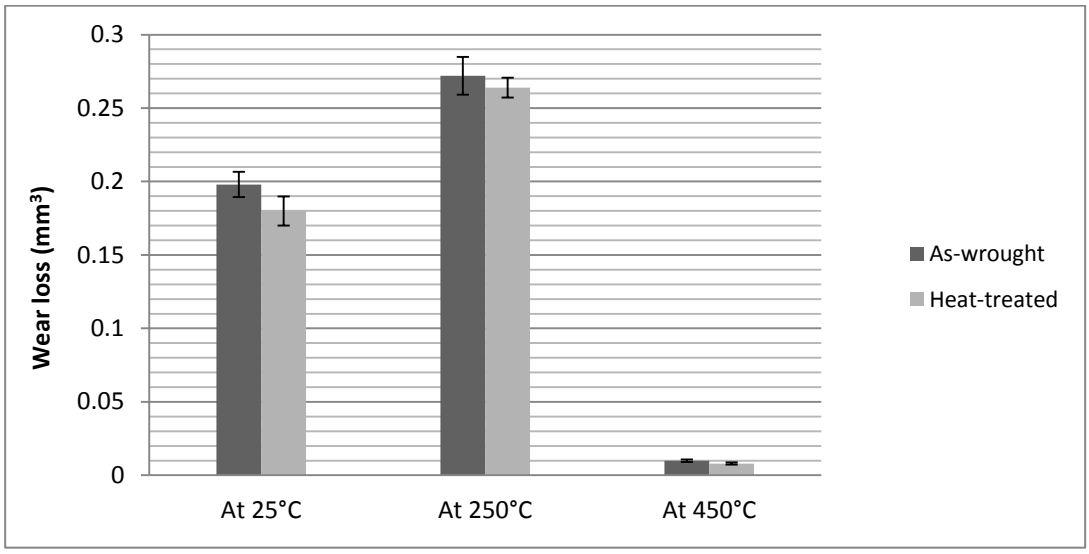

Figure 6-4: Wear loss of AISI 440C under pin-on-disc wear test.

Table 6-4: Maximum error calculations of wear loss for AISI 440C

Temperature / Specimen	25°C	250°C	450°C
As-wrought	4.34%	4.75%	8.69%
Heat-treated	5.52%	2.54%	9.52%

6.2 Worn Surface Analysis

From the wear loss results presented above, each alloy exhibited different wear behavior at room temperature and at elevated temperature; and also the heat treatment affect the wear resistance of these alloy differently. In order to better understand the wear loss results and explore the wear mechanisms of these alloys, the worn surfaces of each specimen were analyzed using SEM/EDX techniques. The SEM images and the EDX spectra are presented

below for each alloy.

6.2.1 Stellite 22

The worn surfaces of as-cast Stellite 22 and heat-treated Stellite 22 specimens tested at room temperature are presented in Figure 6-5 and Figure 6-6, respectively. The morphologies show typical ploughing characteristics; some areas are smooth where the material was scraped away by the pin under normal loading and some area were deformed with large plastic flow, as seen in the images at high magnification. Comparing the wear track sizes between the image in Figure 6-5(a) and that in Figure 6-6(a), it is clear that the wear track in the heat-treated specimen surface is wider, which confirms the wear loss results in Figure 6-1. The microstructural analysis showed the increase of Co_3Mo and $CoMo_6$ intermetallic compounds and the occurrence of $Cr_{23}C_6$ precipitated in the heat-treated specimen. Since Co_3Mo and $CoMo_6$ intermetallic compounds are very brittle, the increase in their volume fraction would result in the decrease of the overall strength of the alloy, thus less resistance to wear attack.

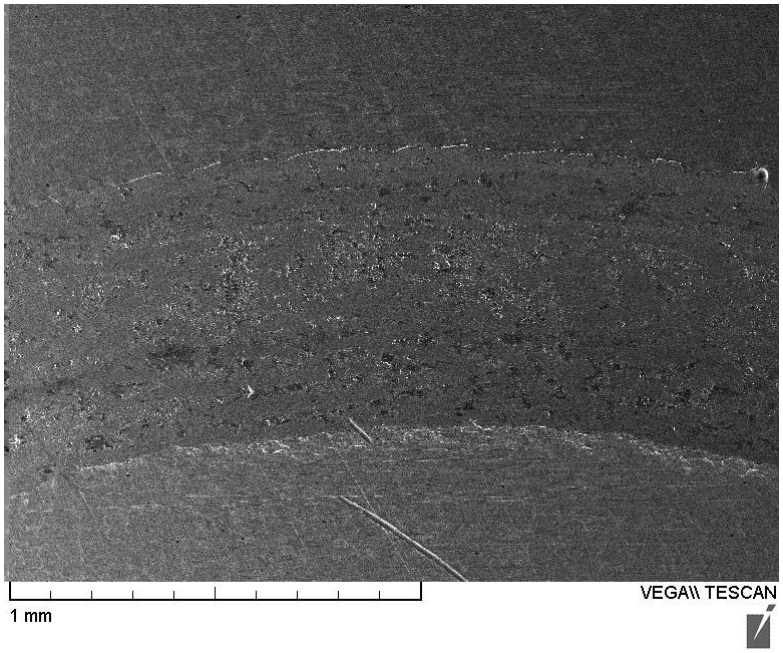

(a)

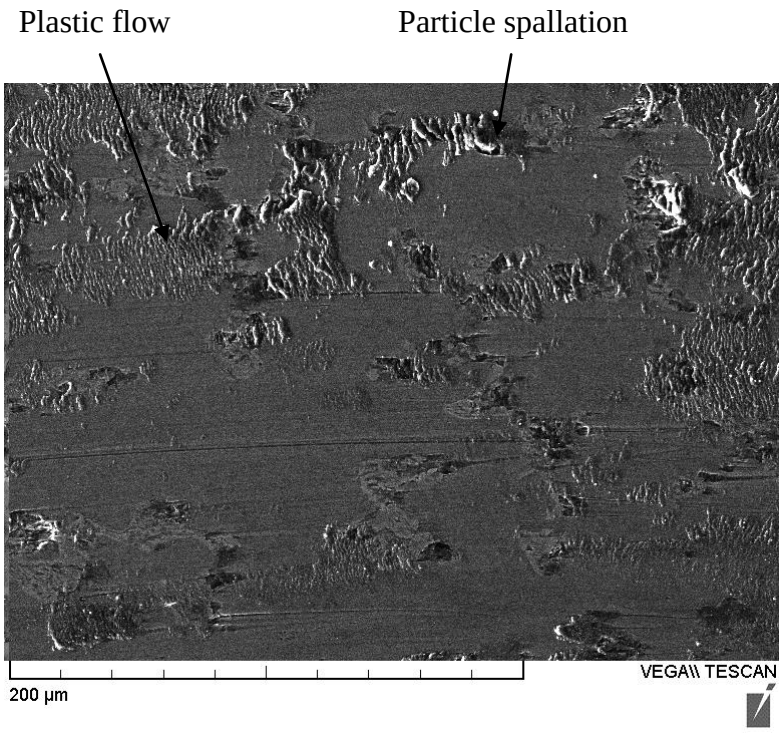

(b)

Figure 6-5: SEM images of worn surface of as-cast Stellite 22 tested at room temperature: (a) at low magnification and (b) at high magnification.

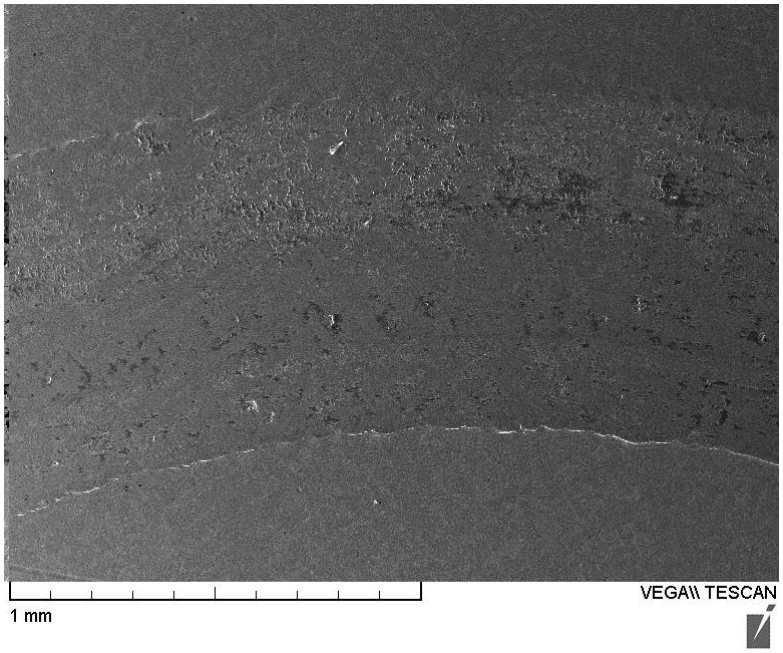

(a)

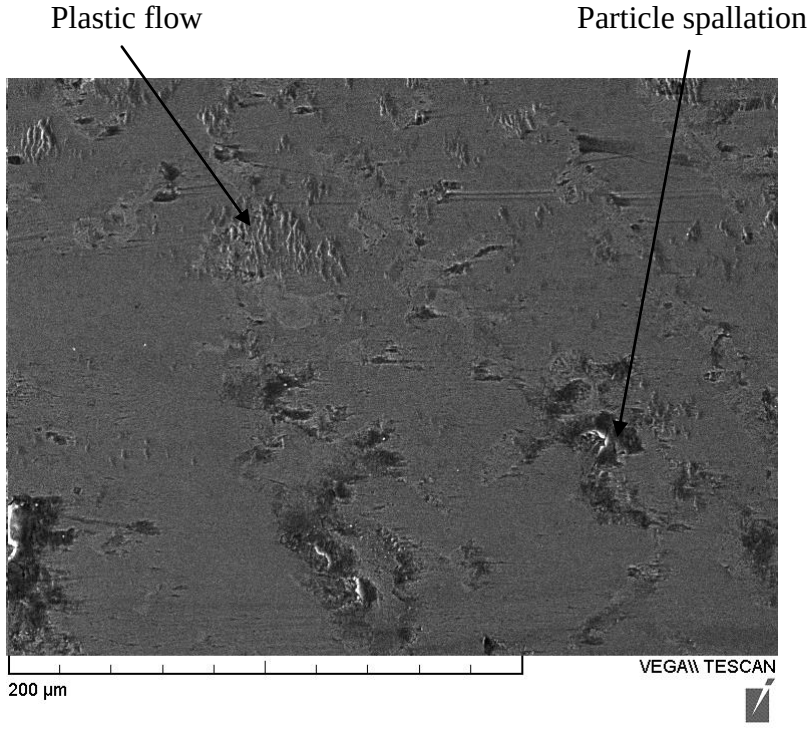

(b)

Figure 6-6: SEM images of worn surface of heat-treated Stellite 22 tested at room temperature: (a) at low magnification and (b) at high magnification.

Regarding the temperature effect, it is clear that the widths of the wear tracks in the specimen surfaces tested at 250°C are double of those of the wear tracks in the specimen surfaces tested at room temperature, as shown in Figure 6-7(a) and Figure 6-8(a), which is consistent with the wear loss results. In general, metallic materials lose strength at high temperatures so that the main reason for the increased wear loss should be the reduced hardness. Comparing the morphologies of worn surface of the specimens tested at room temperature and at 250°C, less plastic deformation is observed in the worn surface image of latter specimen, seen Figure 6-7(b) and Figure 6-8(b). Again, it is shown that the wear track in the heat-treated specimen surface is wider, which indicates more wear loss. The governing wear mechanism may also be due to the increased brittleness by the additional intermetallic compounds precipitated during the heat treatment that made the alloy more vulnerable under wear impact loads.

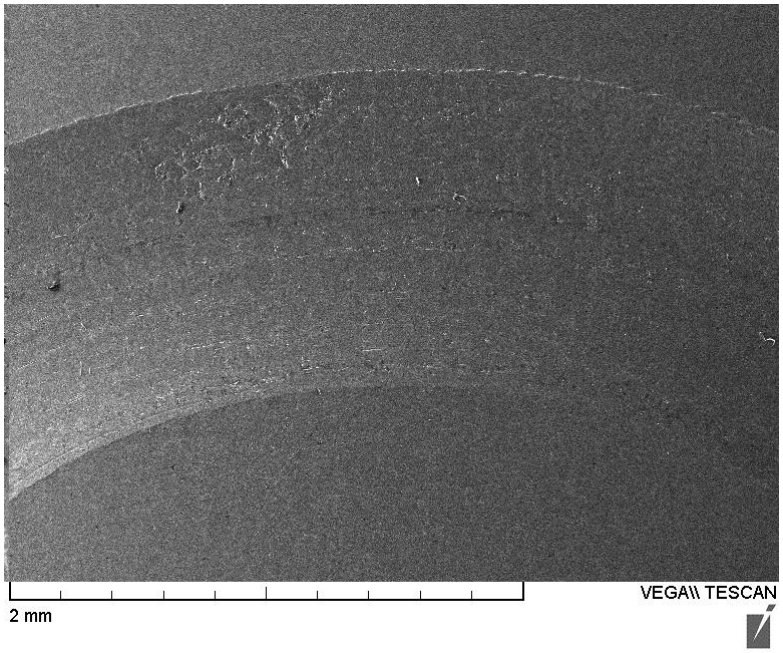

(a)

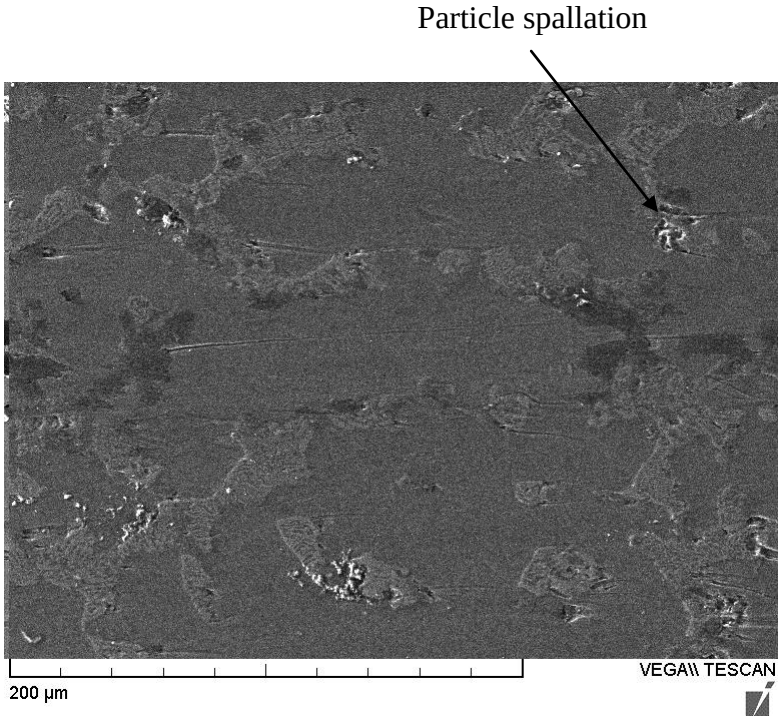

(b)

Figure 6-7: SEM images of worn surface of as-cast Stellite 22 tested at 250°C: (a) at low magnification and (b) at high magnification.

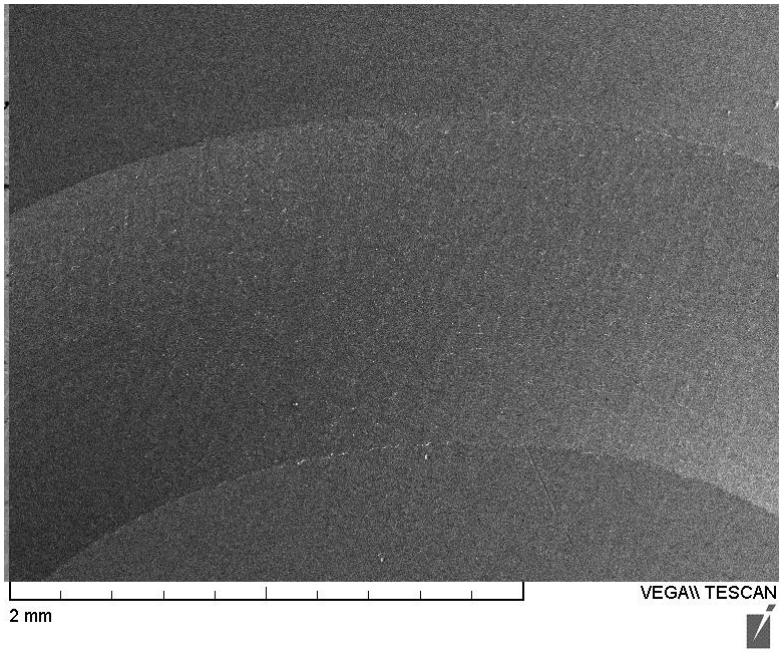

(a)

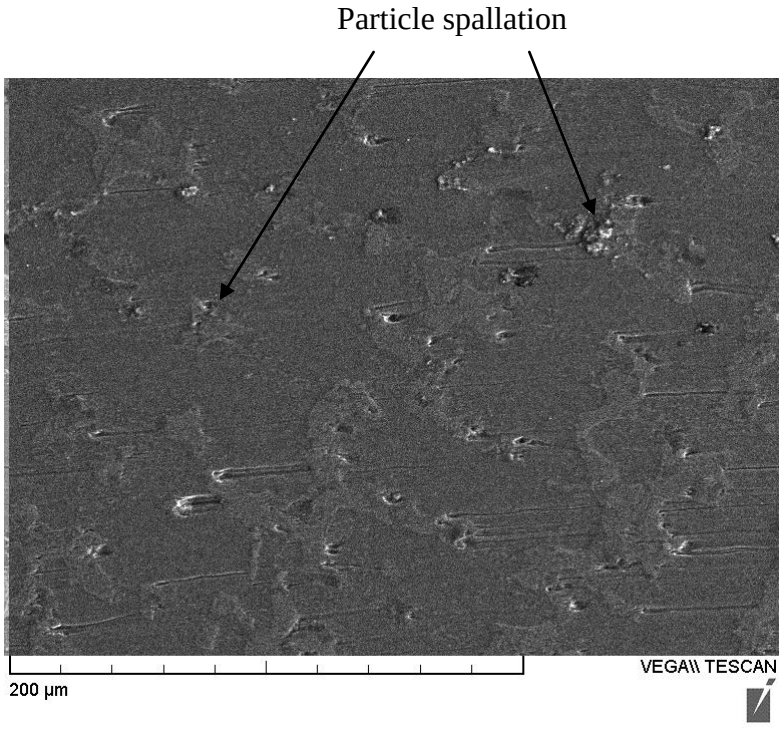

(b)

Figure 6-8: SEM images of worn surface of heat-treated Stellite 22 tested at 250^{o}C: (a) at low magnification and (b) at high magnification.

However, different morphologies are observed in the worn surfaces of the specimens tested at 450^{o}C; surface oxidation is observed obviously, in particular, in the as-cast specimen surface, see the images in Figure 6-9 and Figure 6-10, the white areas are the residuals of Cr-oxides. Owing to the large amount of Cr in the solid solution, at high temperatures, hard and strong Cr-oxide films would be formed on the specimen surface. These oxide films exerted their influences on the wear process through the so-called “glazing” effect; the oxide debris can be squeezed into the specimen surface during the wear process, which can harden the specimen surface against wear. This can explain why the wear loss of the specimen at 450^{o}C is lower than that at 250^{o}C. To confirm the surface oxidation at the high temperature, EDX analysis was conducted on the wear tracks; the spectra are provided in Figure 6-11. It is shown that a large amount of oxygen detected in the wear tracks of both as-cast and heat-treated specimens, which exists as Cr-oxide because high Cr content was also detected. Also, the wear track of as-cast specimen is found contained more oxygen than that of heat-treated one, which may be one of the reasons why as-cast specimen exhibited a better wear resistance than heat-treated one in high temperature wear.

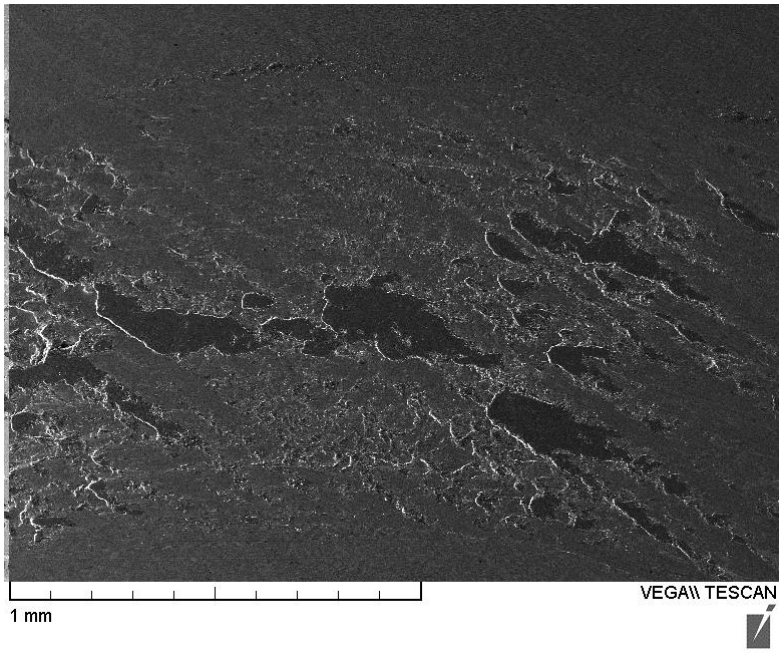

(a)

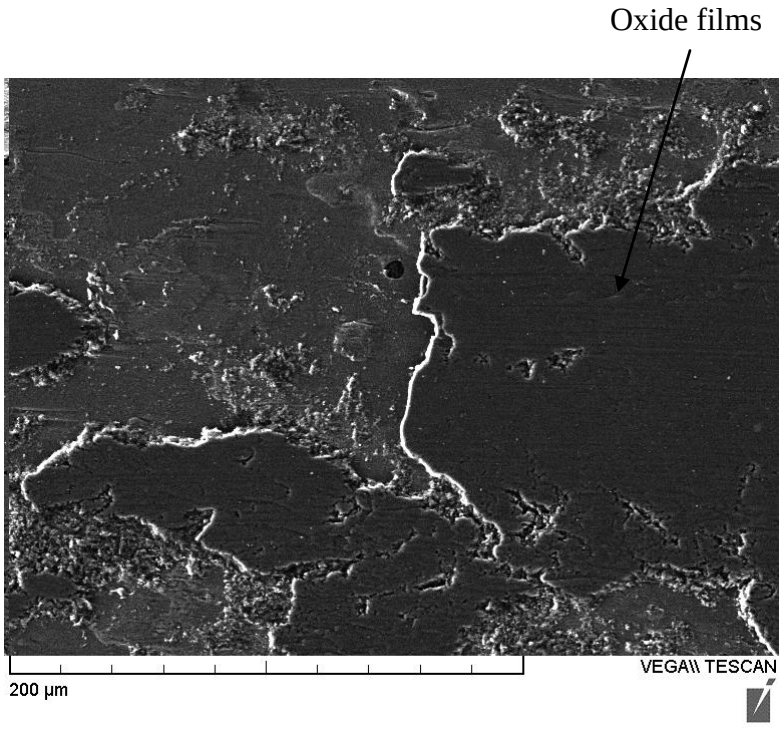

(b)

Figure 6-9: SEM images of worn surface of as-cast Stellite 22 tested at 450^{o}C:

(a) at low magnification and (b) at high magnification.

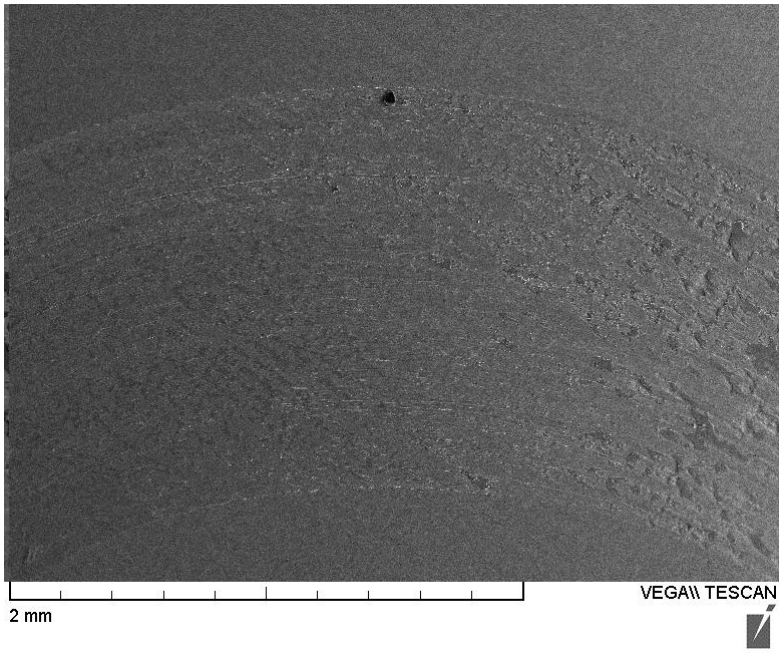

(a)

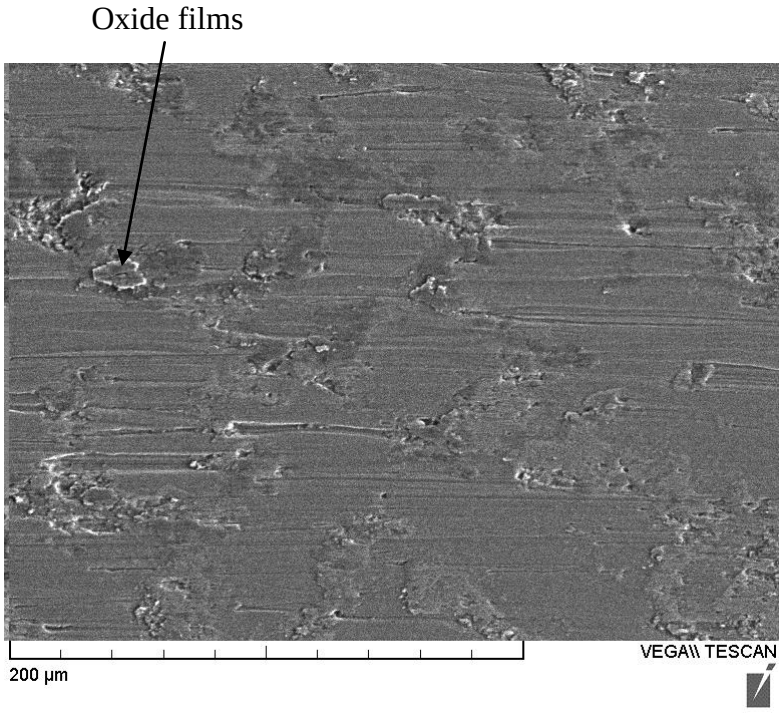

(b)

Figure 6-10: SEM images of worn surface of heat-treated Stellite 22 tested at 450°C: (a) at low magnification and (b) at high magnification.

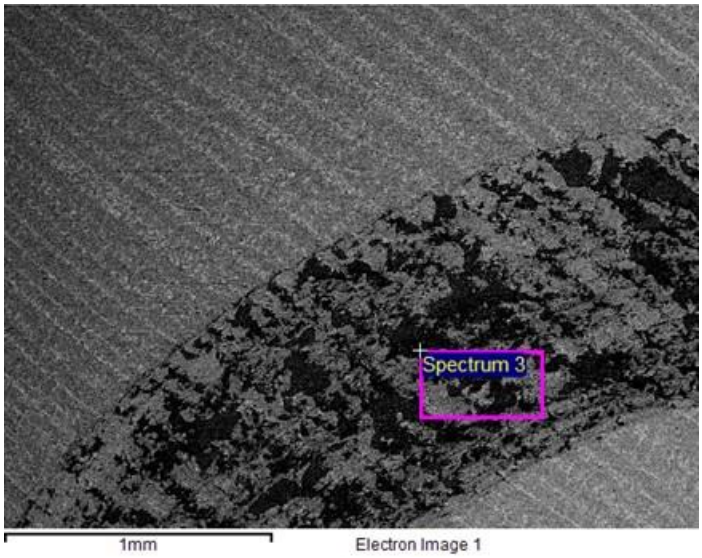

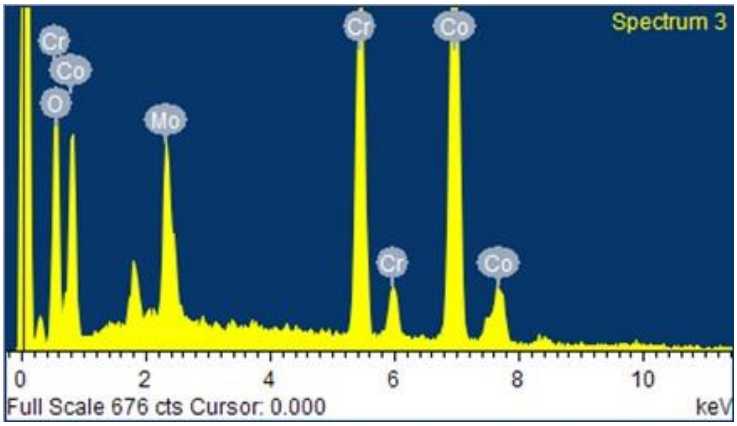

Element	Weight%	Atomic%
O K	19.58	47.78
Cr K	22.18	16.65
Co K	46.62	30.84
Mo L	11.62	4.73
Total	100.00	100.00

(a)

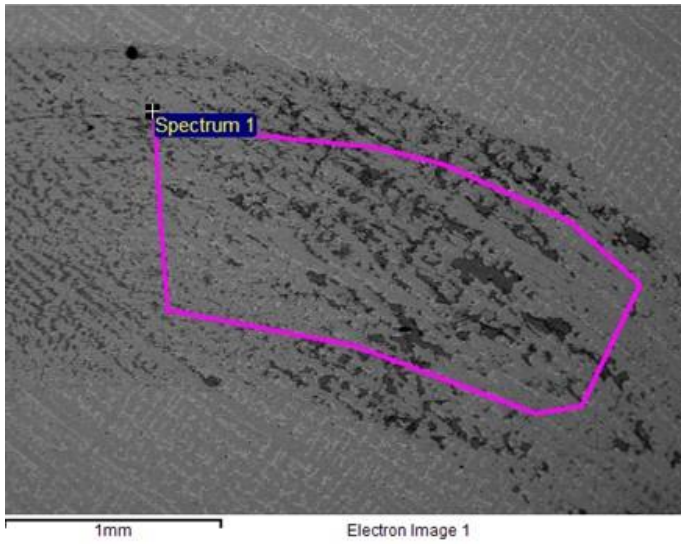

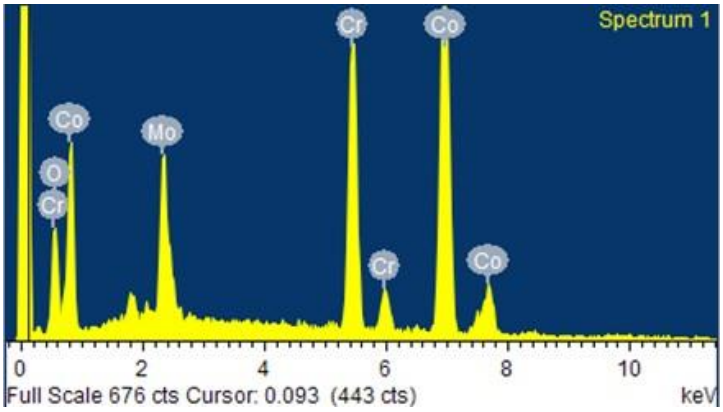

Element	Weight%	Atomic%
O K	9.61	28.69
Cr K	23.98	22.03
Co K	52.05	42.14
Mo L	14.37	7.15
Total	100.00	100.00

(b)

Figure 6-11: EDX spectra of wear track of Stellite 22 tested at 450^{o}C:

(a) as-cast and (b) heat-treated.

6.2.2 T-400C

T-400C exhibited much better wear resistance at room temperature than at elevated temperatures. The SEM images of the worn surfaces of the specimens tested at room temperature are presented in Figure 6-12 and Figure 6-13. The morphologies of the worn surfaces show that oxidation had occurred in the specimen surfaces, characterized by the oxide residuals (in white). The EDX analysis on the wear tracks has confirmed the presence of oxides, as demonstrated by the EDX spectra in Figure 6-14, high oxygen content was detected. Although the specimens were test at room temperature, since this alloy contains a large volume fraction of hard Laves phase, when the hard pin (94% WC and 6% Co, HV1534) rubbed against the specimen during the wear process, friction heat was generated between the contact surfaces, causing the local temperature rising. The Cr in the solid solution would form hard and strong Cr-oxide film that could prevent the surface from further oxidation and could also strengthen the surface for wear resistance by the “glazing” effect. However, the Laves phase may also be oxidized, forming loose and brittle silicates, which added to the wear loss of the specimen. Although oxidation occurred in the specimen surface, the main mechanism of T-400C in room temperature wear is plowing of the solid solution, also possibly accompanied with fracture of the Laves phase, as characterized by the cavities in the worn surfaces. The increased wear resistance of the heat-treated specimens was owing to the Laves phase precipitates within the solid solution, which had strengthened the solution matrix.

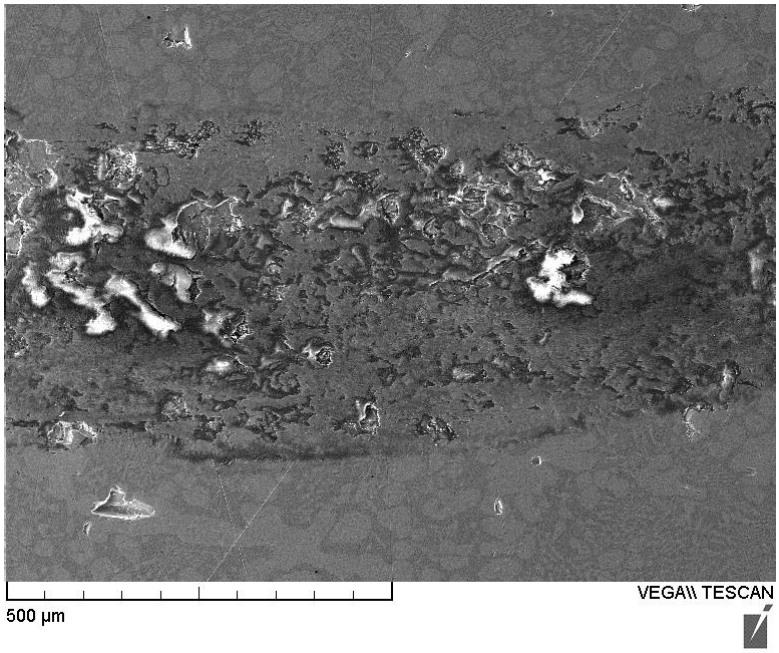

(a)

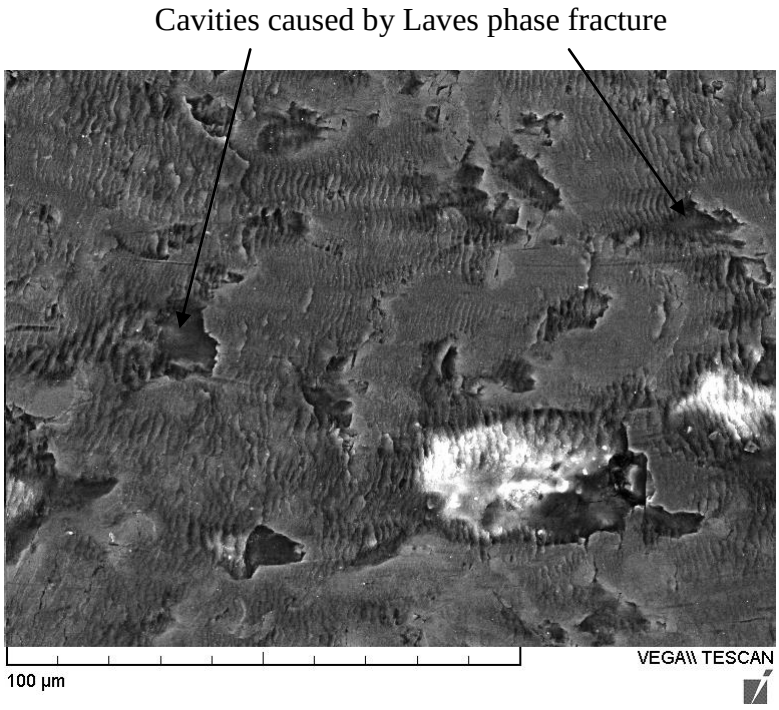

(b)

Figure 6-12: SEM images of worn surface of as-cast T-400C tested at room temperature: (a) at low magnification and (b) at high magnification.

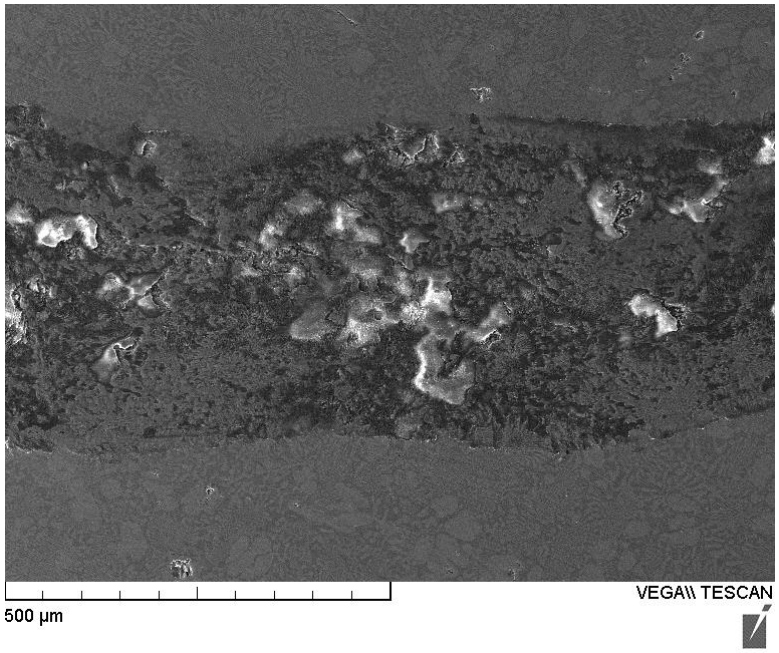

(a)

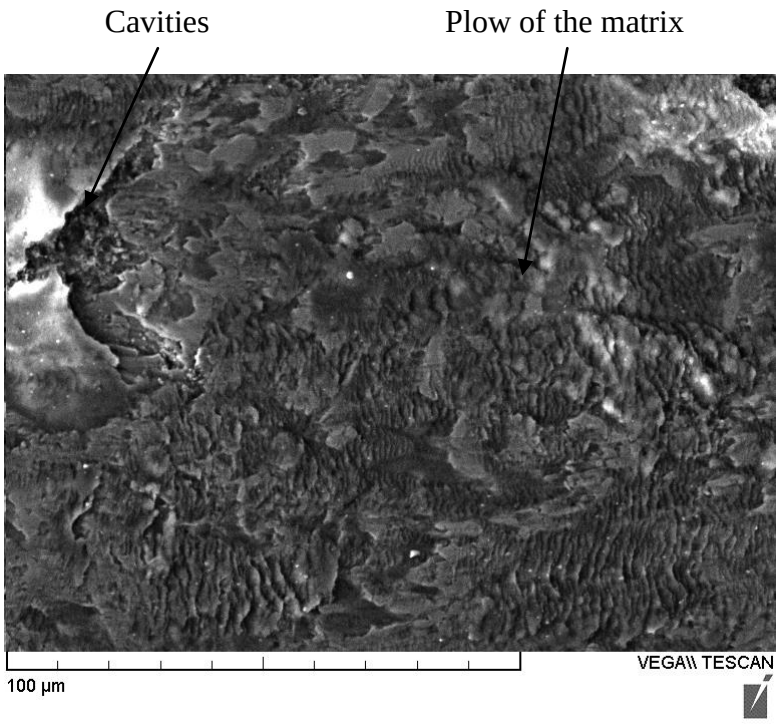

(b)

Figure 6-13: SEM images of worn surface of heat-treated T-400C tested at room temperature: (a) at low magnification and (b) at high magnification.

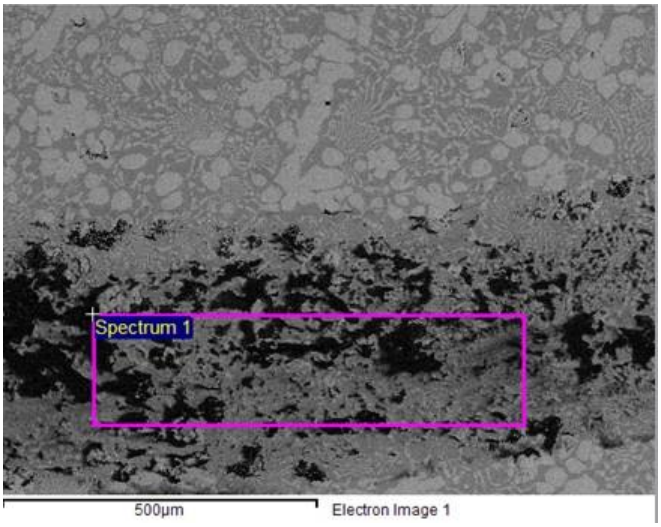

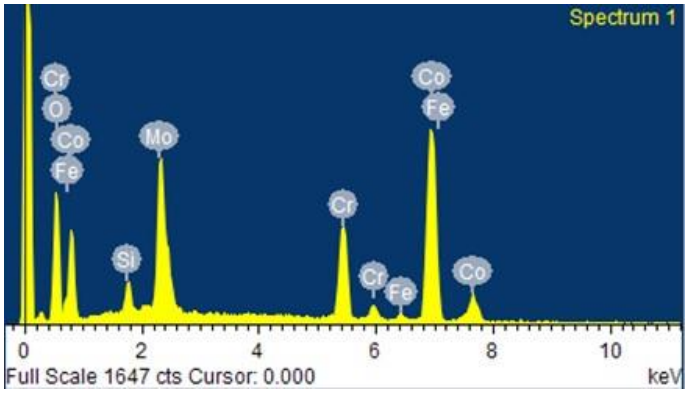

Element	Weight%	Atomic%
O K	22.62	53.29
Si K	1.58	2.13
Cr K	11.93	8.65
Fe K	1.08	0.73
Co K	42.86	27.38
Mo L	19.92	7.82
Total	100.00	100.00

(a)

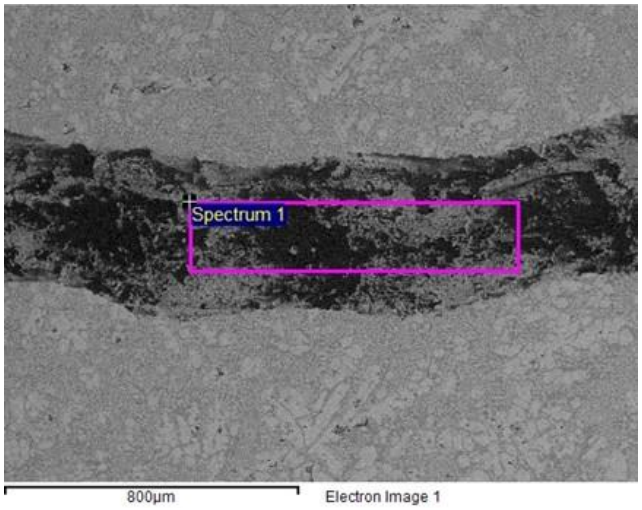

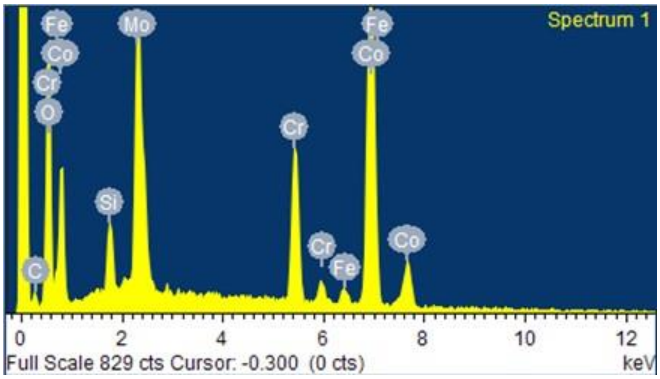

Element	Weight%	Atomic%
O K	27.43	59.48
Si K	1.98	2.45
Cr K	10.14	6.77
Fe K	1.49	0.92
Co K	39.98	23.51
Mo L	18.99	6.87
Total	100.00	100.00

(b)

Figure 6-14: EDX spectra of weak track of T-400C tested at room temperature:

(a) as-cast and (b) heat-treated.

At the elevated temperature of 250°C, the wear resistance T-400C decreased significantly. Unlike the worn surfaces of the specimens tested at room temperature, the morphologies of the worn surfaces of the specimens tested at 250°C look very smooth, and also do not show any oxides, see Figure 6-15 and Figure 6-16. The EDX analysis on the wear tracks also confirmed that no oxygen was detected. However, at 250°C T-400C should be oxidized, in particular, friction heat would promote the temperature rising. It can be inferred that both the Laves phase and solid solution were oxidized during the wear test in the 250°C environment; resulting in loose/brittle silicates and hard/strong Cr-oxides, respectively. As the size and the amount of the Laves phase were both large in this alloy, the Cr-oxides must be less in amount and small in size. Therefore, under the mechanical attack due to wear, these oxides were vulnerable. In the meanwhile, the hardness of both the solid solution and Laves phase was decreased at 250°C, which degraded the wear resistance of this alloy. All the above mentioned factors would lead to the increased wear loss, while the removal of the silicates and oxides, along with scraping off the surface material rendered the worn surfaces smoother. The heat treatment benefited the wear resistance of T-400C at both room temperature and elevated temperatures. This is all owing to the Laves phase precipitates in the solid solution. No noticeable difference in worn surface morphology was found between the as-cast and heat-treated specimens.

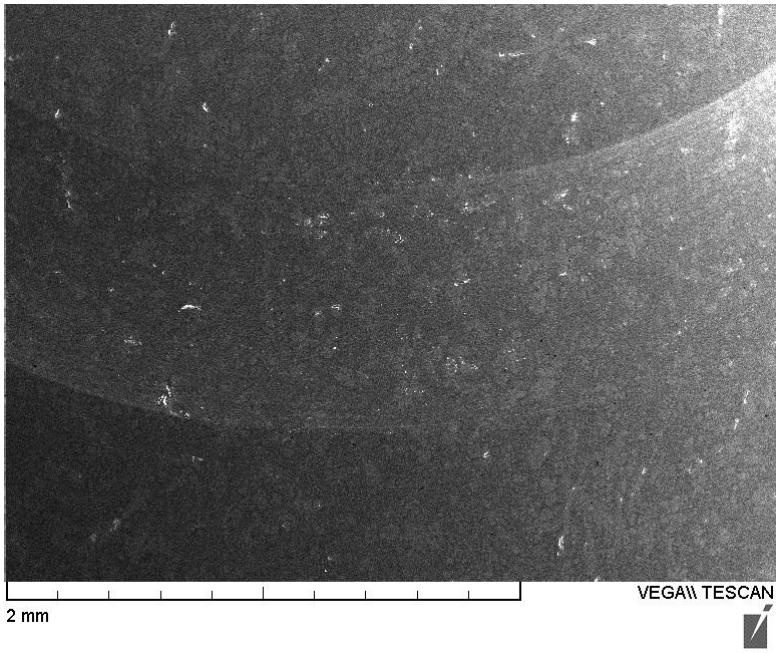

(a)

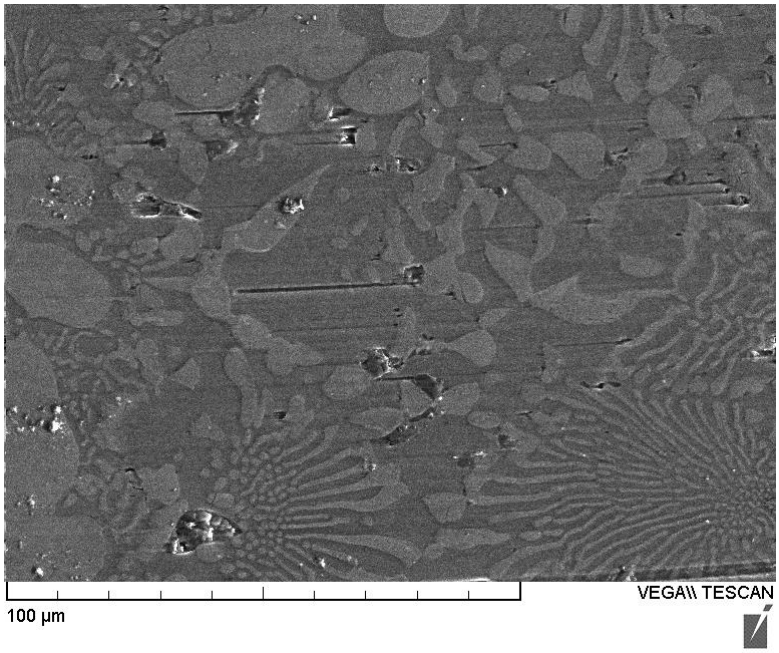

(b)

Figure 6-15: SEM images of worn surface of as-cast T-400C tested at 250°C:

(a) at low magnification and (b) at high magnification.

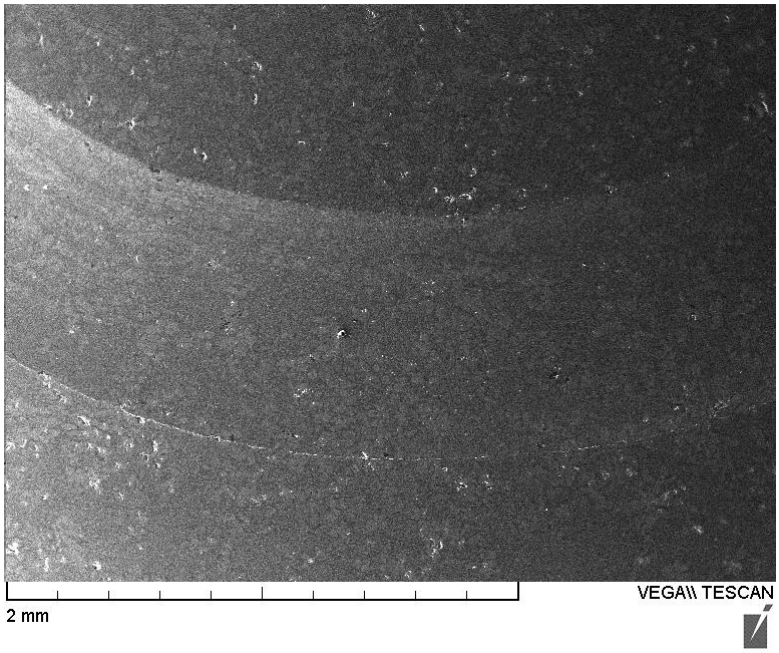

(a)

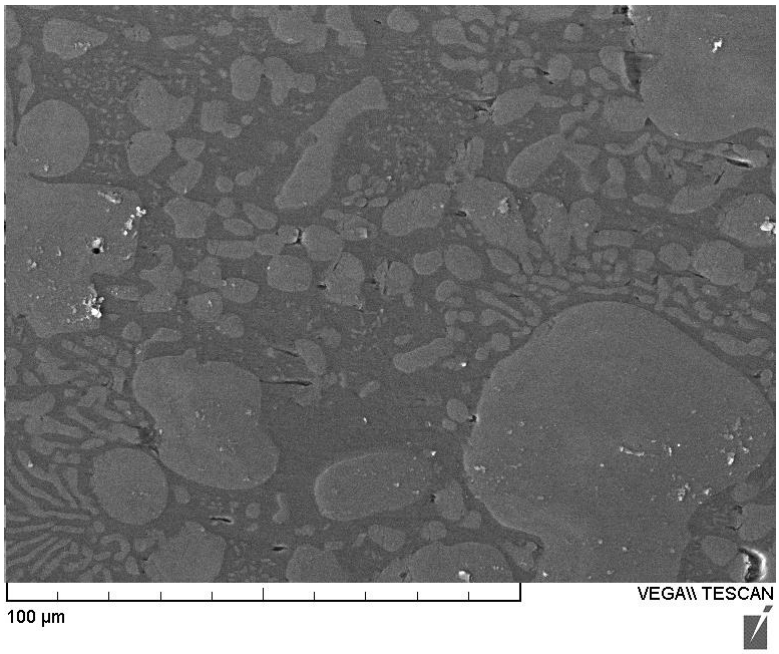

(b)

Figure 6-16: SEM images of worn surface of heat-treated T-400C tested at 250^{o}C: (a) at low magnification and (b) at high magnification.

With specimen temperature further raising to 450^{o}C, the wear losses of the T-400C specimens were reduced, compared with those at 250^{o}C, as illustrated in Figure 6-2. The worn surface morphologies of this alloy tested at these two elevated temperatures are quite different. As shown in Figure 6-17 and Figure 6-18, severe oxidation had occurred in the worn surfaces during the wear test; a large amount of oxide residuals were found in the surfaces. The EDX spectra, shown in Figure 6-19, reveal the presence of very high oxygen content in the wear tracks. At this high temperature, the hardness of both the solid solution and Laves phase continuously decreased, as demonstrated in the microhardness test; concurrently the high temperature promoted the oxidation of both the phases, resulting in a large amount of Cr-oxide and silicates. These oxidation products would be broken due to the wear attack; some of the hard Cr-oxides may be squeezed into the specimen surface layer, which enhanced the wear resistance. The morphologies of the worn surfaces of as-cast and heat-treated T-400C tested at 450^{o}C look the same so that their wear mechanisms may be similar.

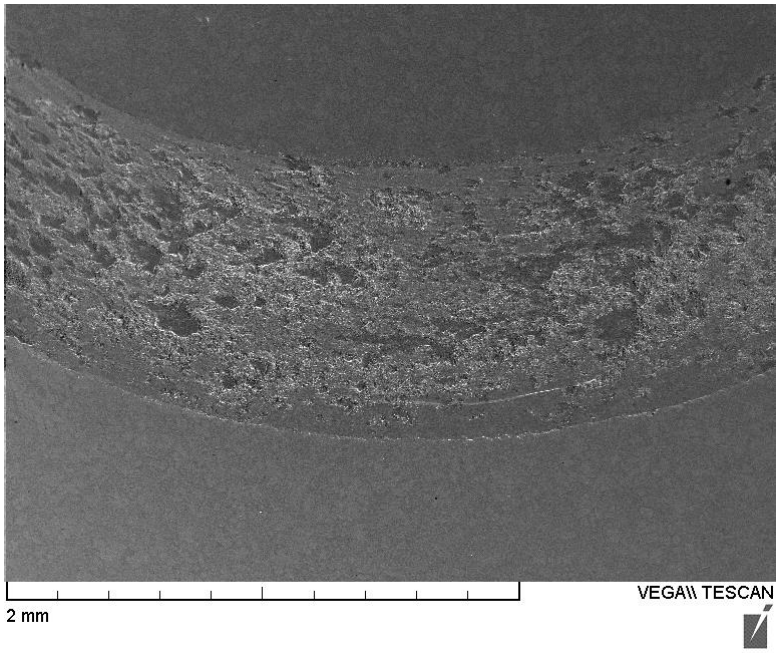

(a)

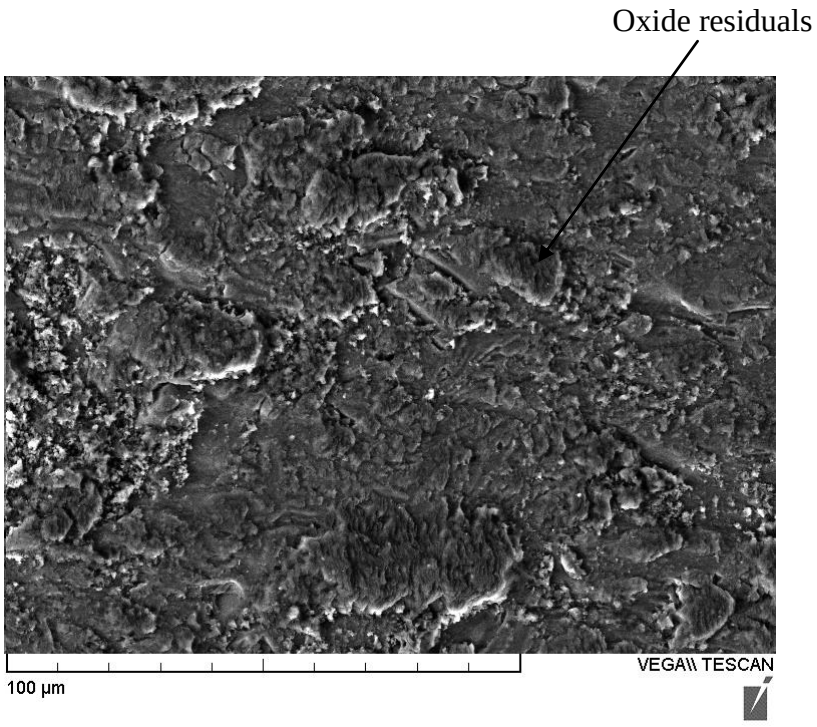

(b)

Figure 6-17: SEM images of worn surface of as-cast T-400C tested at 450^{o}C:

(a) at low magnification and (b) at high magnification.

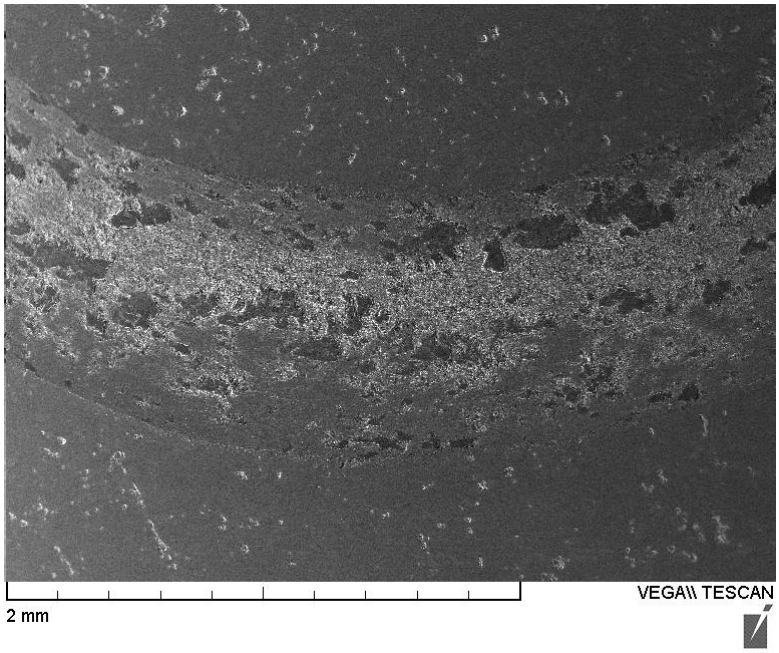

(a)

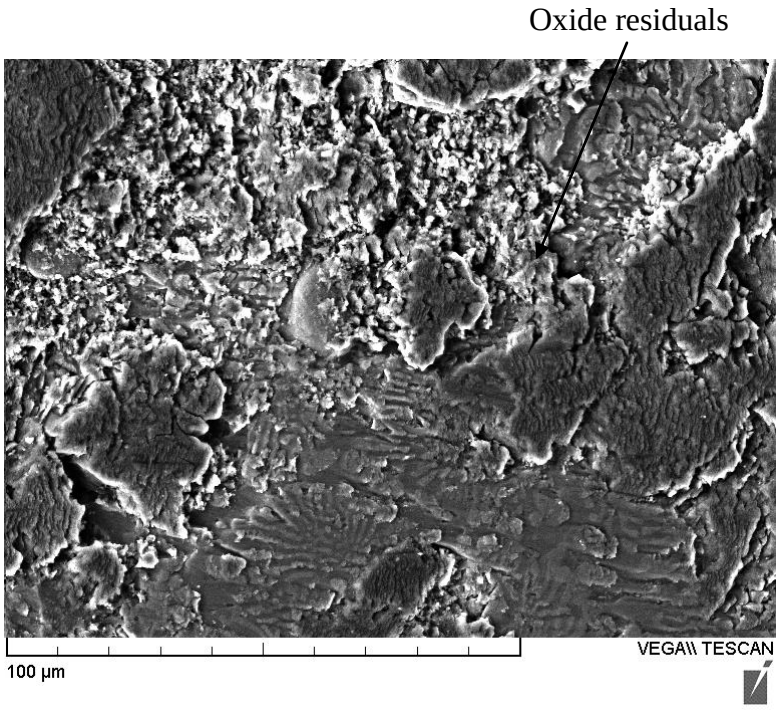

(b)

Figure 6-18: SEM images of worn surface of heat-treated T-400C tested at 450°C: (a) at low magnification and (b) at high magnification.

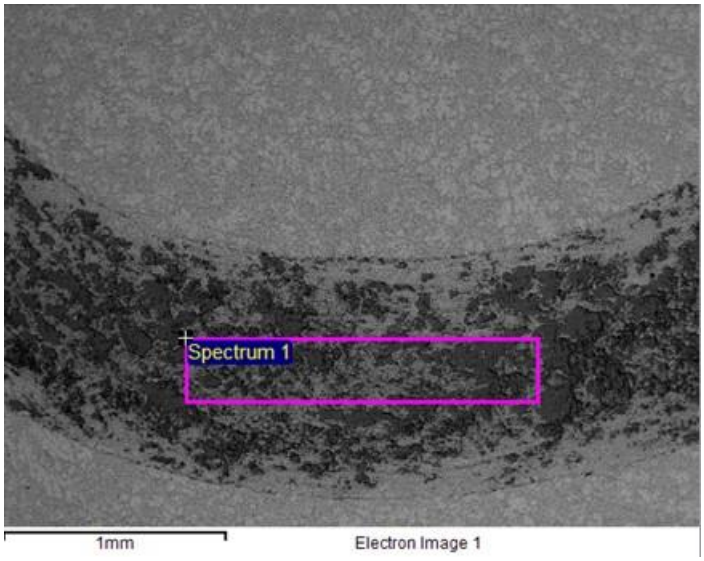

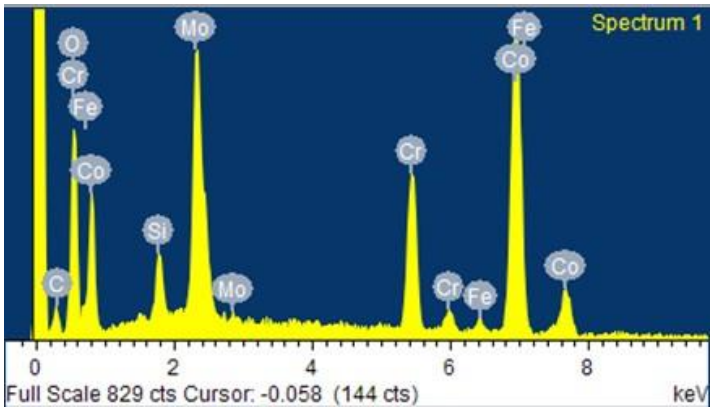

Element	Weight%	Atomic%
O K	24.93	56.38
Si K	1.71	2.21
Cr K	11.47	7.98
Fe K	0.84	0.54
Co K	41.78	25.62
Mo L	19.26	7.26
Total	100.00	100.00

(a)

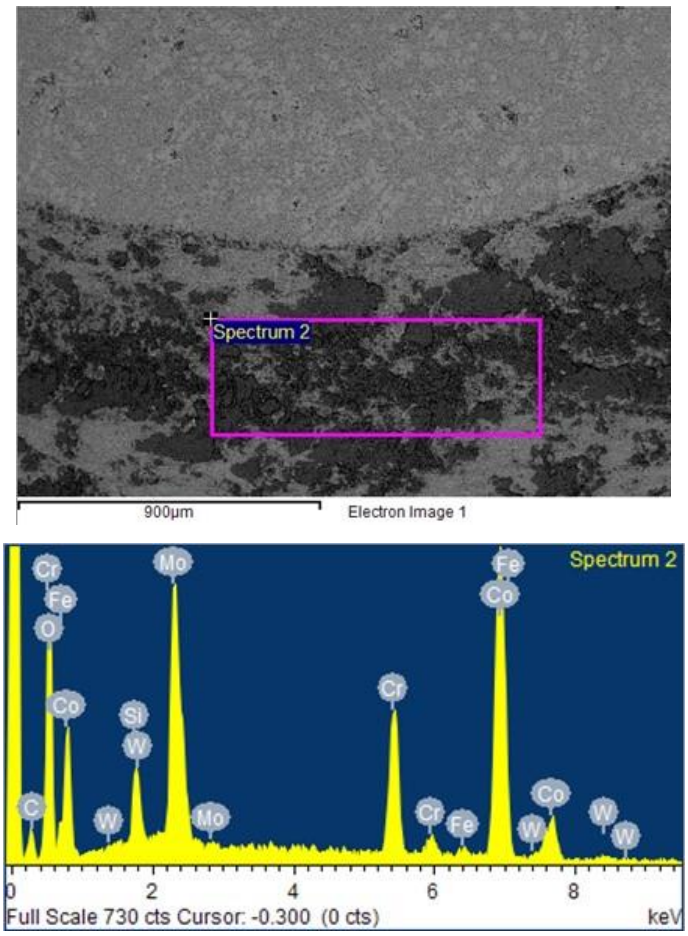

Element	Weight%	Atomic%
O K	28.52	60.88
Si K	1.68	2.06
Cr K	10.61	6.97
Fe K	0.86	0.52
Co K	39.55	22.89
Mo L	18.78	6.68
Total	100.00	100.00

(b)

Figure 6-19: EDX spectra of wear track of T-400C tested at 450^{o}C: (a) as-cast and (b) heat-treated.

6.2.3 AISI 420

The SEM microstructural analysis has shown the significant change in microstructure of AISI 420 after the heat treatment. Accordingly, the wear test demonstrated the great difference in wear resistance at room temperature between the as-wrought and heat-treated specimens, as illustrated in Figure 6-3. Reviewing the worn surface morphologies in Figure 6-20 and Figure 6-21, it is found that both the specimens suffered oxidation during the wear test; the oxide residuals can be observed clearly in the surfaces; and can also be confirmed by the EDX spectra in Figure 6-22, which show high oxygen content in the wear tracks. The temperature that caused oxidation occurrence was a result of friction heating at the contact surfaces. The oxidation products in the alloy surfaces can be Cr-oxide films from solution matrix and brittle and loose carbonates from the carbides. More severe oxide film fracture and more oxide residuals were found in the heat-treated specimen than in the as-wrought specimens, which may be the reason for the higher wear loss.

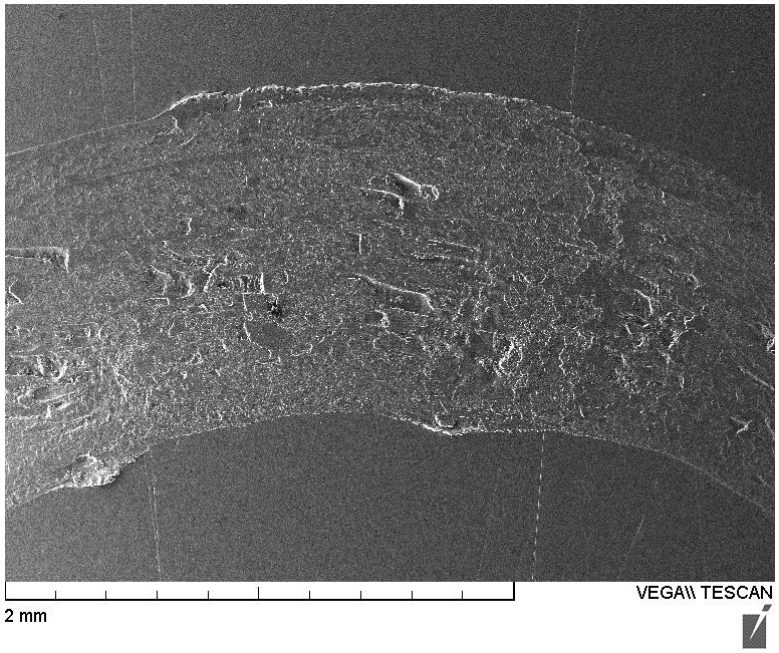

(a)

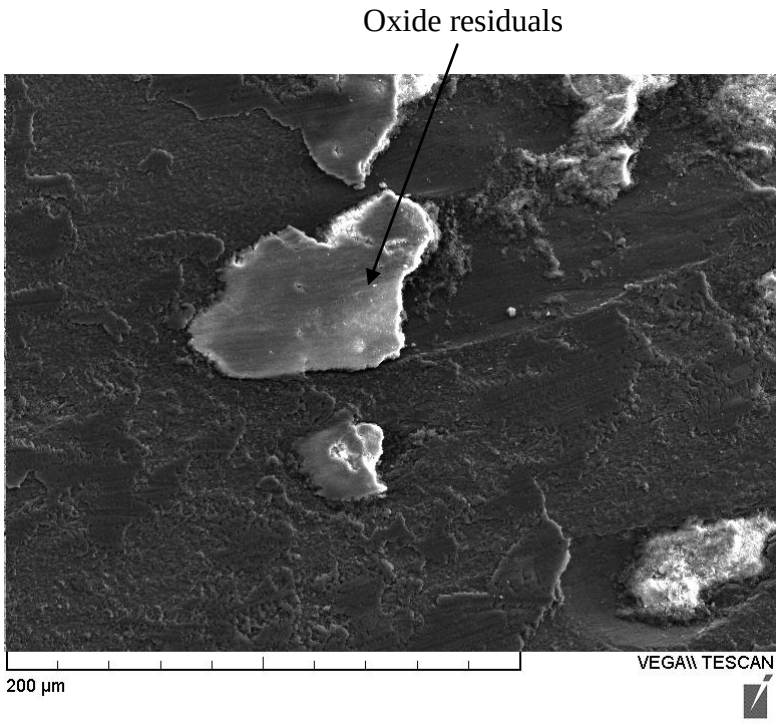

(b)

Figure 6-20: SEM images of worn surface of as-wrought AISI 420 tested at room temperature: (a) at low magnification and (b) at high magnification.

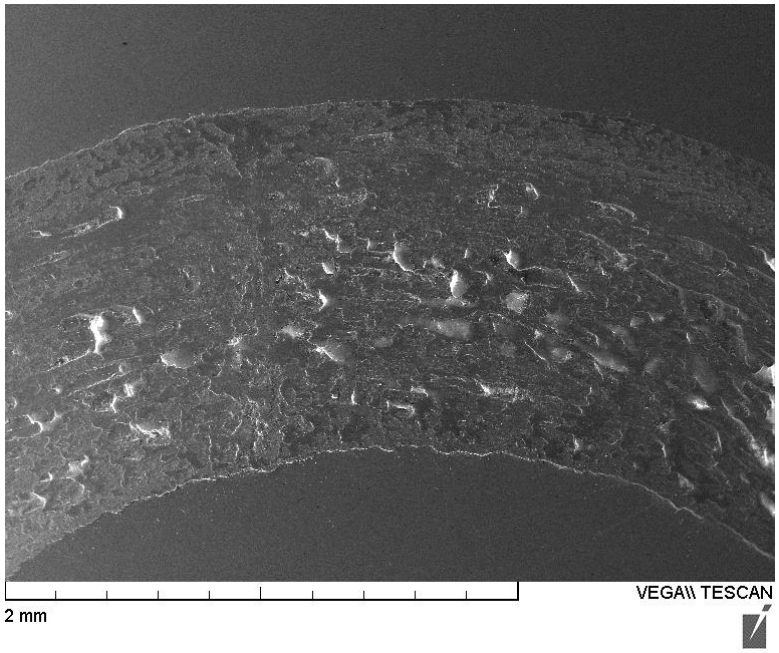

(a)

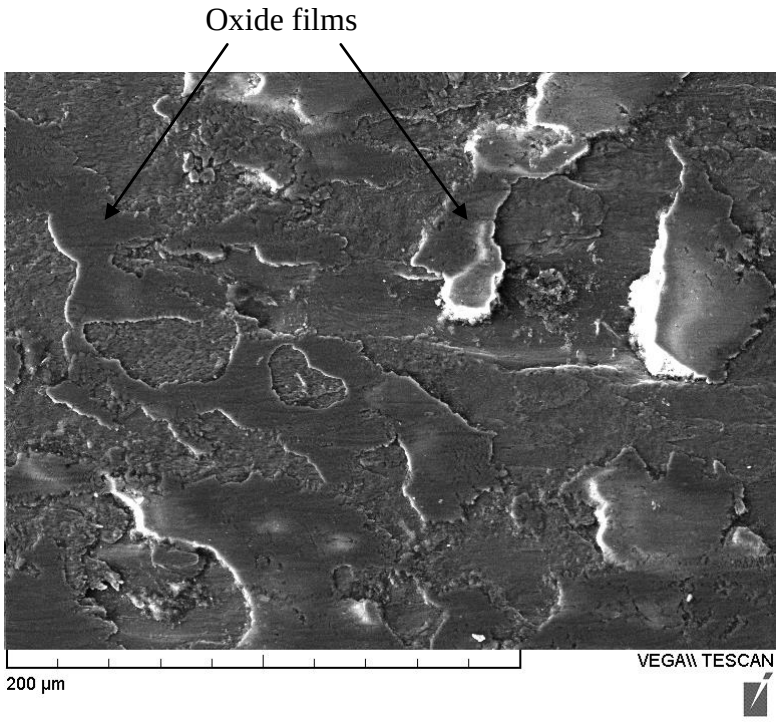

(b)

Figure 6-21: SEM images of worn surface of heat-treated AISI 420 tested at room temperature: (a) at low magnification and (b) at high magnification.

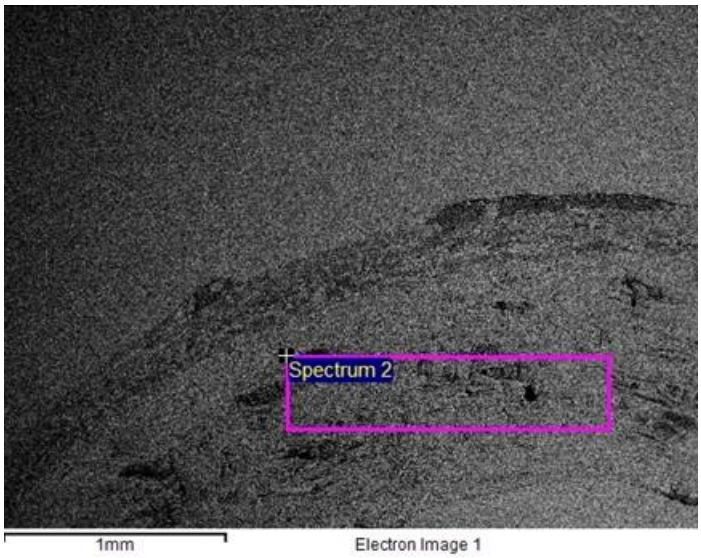

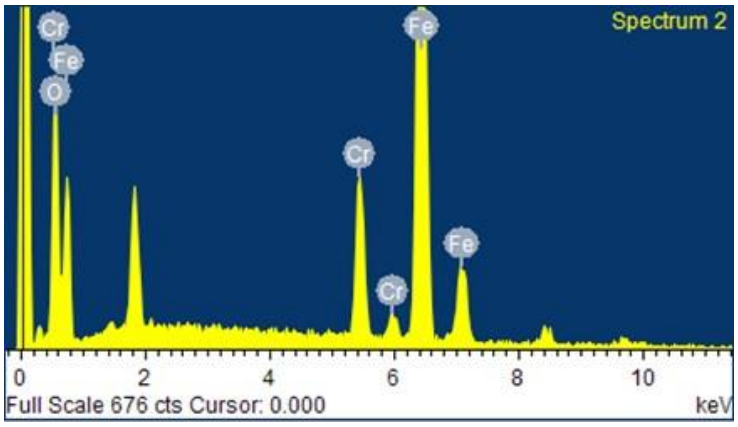

Element	Weight%	Atomic%
O K	15.22	38.34
Cr K	11.49	8.91
Fe K	73.29	52.75
Total	100.00	100.00

(a)

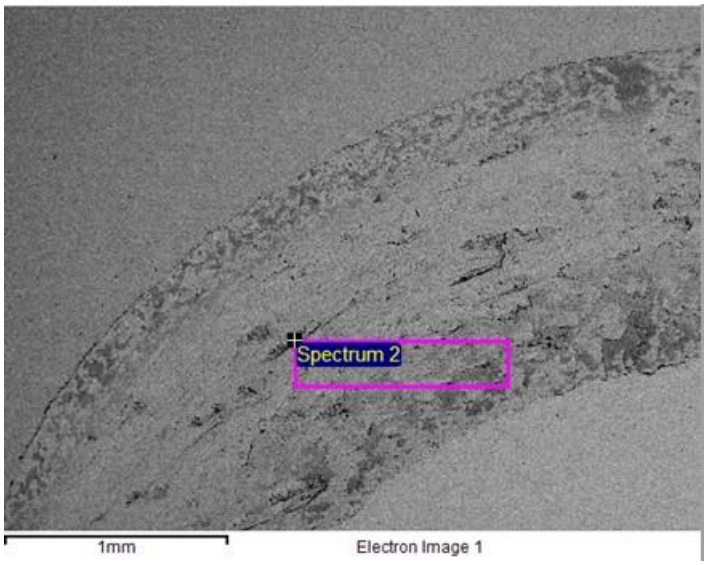

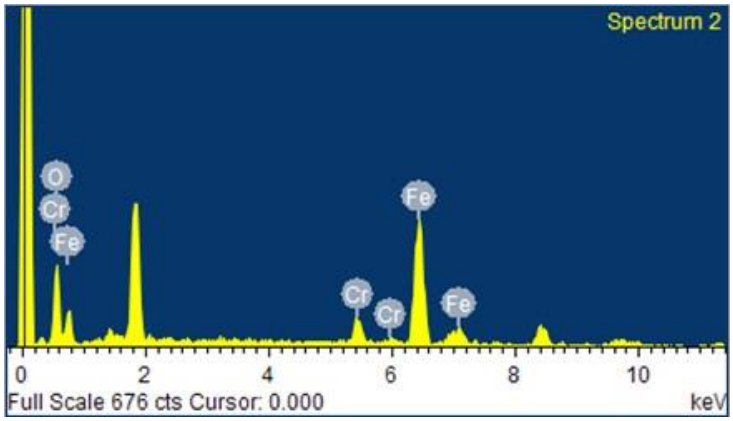

Element	Weight%	Atomic%
O K	20.81	47.64
Cr K	10.83	7.63
Fe K	68.36	44.73
Total	100.00	100.00

(b)

Figure 6-22: EDX spectra of wear tracks of AISI 420 tested at room temperature:

(a) as-wrought and (b) heat-treated.

At the elevated temperature of 250^{o}C, severe oxidation occurred in both the specimen surfaces, as shown in Figure 6-23 and Figure 6-24. The EDX spectra of the wear tracks in Figure 6-25 are consistent with the observation; very high oxygen content was detected in the wear tracks. In addition, the wear track in the as-wrought specimen surface is obviously wider than that in the heat-treated one. The wear resistance of these two specimens is close at this temperature. This implies that the wear loss of this alloy at elevated temperatures was mainly caused by material oxidation; that is, the wear behavior of the microstructure itself was less important. Further confirmation can be obtained from the wear behavior of this alloy at 450^{o}C. As illustrated in Figure 6-3, the wear losses of as-wrought AISI 420 and heat-treated AISI 420 at 450^{o}C are nearly the same. Their worn surfaces contain heavy oxidation products, as shown in Figure 6-26 and Figure 6-27. The EDX spectra in Figure 6-28 show very high oxygen content in the wear tracks. The great reduction in wear loss of this alloy at elevated temperatures was owing to the "glazing" effect. The large amount of Cr-oxide was formed during the wear process; in the meanwhile, the alloy was softer at elevated temperatures, which resulted in a case that oxide debris was embedded into the specimen surface thus enhancing its wear resistance. Although the microstructures of as-wrought AISI 420 and heat-treated AISI 420 are quite different, the high temperatures promoted formation of large amounts of oxides in the specimen surface, which dominated the wear process.

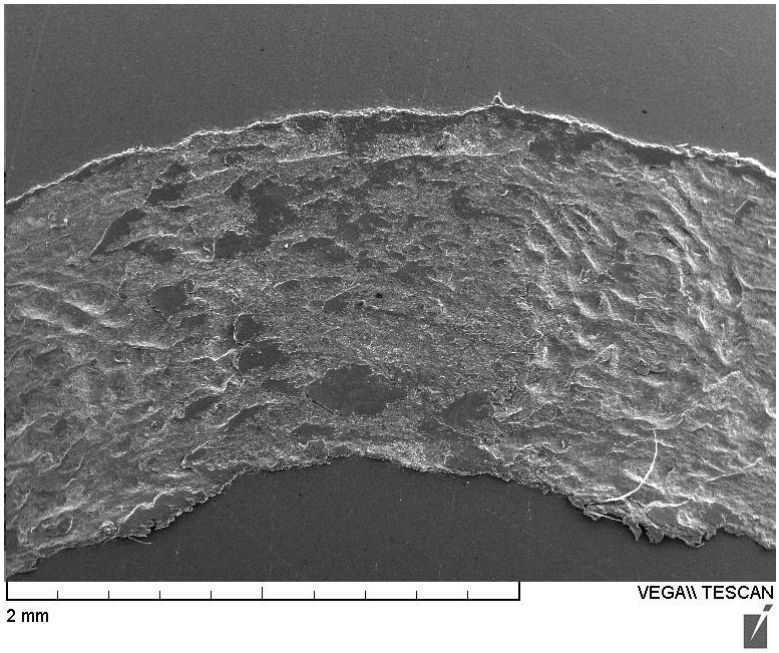

(a)

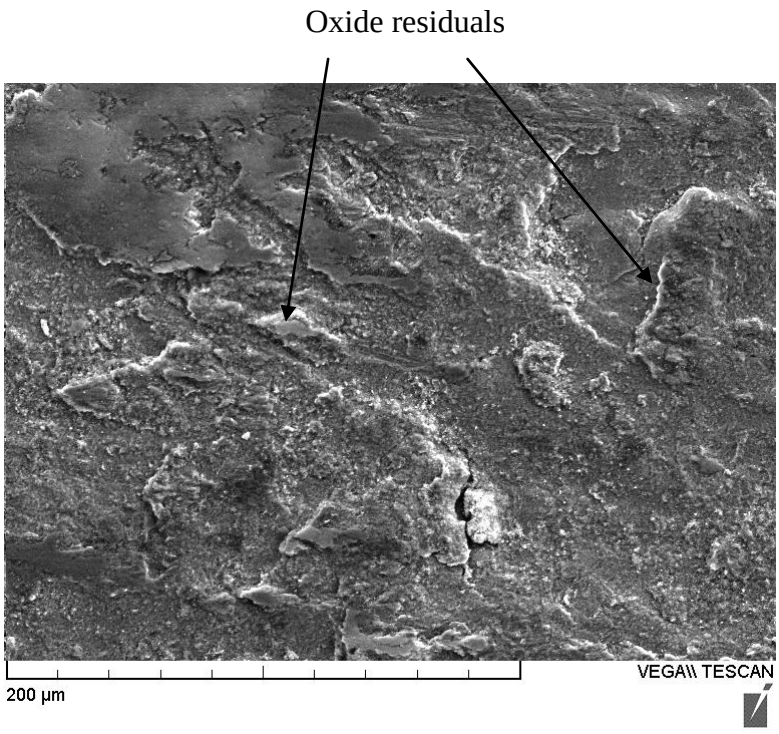

(b)

Figure 6-23: SEM images of worn surface of as-wrought AISI 420 tested at 250^{o}C: (a) at low magnification and (b) at high magnification.

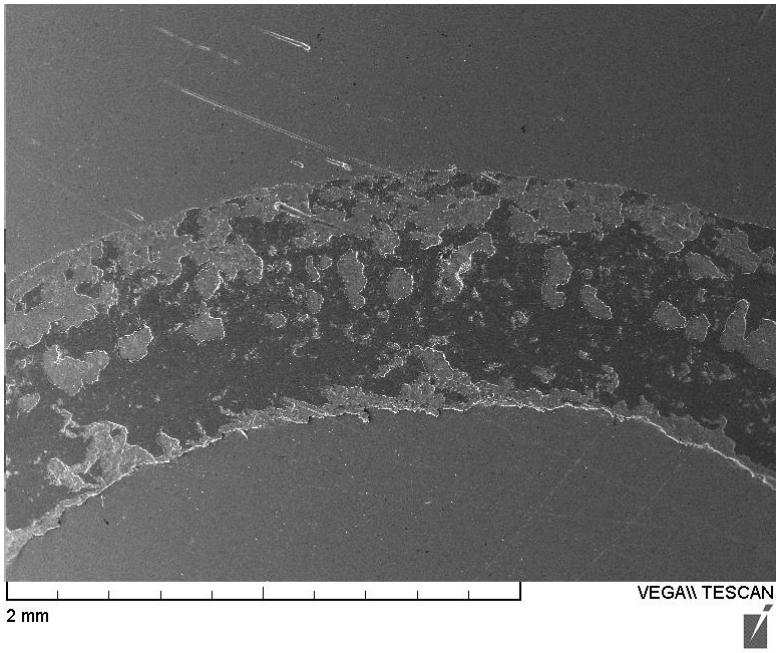

(a)

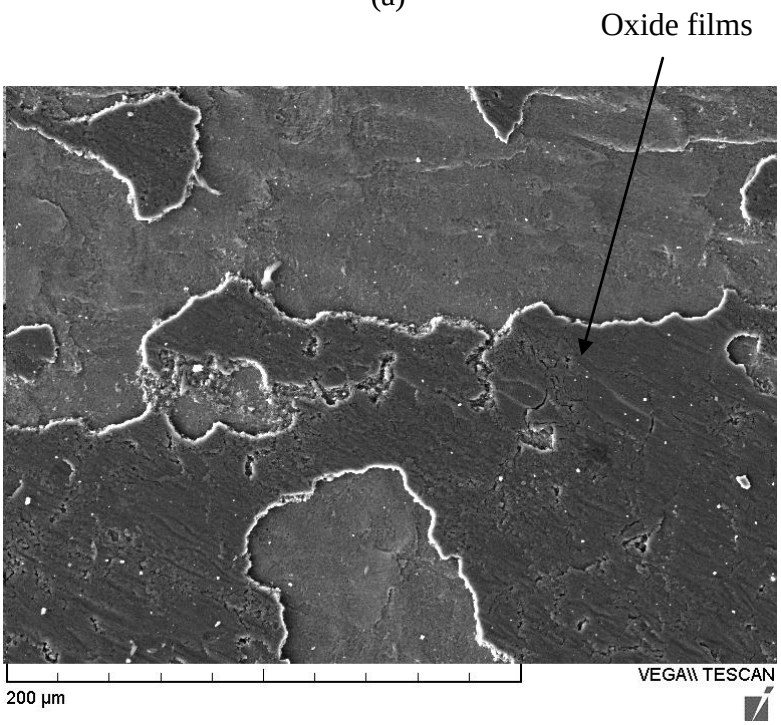

(b)

Figure 6-24: SEM images of worn surface of heat-treated AISI 420 tested at 250^{o}C: (a) at low magnification and (b) at high magnification.

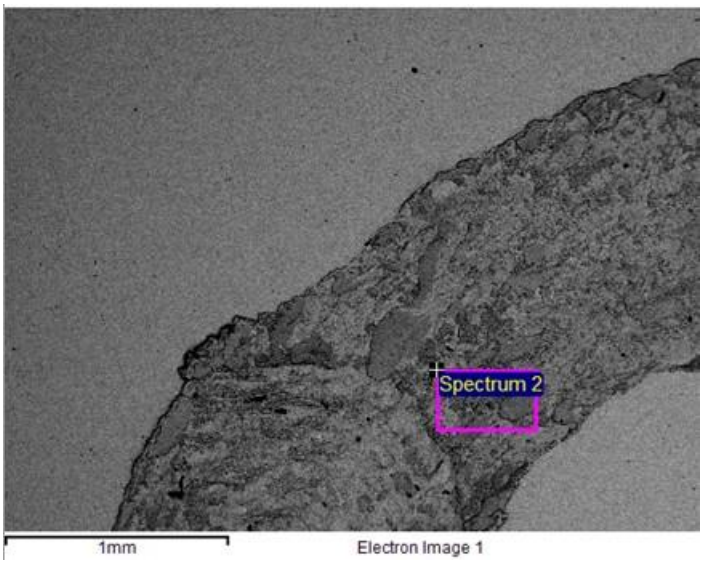

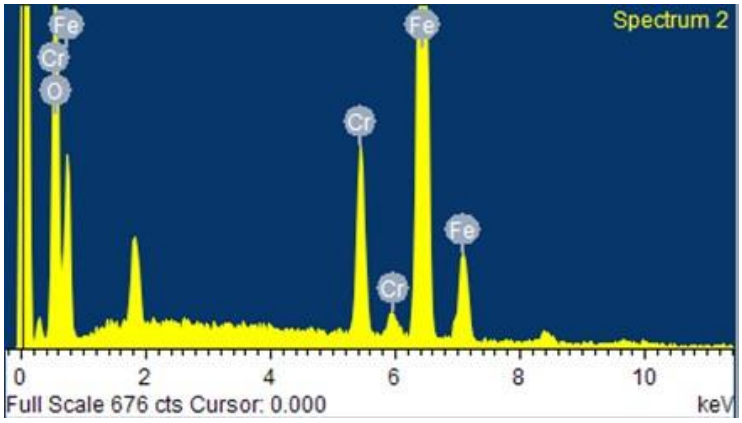

Element	Weight%	Atomic%
O K	27.43	56.68
Cr K	10.23	6.51
Fe K	62.34	36.81
Total	100.00	100.00

(a)

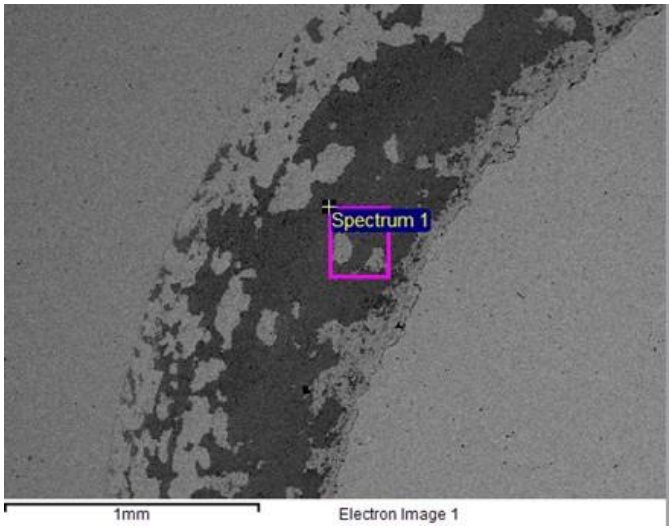

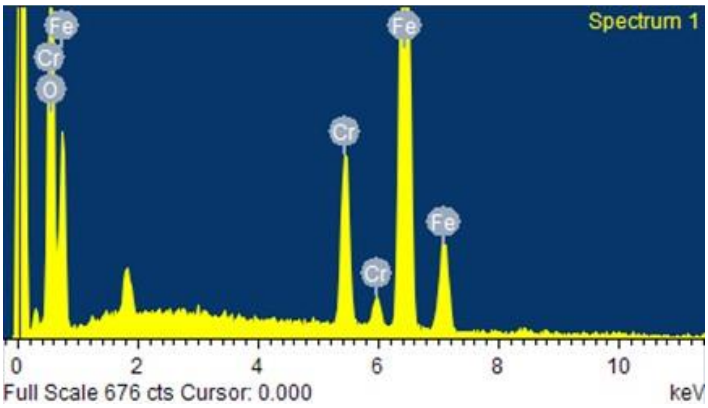

Element	Weight%	Atomic%
O K	29.69	59.40
Cr K	9.44	5.81
Fe K	60.87	34.79
Total	100.00	100.00

(b)

Figure 6-25: EDX spectra of wear track of AISI 420 tested at 250^{o}C:

(a) as-wrought and (b) heat-treated.

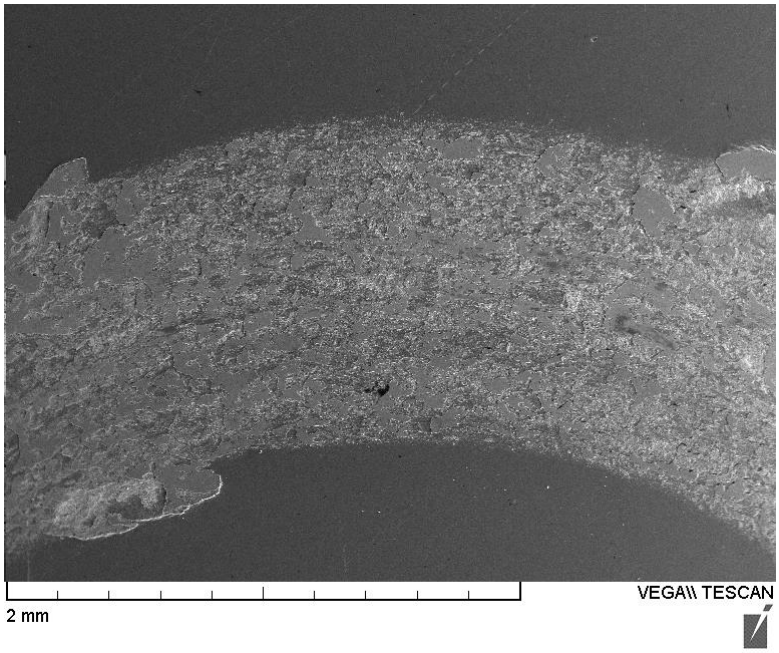

(a)

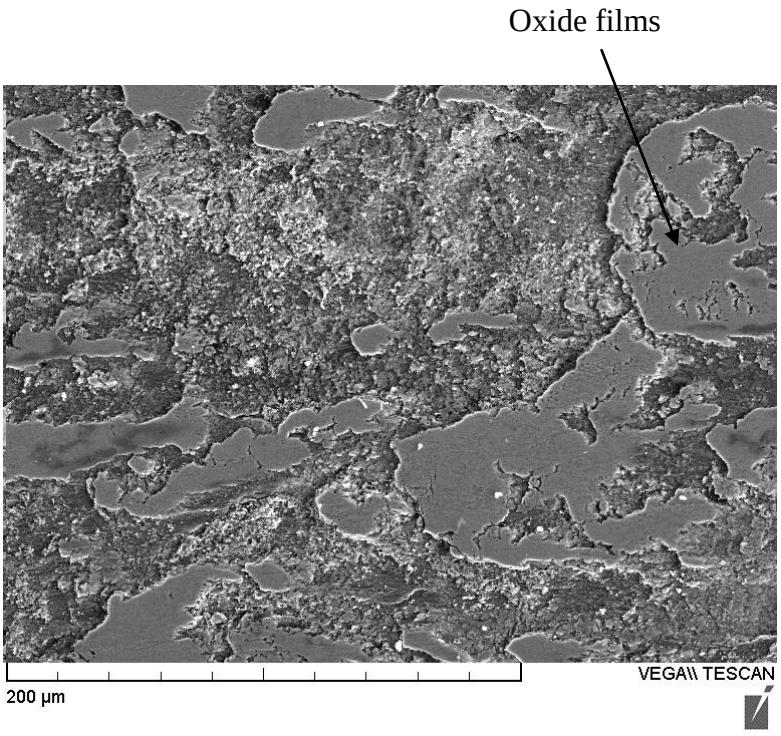

(b)

Figure 6-26: SEM images of worn surface of as-cast AISI 420 tested at 450^{o}C:

(a) at low magnification and (b) at high magnification.

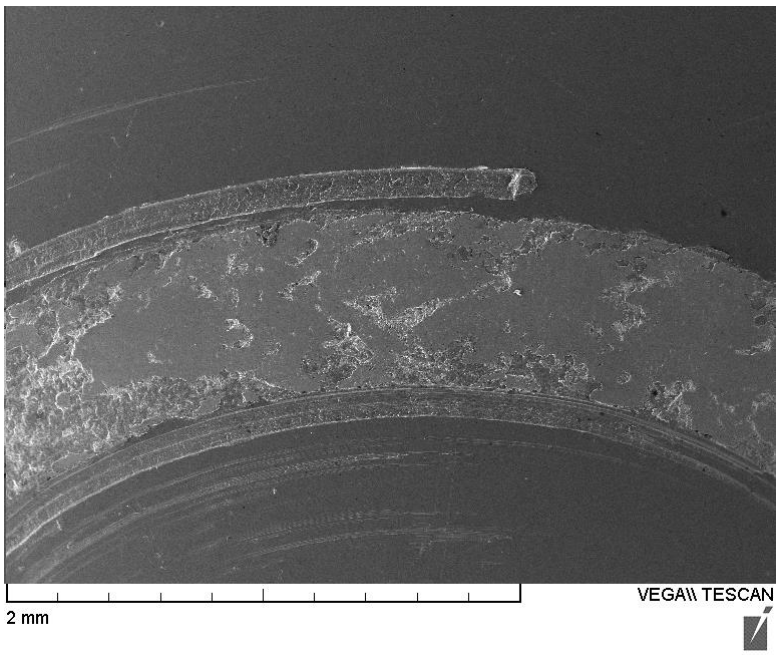

(a)

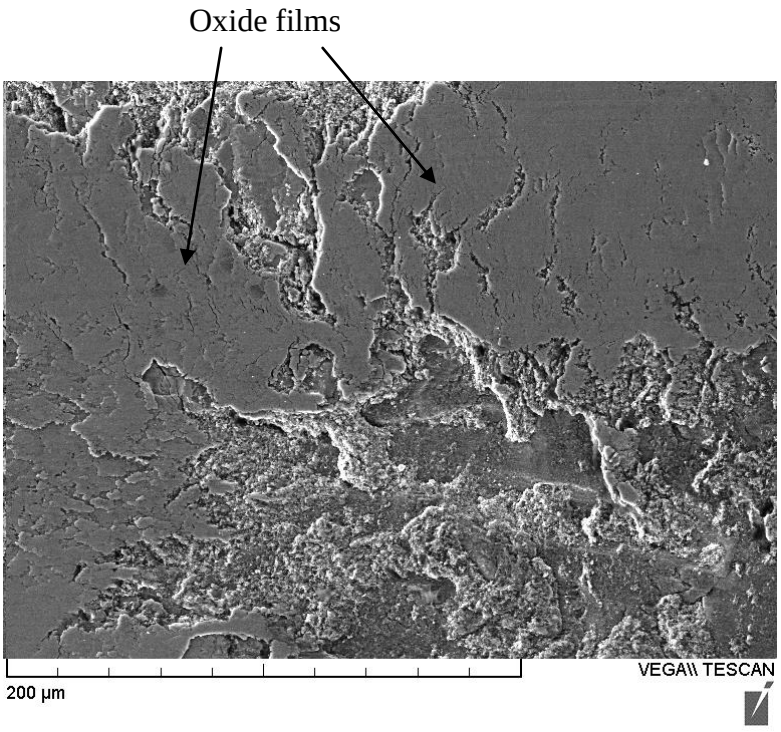

(b)

Figure 6-27: SEM images of worn surface of heat-treated AISI 420 tested at 450^{o}C:

(a) at low magnification and (b) at high magnification.

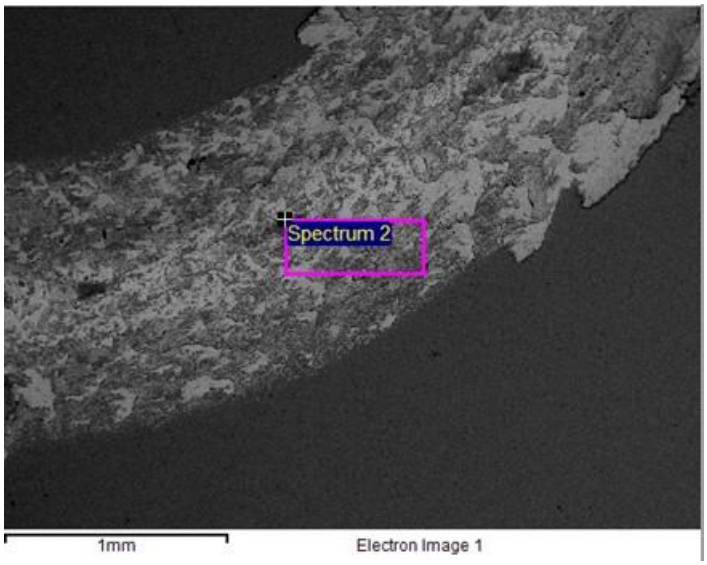

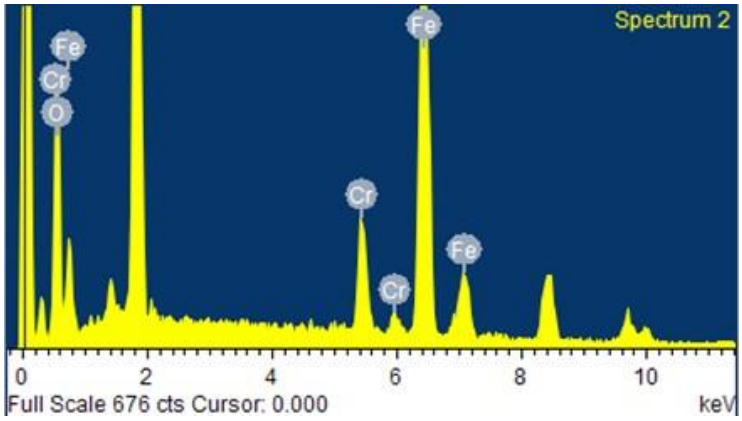

Element	Weight%	Atomic%
O K	33.73	63.79
Cr K	9.55	5.56
Fe K	56.72	30.65
Total	100.00	100.00

(a)

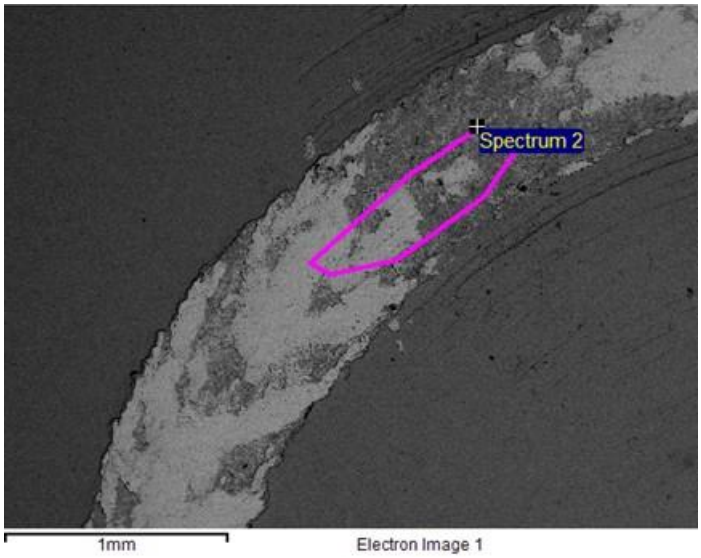

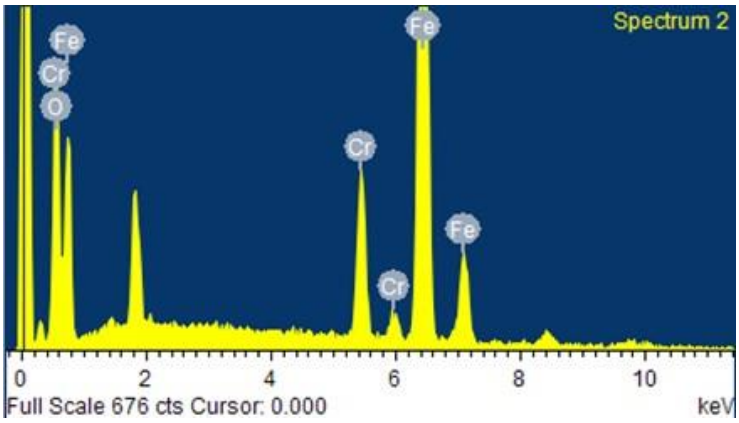

Element	Weight%	Atomic%
O K	35.76	65.86
Cr K	8.22	4.66
Fe K	56.01	29.48
Total	100.00	100.00

(b)

Figure 6-28: EDX spectra of wear track of AISI 420 tested at 450^{o}C:

(a) as-wrought and (b) heat-treated.

6.2.4 AISI 440C

The heat treatment did not induce any phase transformations in AISI 440C, but it caused slight increase in carbide volume fraction, as analyzed previously. These additional carbides enhanced the wear resistance of this alloy, as illustrated in Figure 6-4. The worn surfaces of as-wrought and heat-treated AISI 440C tested at room temperature and at elevated temperatures have a similar morphology, as shown in Figure 6-29 to Figure 6-34. The main characteristic of the morphology is the surfaces partially covered with oxide residuals, which indicates that oxidation had occurred in the surfaces during the wear tests and the amount of the oxides formed on the surfaces increased with the temperature. EDX analysis was performed on the wear tracks of each specimen and the spectra are presented in Figure 6-35 to Figure 6-37. It is shown the presence of a high level of oxygen in all the wear tracks, in particular, in the wear tracks from the high temperature (450^{o}C) wear test, very high oxygen content was detected.

Different from AISI 420, the elevated temperature of 250^{o}C aggravated the wear loss of AISI 440C. The main reason for this can be the difference in chromium and molybdenum content between these two alloys. Since AISI 440C contains much higher chromium and molybdenum content than AISI 420, it exhibits a much better oxidation resistance. Therefore less oxide films are formed on the specimen of AISI 440C. On the other hand, due to the larger volume fraction of carbides, less ferrite solution is in the microstructure of AISI 440C, thus there would be less area that can be strengthen by the "glazing" effect, because the oxide debris can only be squeezed into the soft solution matrix but not the carbides. Finally, at the elevated temperature, the overall hardness of AISI 440C was decreased, which may also be a

factor influencing the wear resistance.

At the high temperature of 450^{o}C, similar to AISI 420, both as-wrought and heat-treated AISI 440C specimens became more resistant to wear, as shown in Figure 6-4; the wear losses of the specimens at 450^{o}C are even less than those of the specimens at room temperature. It is believed that the enhanced wear resistance resulted from the "glazing" effect, as seen in the worn surface morphologies in Figure 6-33 and Figure 6-34, some areas of the wear tracks are glazing glossy. This is because the high temperature promoted Cr-oxide formation, which provided more chances for the "glazing" strengthening of the surfaces. In the meanwhile, the strengthened surfaces with oxide debris embedded could suppress further oxidation thus lead to reduced wear loss. As mentioned previously, when oxidation occurred heavily, the microstructure of the alloy had little effect on the wear behavior; therefore the heat treatment influence was less important. At this temperature, the wear loss of the specimen was mainly determined by the properties of oxide films.

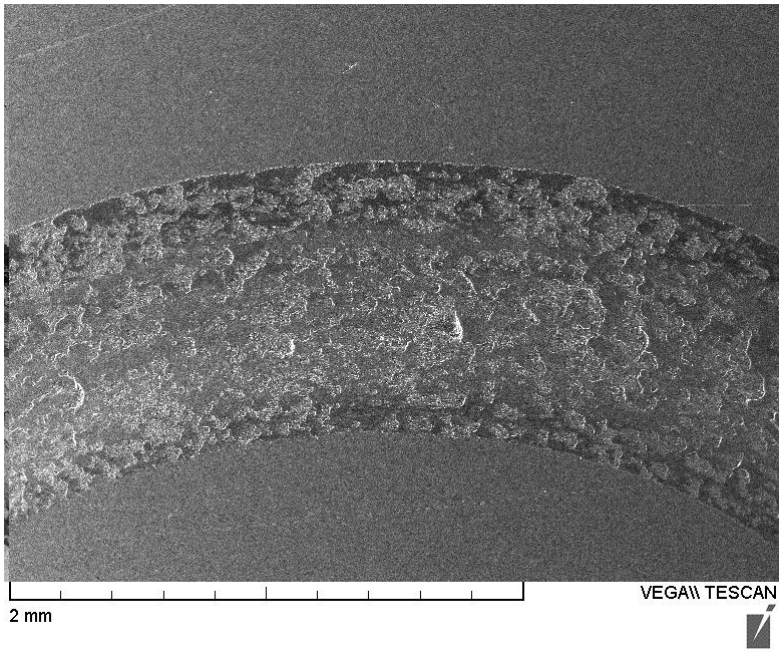

(a)

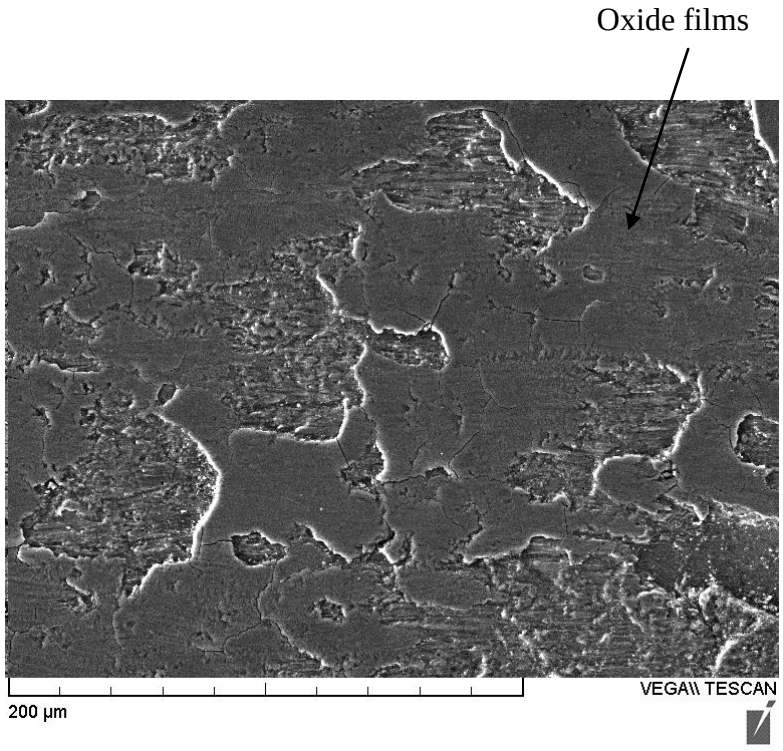

(b)

Figure 6-29: SEM images of worn surface of as-wrought AISI 440C tested at room temperature: (a) at low magnification and (b) at high magnification.

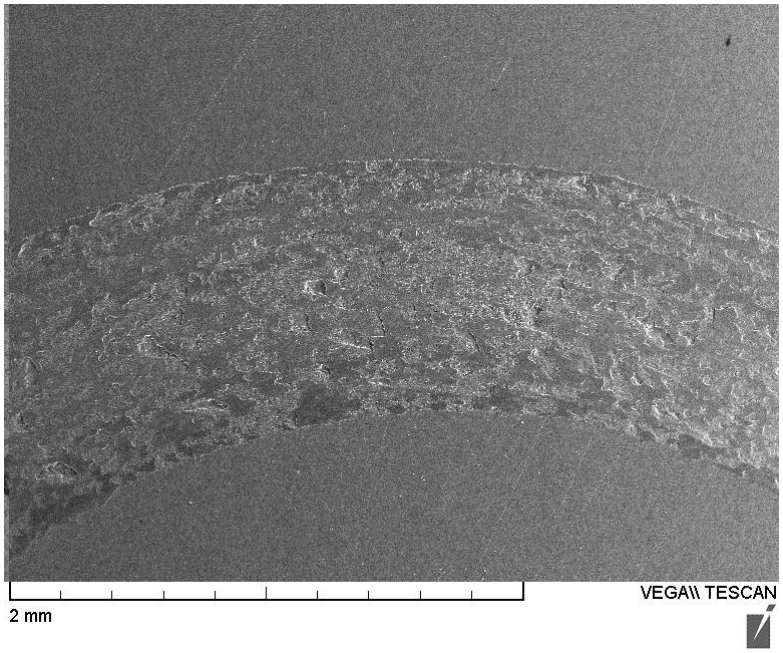

(a)

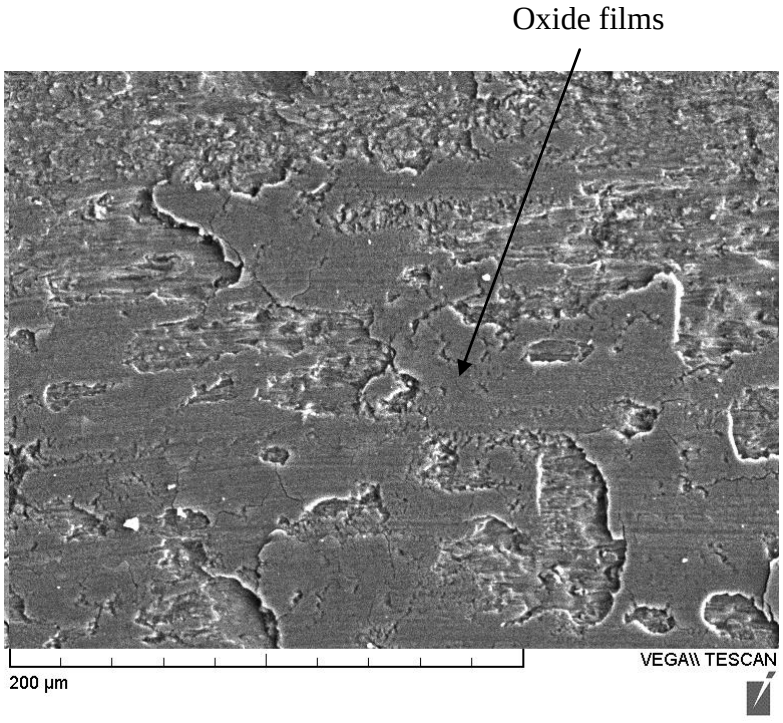

(b)

Figure 6-30: SEM images of worn surface of heat-treated AISI 440C tested at room temperature: (a) at low magnification and (b) at high magnification.

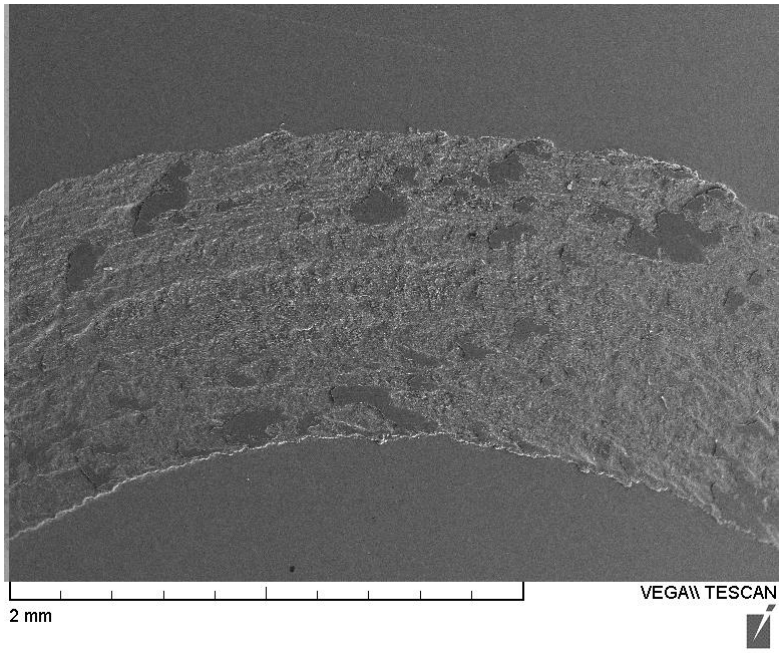

(a)

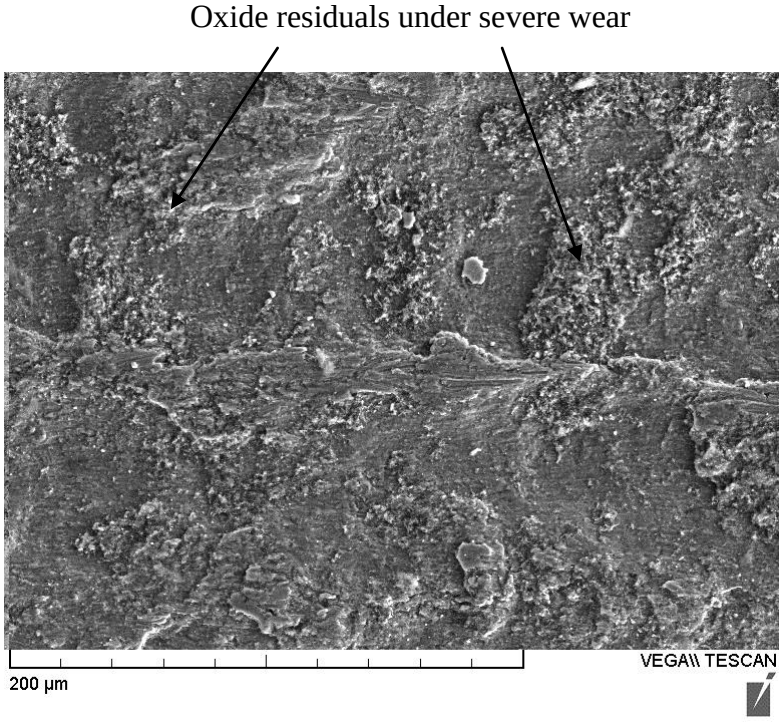

(b)

Figure 6-31: SEM images of worn surface of as-wrought AISI 440C tested at 250^{o}C:

(a) at low magnification and (b) at high magnification.

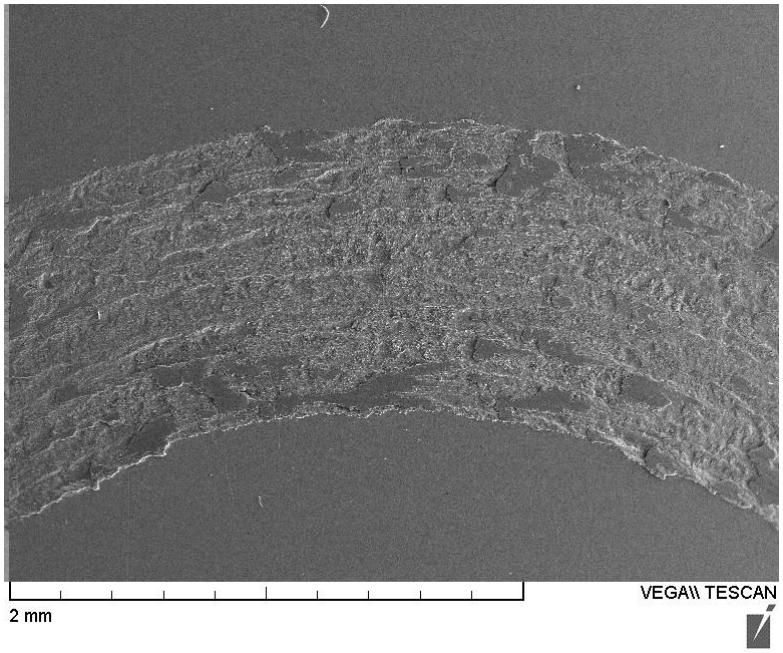

(a)

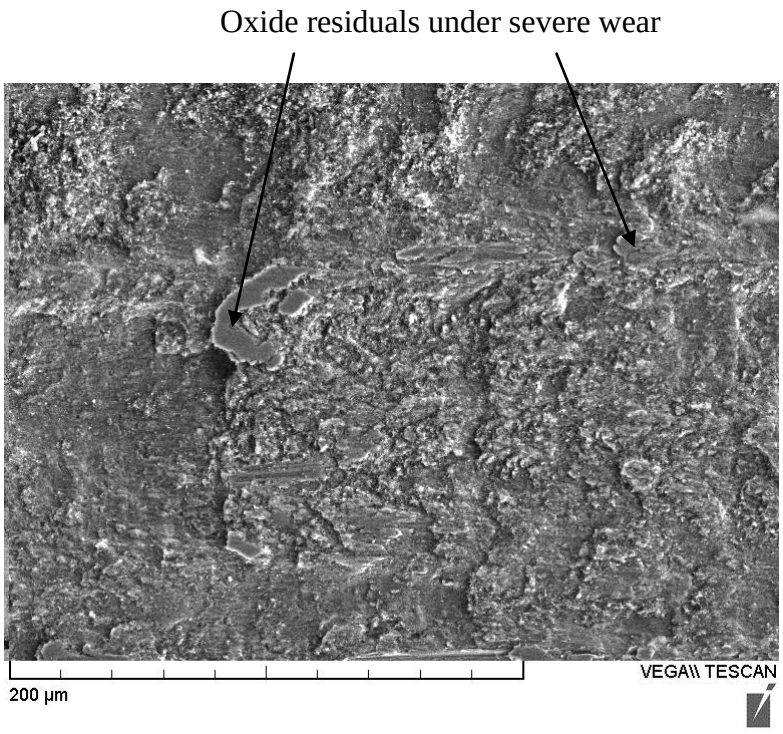

(b)

Figure 6-32: SEM images of worn surface of heat-treated AISI 440C tested at 250^{o}C: (a) at low magnification and (b) at high magnification.

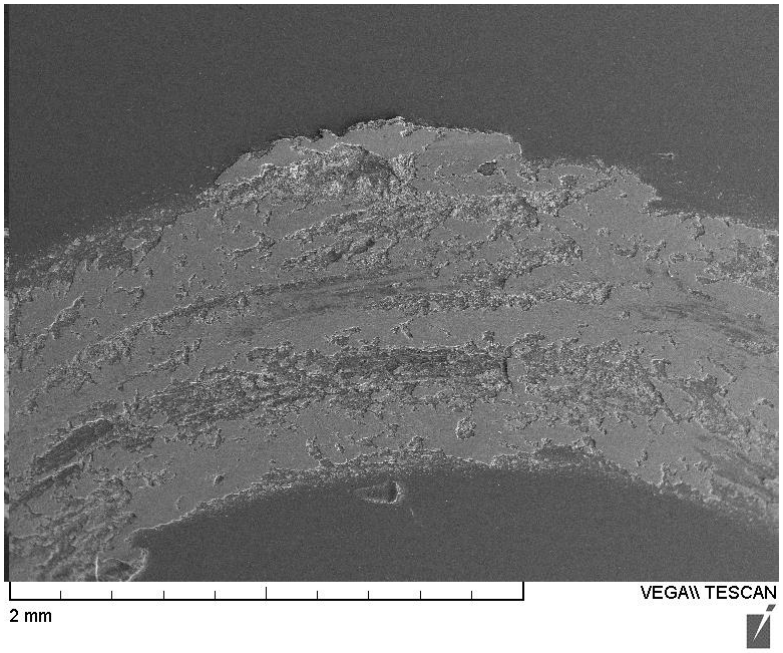

(a)

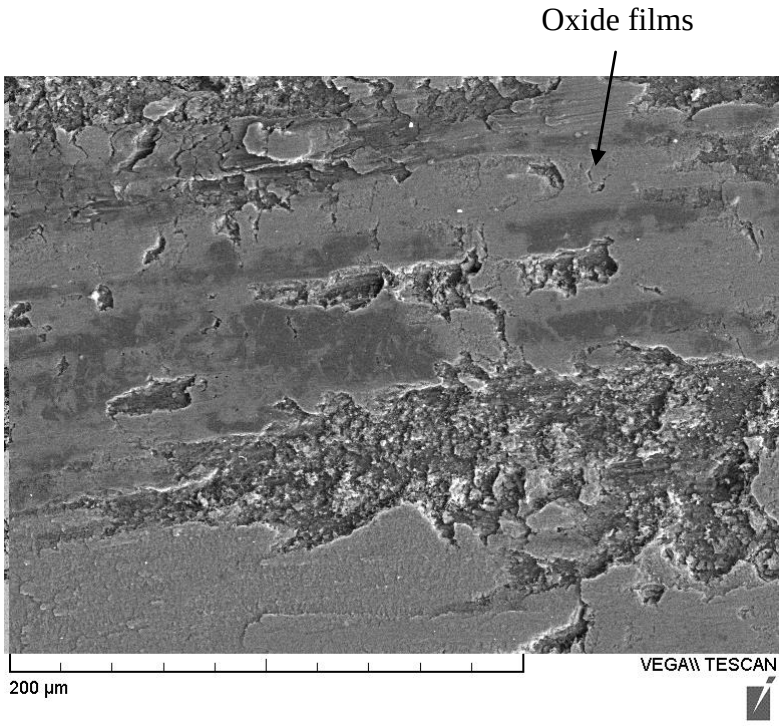

(b)

Figure 6-33: SEM images of worn surface of as-cast AISI 440C tested at 450^{o}C:

(a) at low magnification and (b) at high magnification.

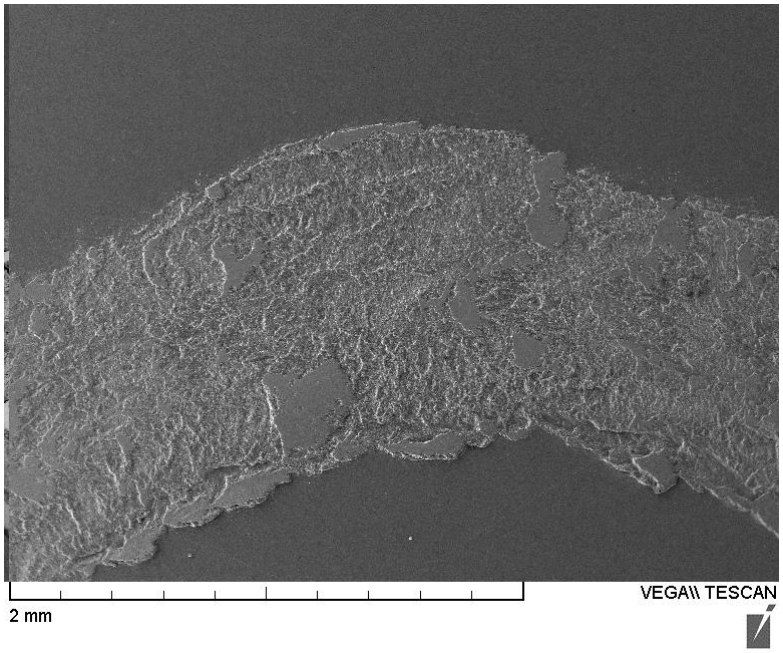

(a)

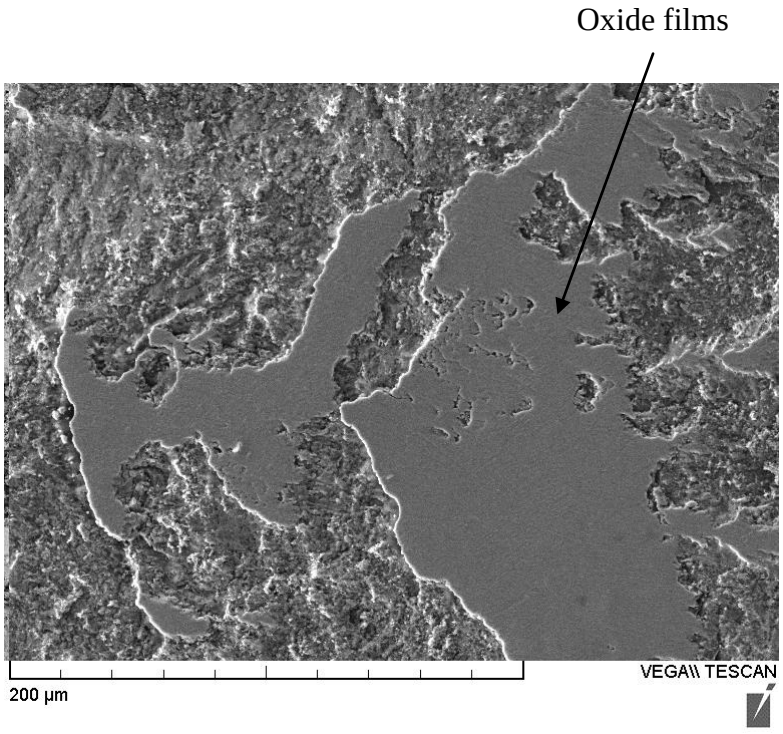

(b)

Figure 6-34: SEM images of worn surface of heat-treated AISI 440C tested at 450^{o}C: (a) at low magnification and (b) at high magnification.

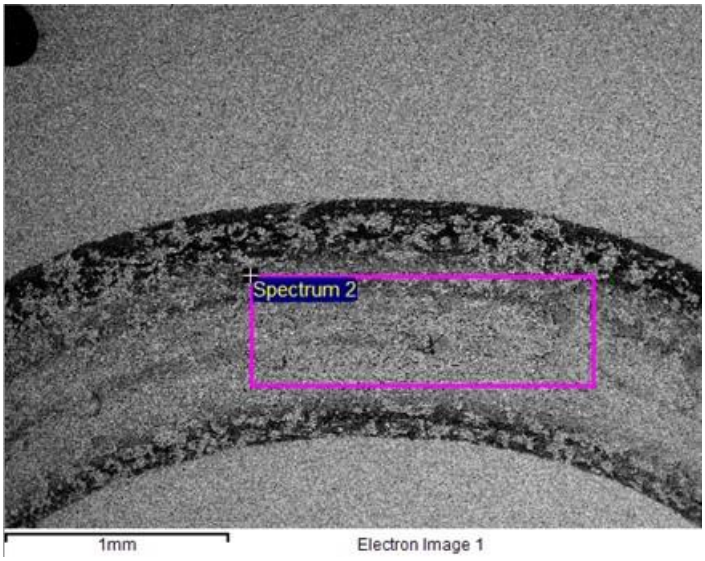

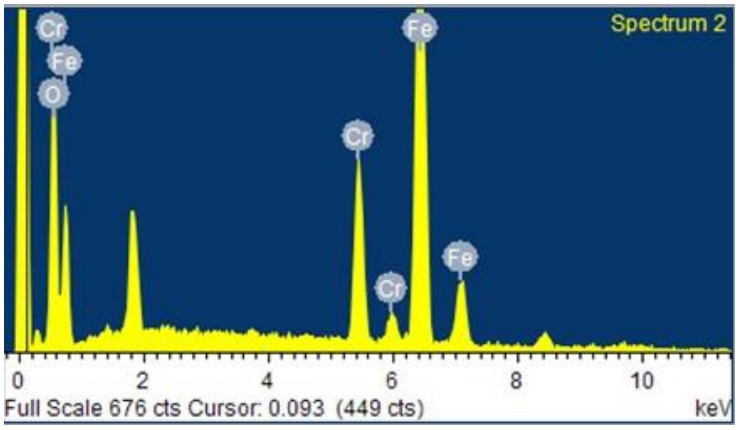

Element	Weight%	Atomic%
O K	23.63	51.65
Cr K	13.87	9.33
Fe K	62.50	39.03
Total	100.00	100.00

(a)

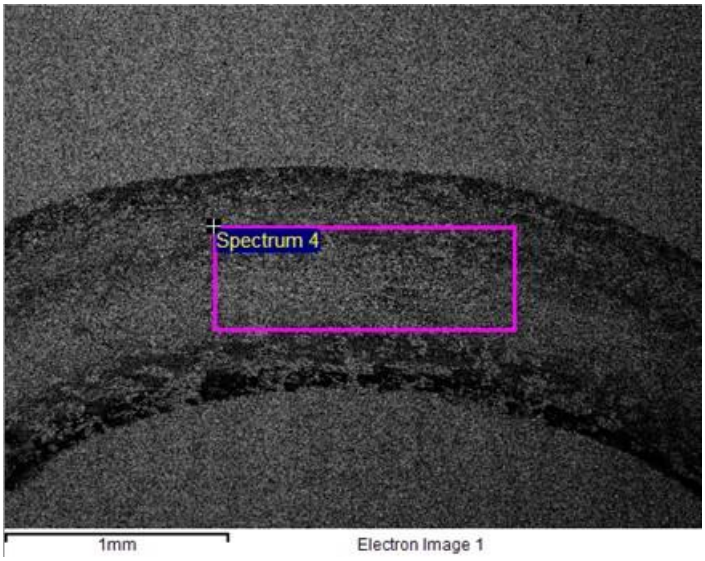

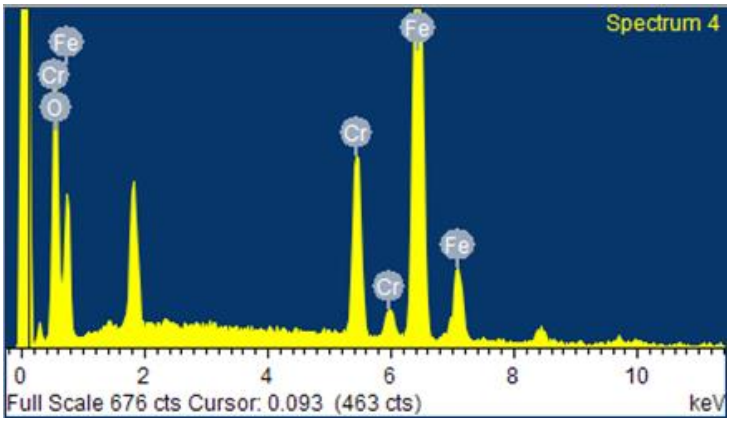

Element	Weight%	Atomic%
O K	22.87	50.57
Cr K	14.40	9.79
Fe K	62.74	39.64
Total	100.00	100.00

(b)

Figure 6-35: EDX spectra of wear track of AISI 440C tested at room temperature: (a) as-wrought and (b) heat-treated.

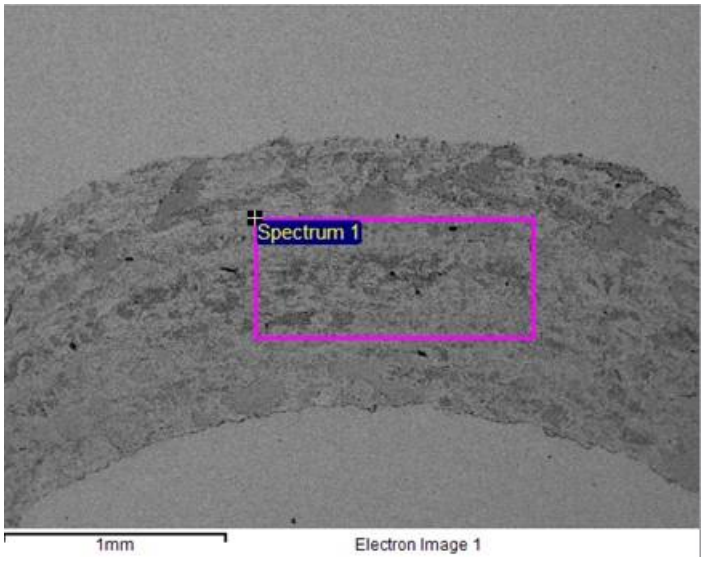

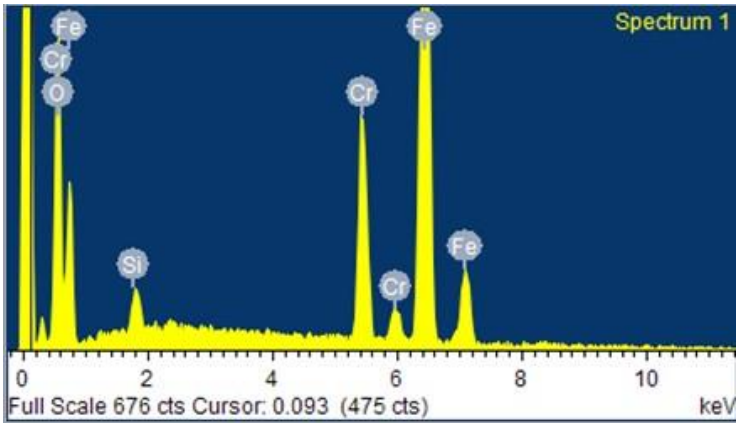

Element	Weight%	Atomic%
O K	21.61	48.57
Si K	0.53	0.68
Cr K	14.81	10.24
Fe K	63.06	40.50
Total	100.00	100.00

(a)

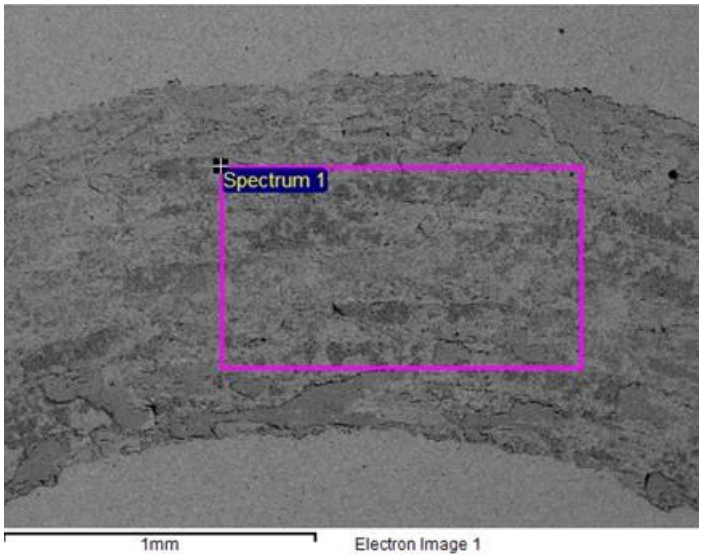

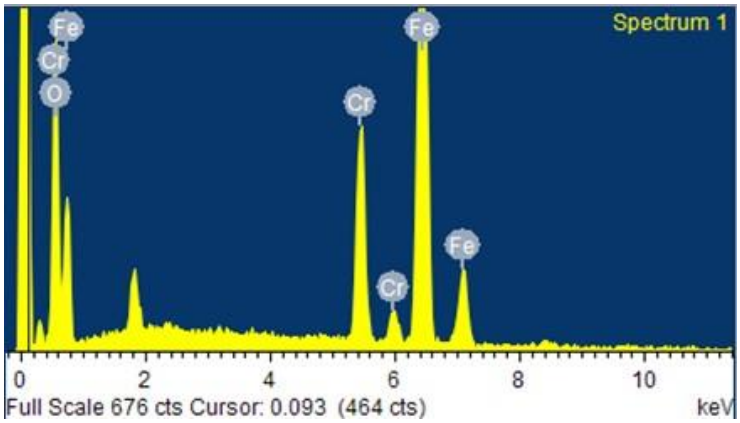

Element	Weight%	Atomic%
O K	22.83	50.51
Cr K	14.79	10.07
Fe K	62.38	39.43
Total	100.00	100.00

(b)

Figure 6-36: EDX spectra of wear track of AISI 440C tested at 250^{o}C:

(a) as-wrought and (b) heat-treated.

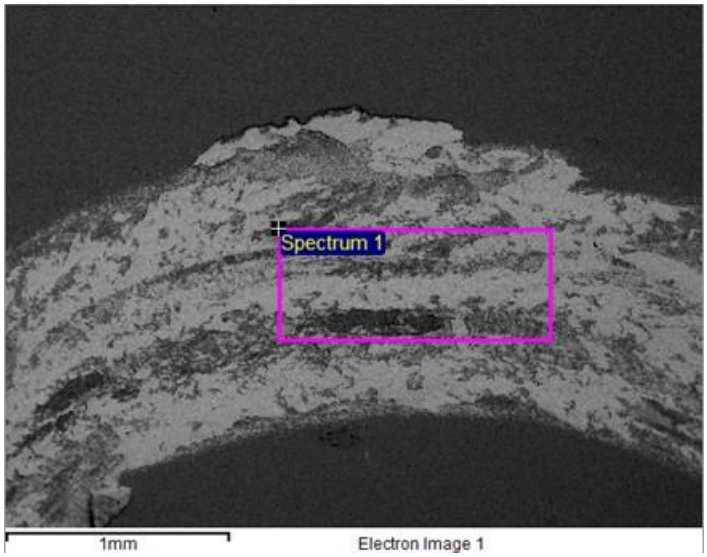

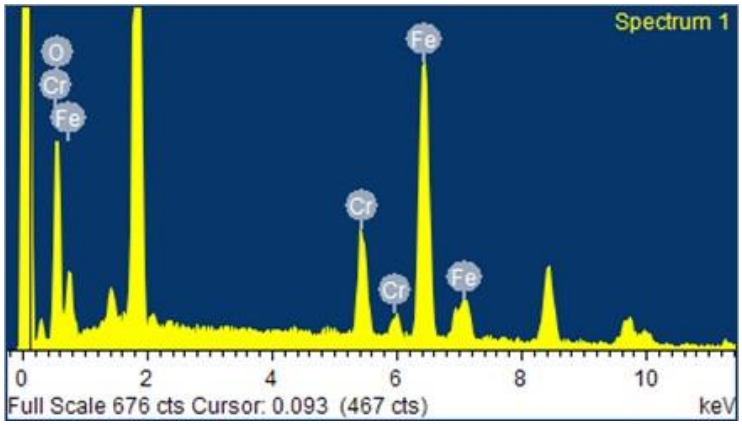

Element	Weight%	Atomic%
O K	37.05	66.98
Cr K	12.91	7.18
Fe K	50.04	25.84
Total	100.00	100.00

(a)

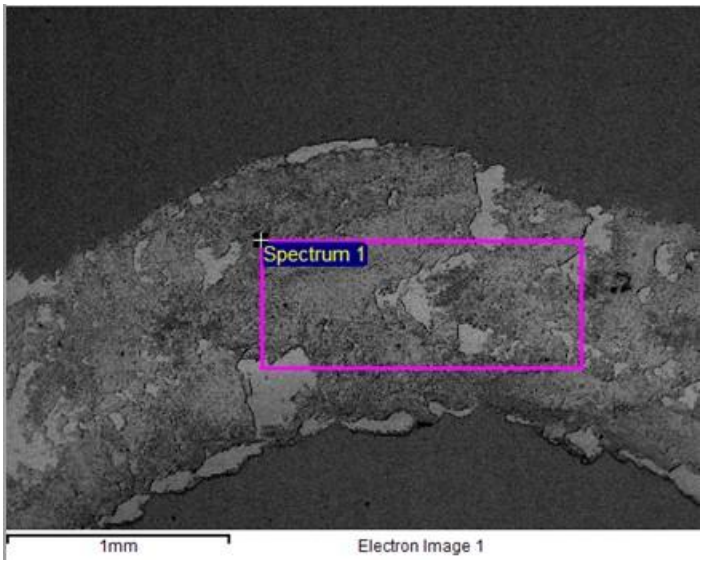

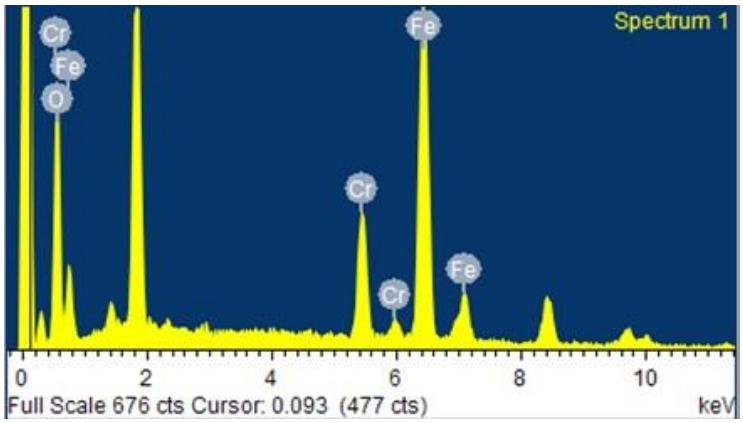

Element	Weight%	Atomic%
O K	33.12	63.06
Cr K	13.45	7.88
Fe K	53.43	29.06
Total	100.00	100.00

(b)

Figure 6-37: EDX spectra of wear track of AISI 440C tested at 450^{o}C:

(a) as-wrought and (b) heat-treated.

7 Discussion on Results

7.1 Heat Treatment Effects

7.1.1 Microstructure development

Chemical composition, altogether with fabrication process and heat treatment controls the microstructure of a material. The heat treatment cycle studied in this research exhibited different effects on each alloy being investigated. For Stellite 22, the maximum temperature (1193°C) in the heating process of the heat treatment is below the melting temperature (1364.9°C) of the alloy. The curve in Figure 7-1 was obtained from the differential scanning calorimetry (DSC) analysis, which shows the phase transformation behavior of Stellite 22 in the melting process. The melting temperature of the eutectic is around 1255.2°C.

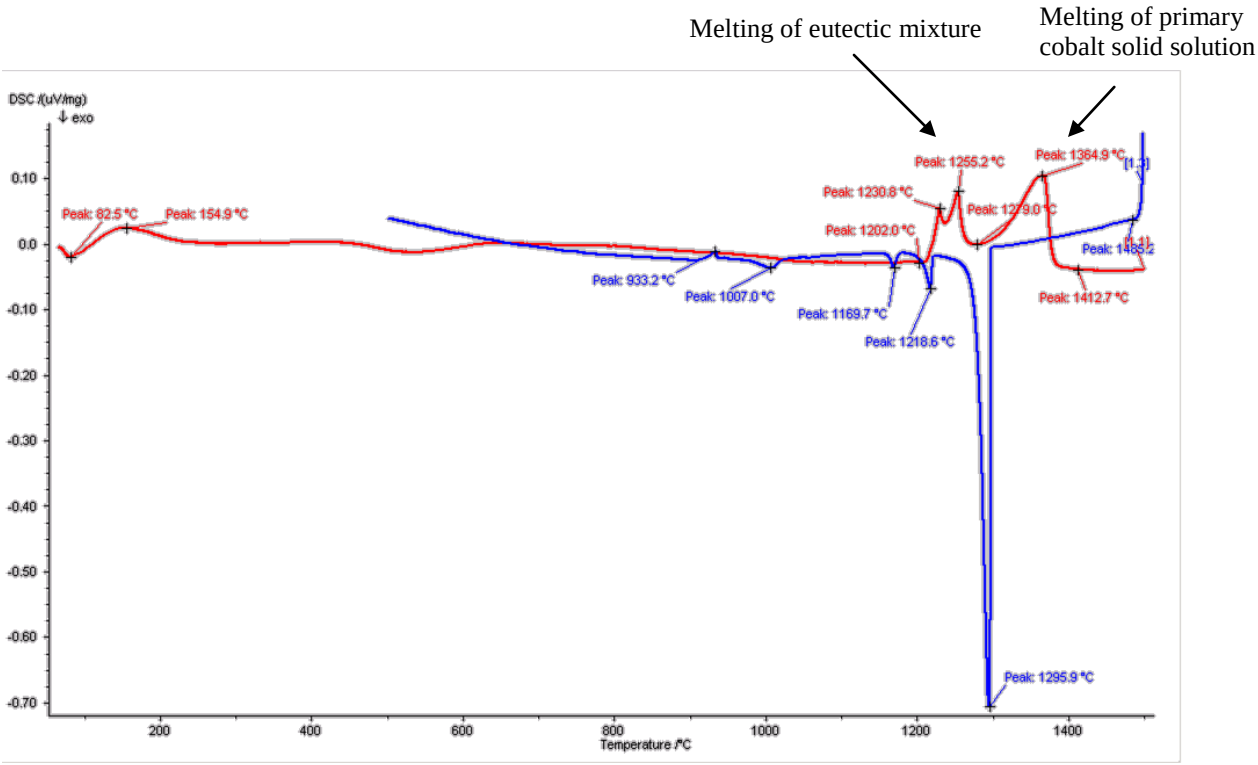

Figure 7-1: DSC curve of Stellite 22 in melting process.

According to the DSC curve, both the eutectic and solid solution did not melt during the heat treatment, therefore no significant change of the microstructure after the heat treatment was observed. However, in the heat treatment process, some of the carbides and intermetallic compounds may dissolve into the solid solution and precipitation of carbides and intermetallic compounds occurred during cooling. The EDX result in Figure 4-4(c) shows very high Cr content in the eutectic mixture, which implies the presence of $Cr_{23}C_6$ precipitates in the alloy after the heat treatment. In addition, the volume faction of the intermetallic compounds was found also increased in this alloy after heat treated.

For T-400C the eutectic phase and primary Laves phase have close melting points thus would melt simultaneously, as shown on the DSC curve in Figure 7-2. The melting temperature of T-400C is 1328.0°C. Therefore, both the eutectic and the Laves phase were still in solidus state during the heat treatment process. Accordingly, from the microstructural analysis, there is no change found in the primary Laves phase after T-400C experienced the heat treatment, but the cooling process resulted in the formation of tiny Laves phase precipitates.

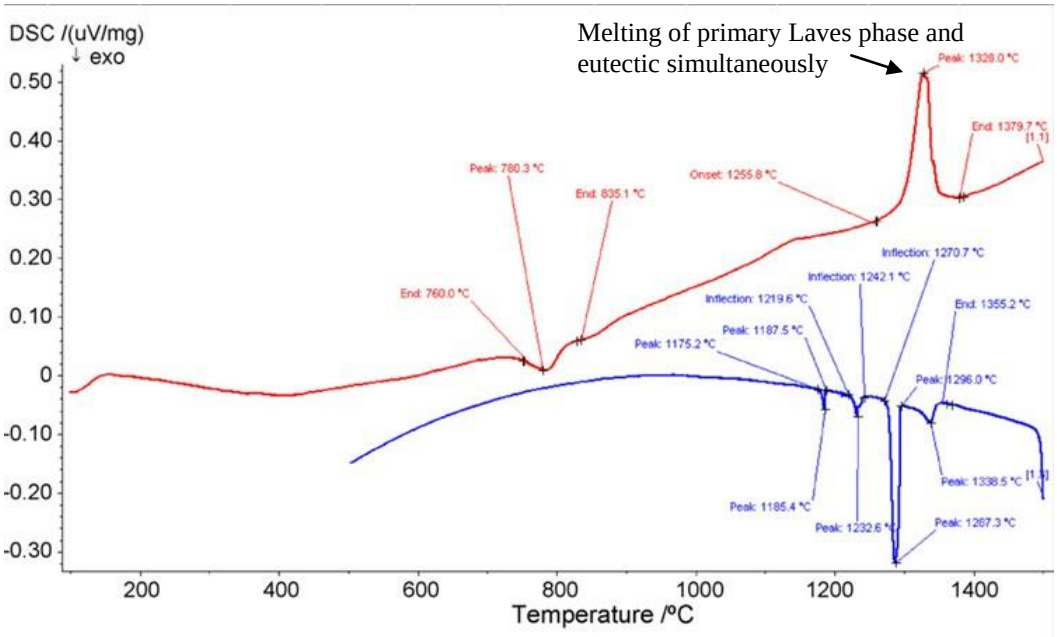

Figure 7-2: DSC curve of T-400C in melting process.

For the two stainless steels, AISI 420 and AISI 440C, their melting points are close, in the range 1475-1510 ℃. Therefore these alloys should be in solidus state during the heat treatment process. From the microstructural analysis, the heat treatment altered the microstructure of AISI 420 significantly and induced the phase transformation but it did not change that of AISI 440C very much. For martensite stainless steels, austenitizing temperature is generally in the range 925 – 1070 ℃. According to this data, at the heat treatment temperature, both alloys had been austenized. As for AISI 420, during the cooling, eutectoid reaction proceeded and resulted in the formation of pearlite phase. However, the cooling rate was not so low to allow austenite → pearlite transformation completely, which caused martensite phase formed when temperature was decreased to austenite → martensite transformation range. As a result, the microstructure of heat-treated AISI 420 steel is the mixture of primary pearlite eutectic phase with martensite matrix.

AISI 440C contains much higher C than AISI 420; owing to the high Cr content, a large amount of Cr-rich carbide precipitated in this alloy. The heat treatment did not induce any phase transformations in AISI 440C, which differed from what it did in AISI 420. The high Cr content in 440C may be responsible for this phenomenon. During the cooling, owing to the large amount of chromium with strong carbide-forming ability, most of C was preferable to form carbides with chromium. In this case there was no enough C in the solid solution to precede the eutectoid transformation. Despite no significant change in the microstructure, it was found that the heat treatment enhanced the carbide precipitation.

7.1.2 Hardness behavior

Hardness of a material is determined by its microstructure. The heat treatment altered more or less the microstructure of each alloy being studied; therefore it influenced their hardness behavior. For Stellite 22, the heat treatment had little effect on the hardness of the solid solution, but it increased the hardness of the eutectic, as shown in Figure 5-2(a), which resulted in the increase of the overall hardness of the alloy. The slight decrease in hardness of the solid solution may be due to the reduction of Cr and C as a result of $Cr_{23}C_6$ precipitation. On the contrary, the heat treatment strengthened the solid solution but almost did not change the hardness of the Laver phase of T-400C, as seen in Figure 5-4 (a), which slightly increased the overall hardness of T-400C. The microhardness test results in Figure 5-6 and Figure 5-8 show that the overall hardness of AISI 420 was greatly increased by the heat treatment but that of AISI 440C was only increased slightly. For convenient comparison, the percentages of hardness change of the alloys after the heat treatment were calculated and reported in Table

7-1. It is evident that the heat treatment increased hardness for all the alloys. The main contribution to the increased hardness of Stellite 22 may be $Cr_{23}C_6$ precipitates and more intermetallic compounds formed. For T-400C, the Laves phase precipitates in the solid solution matrix increased the overall hardness of T-400C, as the Laves phase is much harder than the solid solution. Regarding the stainless steels, significant increase in hardness through the heat treatment was found on AISI 420. This was attributed to the phase transformation; martensite is known possessed with very high harden strength. Since the heat treatment made little change in the microstructure of AISI 440C, the hardness was almost not influenced.

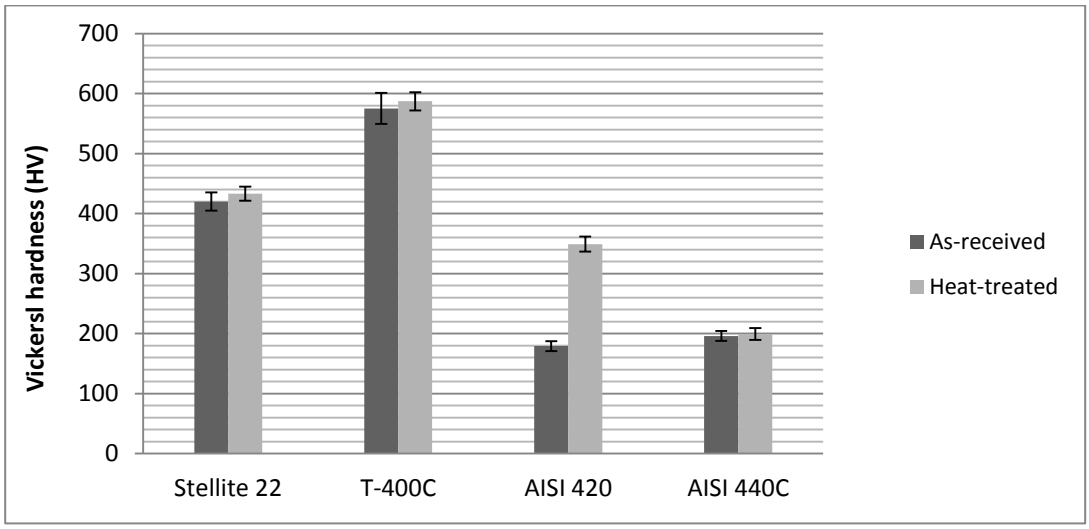

Figure 7-3: Overall Vickers hardness of the alloys before and after the heat treatment.

Table 7-1: Percentages of hardness change of the alloys after heat treated.

Stellite 22	T-400C	AISI 420	AISI 440C
3.1%	2.1%	95%	1.5%

7.1.3 Wear resistance at room temperature

The effect of the heat treatment on the wear resistance of the alloys is more complex than on the hardness. At room-temperature, the wear resistance of the alloys was controlled mainly by their microstructures, but local oxidation of the surface may occur due to the frictional heating. However, at high temperatures oxidation played a significant role, which determined the wear loss of the alloys, in particular, for the stainless steels.

The sliding wear test revealed that the heat treatment did not enhance the wear resistance of Stellite 22, as shown in Figure 6-1. This behavior was also investigated and reported by other researchers [18]. Comparing the microstructures of this alloy before and after the heat treatment, the main change is the increase in the volume fraction of the intermetallic compounds and the occurrence of $Cr_{23}C_6$ precipitates. These hard phases increased the hardness of the alloy but, on the other hand, reduced the ductility, resulting in the decrease of the overall strength to resist wear attack. Regarding the room-temperature wear behavior of T-400C, the heat-treated specimen exhibited better wear resistance. This is definitely attributed to the precipitation of more tiny Laves phase in solid solution matrix during cooling of the heat treatment.

The two stainless steels responded differently to the heat treatment and also behaved differently in room-temperature wear. From Figure 6-3, the AISI 420 specimen after heat treated exhibited much poorer wear resistance than the as-wrought one. Referring to the microstructure change of this alloy after the heat treatment, the original ferrite matrix was transformed to pearlite and martensite mixture. Martensite is known wear resistant owing to

the high hardness; pearlite is a two-phased, lamellar structure composed of alternating layers of alpha-ferrite and cementite; it can be wear resistant because of a strong lamellar network of ferrite and cementite, but is not particularly tough. Compared with the fine Cr-carbide reinforced tough ferrite matrix of as-wrought AISI 420, the integrated microstructure of pearlite and martensite of heat-treated AISI 420 was more vulnerable under the mechanical impact in the wear process due to the lack of enough toughness, which led to more wear loss. Regarding AISI 440C, the enhanced wear resistance after the heat treated resulted from the increase of Cr-rich carbides. Compared with the as-wrought specimen, more uniformly distributed carbides were formed in the heat-treated one, which strengthened the alloy thus reduced wear loss.

7.1.4 Wear resistance at high temperature

In high-temperature wear, microstructures themselves of the alloys play a less important role in controlling the wear loss than in room-temperature wear. As the analysis of the worn surfaces shown, all the alloys whether in as-received state or in heat-treated state were severely oxidized during the wear process, forming hard and strong Cr-oxide films on the specimens. These oxide films had a protective effect for the surfaces from further oxidation. Moreover, they exerted a noticeable beneficial influence, known as the “glazing” effect, on wearing surface by the oxide debris embedded in the surface layer as from the oxide debris. As a result, the wear losses of all the specimens at the high temperature of 450°C decreased, compared to those at 250°C, as shown in Figure 6-1 to Figure 6-4. This beneficial effect was observed more obviously on the stainless steels, especially on AISI 420. Two main reasons can explain this observation; one is the hardness of solid solution matrix; the other is the

volume fraction of solid solution. Since the solid solution matrices of stainless steels are softer than those of superalloys, which made the oxide debris easier squeezed into the specimen surfaces. AISI 420 contains the least volume fraction of carbides, thus the largest volume fraction of solid solution, which provided more surface area for the oxide debris getting into the alloy. Stellite 22, although, contains less carbides than AISI 420, it contains a large amount of intermetallic compounds, which rendered the solid solution less.

As concerns the heat treatment influence on the wear resistance of the alloys at high temperatures, since oxidation played an important role in temperature environments, rather than microstructure, the heat treatment effect was not as pronounced as at room temperature, but compared with the stainless steels, the "glazing" effect on the superalloys was relatively small, as discussed above, therefore, microstructure still governed the wear resistance of these alloys, as depicted in Figure 6-1 and Figure 6-2. More brittle intermetallic compounds were precipitated in Stellite 22 through the heat treatment, which decreased the resistance to wear impact of the alloy, leading to more wear loss. Regarding T-400C, the heat treatment promoted tiny Laves phase precipitates within the solid solution, which strengthened the matrix, thus enhanced the wear resistance of the alloys. For the stainless steels, the wear resistance of each alloy was the result of the beneficial "glazing" effect, therefore, the as-wrought and heat-treated specimens behaved similarly; the heat treatment or microstructure made little influence on high temperature wear behavior of stainless steels.

7.2 Correlations between Properties

7.2.1 Microstructure versus hardness

The hardness of an alloy relates to its microstructure, in particular, for a multi-phase alloy, the overall hardness is determined by the hardness of each individual phase and their proportions in the alloys. The four alloys being studied are all multi-phase alloys; therefore the change in microstructure of the alloys after the heat treatment influenced the overall hardness of the alloys.

As discussed above, the heat treatment promoted more Co_3Mo and $CoMo_6$ intermetallic compounds formation and $Cr_{23}C_6$ carbide precipitation in Stellite 22. Since these intermetallic compounds and carbides are harder than Co solid solution, the increase in their amounts would certainly raise the overall hardness of the alloy. Similarly for T-400C, the main alteration in microstructure through the heat treatment was introduction of Laves phase precipitates in the solution matrix. The hard Laves phase strengthened the matrix, resulting in the increase of the overall hardness.

The heat treatment induced phase transformation in AISI 420, from original ferrite matrix to pearlite and martensite mixture. Ferrite is softer than martensite, but the Cr-rich carbides should provide additional strength to the original ferrite matrix. However, the amount of Cr-rich carbide is small due to the low carbon content in the alloy, while the martensite in the heat-treat specimen takes about 50% volume fraction. As a result of comparison, the overall hardness of heat-treated AISI 420 is higher than that of as-wrought one. The heat treatment

slightly increased the volume fraction of Cr-rich carbides in AISI 440C, which contributed to the light increase of the overall hardness.

7.2.2 Hardness versus wear resistance

Hardness is always related to wear resistance for a material. It is generally accepted that the harder a material, the more resistant to wear the material is, for most metallic materials. However, from the wear analysis of the alloys above, this view has been found not applicable for all cases, especially when temperature is involved.

The hardness measurement has demonstrated that the hardness of the four alloys was all increased by the heat treatment, as illustrated in Figure 7-3. However, the wear test results are not consistent with the hardness behavior. For comparison, the wear losses of the alloys before and after the heat treatment are plotted in Figure 7-4. For convenient comparison, the percentages of wear loss change of the alloys after the heat treatment were calculated and reported in Table 7-2. The enhanced wear resistance of T-400C and AISI 440C after heat treated was attributed to the precipitated hard phases that contributed to the increase of the overall hardness. The higher wear loss of Stellite 22 after the heat treatment was not related to hardness, but the overall strength of the alloy. In this alloy the additional intermetallic compounds from the heat treatment increased the overall hardness of the alloy but also increased the brittleness of the alloy, causing the spallation of the intermetallic compounds from the surface and resulting in more wear loss. Similar mechanism can be applied on AISI 420; the hard martensite and pearlite mixture in the heat-treated specimen enhanced the hardness of the alloy, but rendered the alloy not as tough as the as-wrought specimen which

has a ferrite matrix with fine carbide particles embedded. Under continues impact loading, the tougher surface is more resistant to wear attack and suffered less material removal loss.

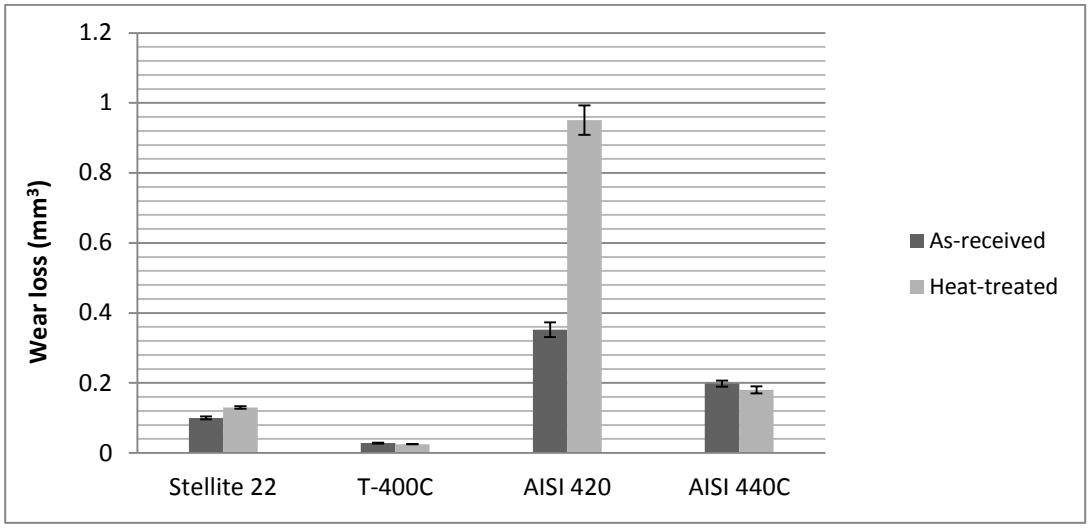

(a)

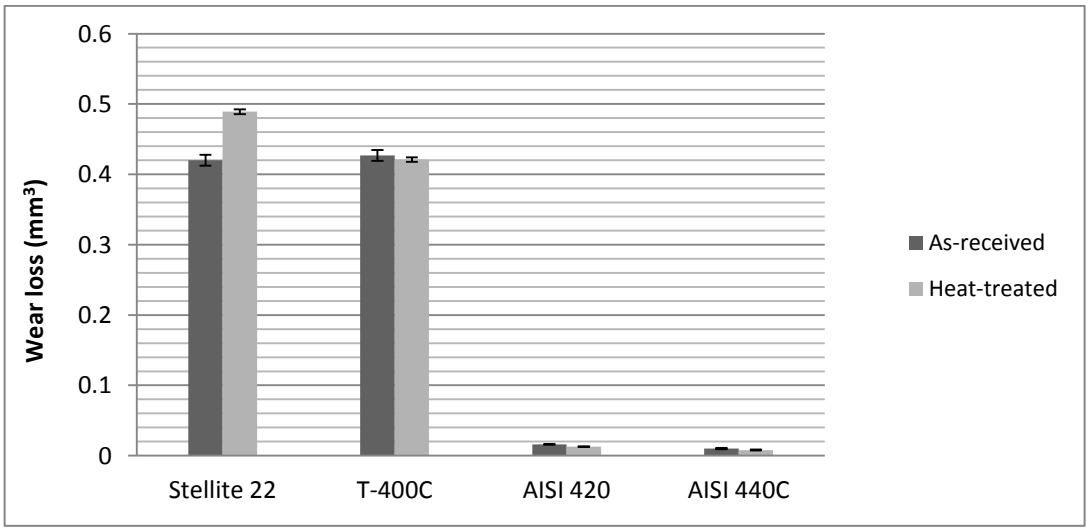

(b)

Figure 7-4: Comparison of wear loss of the alloys before and after heat treatment: (a) at room temperature and (b) at 450 ℃.

Table 7-2: Percentages of wear loss change of the alloys after heat treated.

Alloys / Temperature	Stellite 22	T-400C	AISI 420	AISI 440C
25 ℃	30.00%	-10.71%	170.17%	-9.09%
450 ℃	16.43%	-1.41%	-18.75%	-20.00%

7.2.3 Temperature-dependence of hardness

The hardness of metallic materials usually decreases with temperature. It is especially obvious when the temperature reaches a critical level, the hardness drops steeply, depending on individual materials. Therefore, in order to extend the applications of wear-resistance materials from room temperature to elevated temperatures, it is necessary to understand the shifts of hardness over a range of operating temperatures, which is the hardness variation with temperature.

From the microhardness test, the hardness of individual phases and overall hardness of the alloys all decreased with temperature. This may be the results of enhanced atomic motion and release of dislocations at high temperatures. For convenient comparison, the overall hardness reductions of the alloys at 600°C before and after the heat treatment are plotted in Figure 7-5. Also, the percentages of hardness reduction change of the alloys after the heat treatment were calculated and reported in Table 7-3. Among the alloys under study, AISI 420 was the most sensitive to temperature while T-400C was the least. The heat treatment influenced hardness reduction of the alloys unequally. Again, the heat treatment had the most significant effect on AISI 420 in regard of hardness reduction; and the least effect on T-400C.

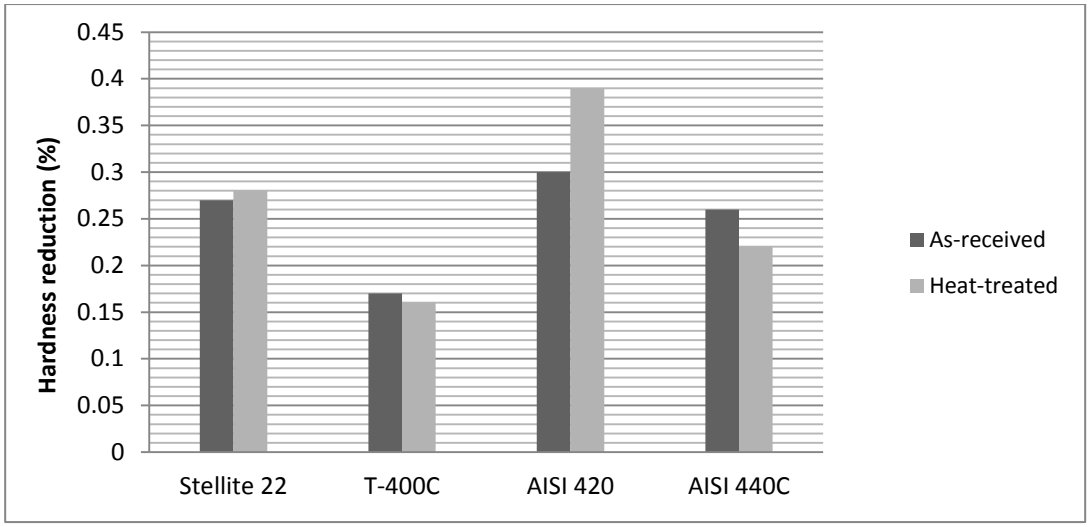

Figure 7-5: Hardness reductions of the alloys at 600°C.

Table 7-3: Percentages of hardness reduction change of the alloys after heat treated.

Stellite 22	T-400C	AISI 420	AISI 440C
3.70%	-5.88%	30.00%	-15.38%

8 Conclusions and Future Work

8.1 Current Work

8.1.1 Summary

The present research was initiated and sponsored by the industry partner, Kennametal Stellite Inc. The primary motivation of this research was to investigate the effect of the thermal cycle in a slurry/sintering coating process on the wear behavior of the materials involved in the coating systems. The heat treatment cycle concerned in this research was a sintering cycle for slurry coating of superalloys and stainless steels, designed by Kennametal Stellite Inc. The two superalloys and two stainless steels investigated in this research are examples of the common materials applied in this coating system either as coating materials or as substrate materials. Stellite 22 is a low-carbon Stellite alloy but contains a high amount of molybdenum and chromium; as a result, in addition to minor Cr-rich carbides, a large amount of Co_3Mo and $CoMo_6$ intermetallic compounds are formed in this alloy. T-400C is a hypereutectic Tribaloy alloy, with the microstructure consisting of primary Laves phase and the eutectic. Both AISI 420 and AISI 440C are martensitic stainless steels; the microstructures of the as-received alloys contain ferrite matrix with (Cr, Fe) carbides embedded. AISI 420 has a low carbon content so that the carbides in its microstructure are fine and less, while AISI 440C contains high carbon content, which renders this alloy with a large amount of carbides in large size.

The objective of this research was to investigate the influence of the sintering cycle on the wear behavior of these materials at both room temperature and high temperatures. The above four alloys experienced a heat treatment simulating the sintering cycle. According to the phase transformation temperatures, at the maximum sintering or heat treatment temperature

(1193°C), all the alloys were still in a solidus state. All the alloys experienced the so-called annealing treatment. To complement this research, the microstructures developed in the heat treatment of the four alloys were studied, compared with the as-received microstructures. Following the microstructural analysis, the hardness and wear resistance of these alloys at room temperature and at high temperatures were evaluated on a microhardness tester and a pin-on-disc tribometer, respectively. The effects of the heat treatment on the microstructure, hardness and wear resistance were analyzed and discussed. The worn surfaces of each specimen were studied using SEM/EDX to understand the wear test results and also to explore the wear mechanisms.

8.1.2 Conclusions

From the experimental results and discussion, the following conclusions can be drawn from this research:

1. The heat treatment can alter microstructure for all the alloys being studied, but it influenced differently each alloy. For Stellite 22, the heat treatment induced new carbide precipitates ($Cr_{23}C_6$) and also promoted the formation of Co_3Mo and $CoMo_6$ intermetallic compounds. The heat treatment resulted in Laves phase precipitates within the Co solid solution matrix of T-400C. The microstructure of AISI 420 was altered significantly by the heat treatment; the original ferrite matrix was transformed to martensite and pearlite (alpha-ferrite and cementite) mixture. However, the heat treatment on AISI 440C only slightly increased the volume fraction of the (Cr, Fe) carbides.

2. The overall hardness of the alloys strongly depends on their microstructures. Since the heat treatment altered the microstructures, the hardness of the alloys was influenced by the heat treatment. As the heat treatment increased the carbide and intermetallic compound amounts in Stellite 22, and these two phases are all harder than the Co solid solution, the overall hardness of this alloy was increased after heat treated. Similar to Stellite 22, tiny hard Laves phase was precipitated by the heat treatment within the solid solution matrix of T-400C, which increased the overall hardness of the alloy. The martensite and pearlite integrated microstructure obtained from the heat treatment on AISI 420 exhibited higher hardness than the original ferrite matrix with fine carbide particles embedded. The heat treatment increased slightly carbide precipitates in AISI 440C thus strengthened the alloy to a small extent.

3. The hardness of individual phases and overall hardness of these alloys all decreased with temperature. AISI 420 was the most sensitive to temperature while T-400C was the least. The heat treatment influenced hardness reduction of the alloys. Again, the heat treatment had the most significant effect on AISI 420 in regard of hardness reduction; and the least effect on T-400C.

4. The effects of the heat treatment on the wear behavior of the alloys were more complex than on hardness, in particular, when temperature was involved. These alloys behaved differently in room temperature wear and in high-temperature wear.

5. At room temperature, the wear resistance of these alloys was mostly controlled by their microstructures; but hardness was not the unique factor. For Stellite 22, the heat treatment

increased the volume fraction of the intermetallic compounds and induced $Cr_{23}C_6$ precipitates, which provided this alloy with additional hardness. However, the increase of these hard and brittle phases caused this alloy more brittle and more vulnerable under the wear impact load. The tiny Laves phase precipitates in T-400C from the heat treatment strengthened the solid solution matrix thus enhanced the wear resistance of this alloy. Although the martensite and pearlite mixture obtained from the phase transformation during the heat treatment of AISI 420 had higher hardness than the original ferrite matrix with fine hard carbide particles embedded, the microstructure exhibited poorer wear resistance due to the brittleness. The heat treatment increased slightly the carbide amount in AISI 440C, thus increased the hardness, also the wear resistance.

6. At high temperatures, all the alloys were severely oxidized with hard and strong Cr-oxide films formed on the specimen surfaces. The wear resistance of these alloys at high temperatures was influenced significantly by oxidation. The oxide films produced the, so-called “glazing” effect, which hardened the specimen surface thus enhanced the wear resistance.

7. The “glazing” effect was more pronounced on stainless steels than on superalloys in which the former has softer solid solution matrix and also larger volume fraction of solid solution. At high temperatures, although the “glazing” effect played an important role in enhancing the wear resistance of the superalloys, the microstructures were still predominant; therefore the heat treatment affected the wear resistance. However, for the stainless steels, the “glazing” effect was predominant over microstructure so that the heat treatment had little effect on the wear resistance.

8.1.3 Significant contributions

Superalloys and stainless steels are two groups of popular alloys known for their excellent corrosion, wear and mechanical properties. They are commonly employed as either coating materials or substrate materials in the coating products. The slurry coating process requires a relatively high temperature (> 1000^{o}C) environment. This high temperature sintering process may alter the microstructure and the properties of superalloys and stainless steels, thus influence the lifetime of the coated mechanical components. However, according to the literature review and information from the material industry, Kennametal Stellite Inc., influences of heat treatment, especially sintering heat treatment, on superalloys and stainless steels are rarely investigated, which has greatly limited the application of superalloys and stainless steels in industry. This research has provided material industry with experimental results of mechanical and tribological properties of two newly-developed superalloys (as-cast Stellite 22 and T-400C) and two popular stainless steels (as-wrought AISI 420 and AISI 440C) after sintering heat treatment. Moreover, wear mechanisms of these four high temperature alloys at room temperature and elevated temperatures are also explored in the research. It is indicated that sintering heat treatment alters the microstructure of all the alloys being studied. It promotes the formation of intermetallic Co_3Mo and $CoMo_6$ in Stellite 22 and Laves phase precipitates in T-400C. Concurrently, it induces new martensite matrix and pearlite phase in AISI 420 and increases the volume fraction of the (Cr, Fe) carbides in AISI 440C. It is demonstrated that the effects of heat treatment on the wear behavior of these four high temperature alloys is very complex, in particular when temperature is involved. At room temperature, the wear resistance of these alloys is governed by their microstructures. However, at high temperatures, oxidation, resulting in formation of oxide films on the specimen surface,

influences the wear resistance significantly. These research outcomes are beneficial for extending the application of existing superalloys and stainless steels. Moreover, this research can provide the scientific guidance for designing and manufacturing functional coatings for various severe conditions.

8.2 Future Work

1. In order to better understand the effect of the heat treatment on superalloys and stainless steels, more various alloys will be selected to study, and also to verify the findings derived from this research.

2. The coatings fabricated from this slurry/sintering process also commonly sever in corrosive environments; therefore the influence of this heat treatment on the corrosion behavior of these alloys needs to be investigated.

3. The coatings fabricated from this slurry/sintering process may also be applied in erosive environments so that the influence of this heat treatment on the erosion behavior of these alloys should be studied too.

4. These alloys showed a general trend in wear resistance with temperature as the wear loss increased with temperature at lower temperatures and then decreased at high temperatures except AISI 420. It is necessary to find out where is the turning temperature for these alloys.

Reference

[1] G.L. Dolland and A. Matthews, Handbook of Lubrication and Tribology, Volume II, CRC Press, 2012.

[2] D. Matthew J and D.S. James, Superalloys: A Technical Guide (2nd edition), Materials Park: ASM International, 2002.

[3] J. Davis, Cobalt-base alloys, in Nickel, Cobalt, and Their Alloys, Materials Park: ASM International, 2000.

[4] Anon, Unique intermetallics combat wear and corrosion, Metal. Prog., 107(5), 1975, 90-92.

[5] R.I. Jaffee, R. Perkins and G. Marshall Pound, High-temperature Oxidation-Resistant Coatings, National Academy of Sciences/ National Academy of Engineering, Washington, D.C. 1970.

[6] A.W. J. Frenk, "Laser cladding with cobalt-based hardfacing," J. Phys. IV France, vol. 1, no. C7, pp. 65-68, 1991.

[7] S. Zhang and D. Zhao, Aerospace Materials Handbook, CRC Press, 2013.

[8] R. Liu, W. Xu, M.X. Yao, P.C. Patnaik and X.J. Wu, “A newly developed Tribaloy alloy with increased ductility,” Scripta Materialia, 53(12), 2005, 1351-1355.

[9] M.X. Yao, J.B.C. Wu, S. Yick, Y. Xie and R. Liu, “High temperature wear and corrosion resistance of a Laves phase strengthened Co–Mo–Cr–Si alloy,” Materials Science & Engineering A, Volume 435-436, issue (November 5, 2006), p. 78-83.

[10] C.T. Sims, Journal of Metals 12 (1969) 36.

[11] K.C. Antony, Journal of Metals 35 (1983) 52.

[12] J. Przybylowicz, J. Kusinski, Surf. and Coating Tech. 125 (2000) 13.

[13] G. Krauss, Steels, Processing, Structure, and Performance, Materials Park: ASM International, 2005.

[14] M.G. Fontana and N.D. Greene, Corrosion Engineering, McGrawHill, 1977

[15] D. Peckner and I.M. Bernstein, Handbook of Stainless steels, McGraw-Hill, 1977

[16] M. McGuire, Stainless Steels for Design Engineers, ASM International, 2008

[17] A. Osma, E.S. Kayali and M.L. Öveçoglu, "The effect of elevated temperature and silicon addition on a cobalt-based wear resistant superalloy," J. Mater. Sci., 31 (1996), p. 4603

[18] P. Huang, R. Liu, X.J. Wu and M.X. Yao, "Effects of molybdenum content and heat treatment on mechanical and tribological properties of a low-carbon Stellite alloy," Journal of Engineering Materials and Technology, 129(4), 2007, 523-529.

[19] A. Nasery Isfahany; H. Saghafian and G. Borhani, "The effect of heat treatment on mechanical properties and corrosion behavior of AISI420 martensitic stainless steel," Journal of Alloys and Compounds (March 2011), 509 (9), pg. 3931-3936.

[20] C. Garcia de Andres, G. Caruana, L.F.Alvarez, "Control of $M_{23}C_6$ carbides in 0.45 C-13Cr martensitic stainless steel by means of three representative heat treatment parameters," Material Science and Engineering A 241 (1998) 211-215.

[21] M.X. Yao, J.B.C. Wu, W. Xu and R. Liu, "Metallographic study and wear resistance of a high-C wrought Co-based alloy Stellite 706K," Materials Science and Engineering: A, Volume 407, Issues 1–2, 25 October 2005, Pages 291-298.

[22] V. Kuzucu, M. Ceylan, H. Celik and I. Aksoy, "Microstructure and phase analyses of Stellite 6 plus 6 wt.% Mo alloy," J. Mater. Process. Technol., 69 (1997), p. 257

[23] R. Liu, M.X. Yao, P.C. Patnaik and X.J. Wu, "Effects of heat treatment on mechanical and tribological properties of Laves intermetallic cobalt-based alloys," Journal of Materials Engineering and Performance, 14(5), 2005, 634 -640.

[24] I. Alphonsa, A. Chainani, P.M. Raole, B. Ganguli, P.I. John, “A study of martensitic stainless steel AISI 420 modified using plasma nitriding” Surf. Coat. Technol. 150 (2002) 263.

[25] Y. Xi, D. Liu, D. Han, “Improvement of corrosion and wear resistances of AISI 420 martensitic stainless steel using plasma nitriding at low temperature,” Surface and Coatings Technology, Volume 202, Issue 12, 15 March 2008, Pages 2577-2583.

[26] R.L. Liu, M.F. Yan, “The microstructure and properties of 17-4PH martensitic precipitation hardening stainless steel modified by plasma nitrocarburizing,” Surface and Coatings Technology, Volume 204, Issue 14, 15 April 2010, Pages 2251-2256.

[27] F. Alonso, A. Garcia, J.J. Ugarte, J.L. Viviente, J.I. Ofiate, P.S. Baranda, C.V. Cooper , “Changes in tribological properties of an AISI 440C martensitic stainless steel after ion implantation of carbon at very high doses,” Surface and Coatings Technology 83 (1996)2 63-268.

[28] J.I. Oñate, J.K. Dennis, S. Hamilton, “Wear behaviour of nitrogen-implanted AISI 420 martensitic stainless steel,” Surface and Coatings Technology, 42 (1990) 119—131.

[29] J. F. Archard, “Contact and Rubbing of Flat Surfaces,” J. Appl. Phys. 24, 981 (1953).

[30] J.F. Archard, W. Hirst, “The Wear of Metals under Unlubricated Conditions”, Proc Royal Society London, A 236 (1956) 397-410.

[31] J.D. Bressan, D.P. Daros, A. Sokolowski, R.A. Mesquita, C.A. Barbosa, “Influence of hardness on the wear resistance of 17-4 PH stainless steel evaluated by the pin-on-disc testing,” Journal of Materials Processing Technology, Volume 205, Issues 1–3, 26 August 2008, Pages 353-359.

[32] J.K. Lancaste, “The Influence of Temperature on Metallic Wear,” Proc. Phys. Soc. B (4th edn.), 70 (1957), pp. 112–118.

[33] F.H. Stott, G.C. Wood, “The influence of oxides on the friction and wear of alloys,” Tribology International, Volume 11, Issue 4, August 1978, Pages 211-218.

[34] Peter J. Blau, “Elevated-temperature tribology of metallic materials,” Tribology International, Volume 43, Issue 7, July 2010, Pages 1203-1208.

[35] KJ Bhansali, “Adhesive wear of nickel-and cobalt-base alloys,” Wear, 60 (1980), pp. 95–110.

[36] A. Babilius, P. Ambroza, "Effect of Temperature and Sliding Speed on the Adhesive Wear." ISSN 1392-1320 Materials Science. Vol. 9, No. 4. 2003.

[37] A. Frenk and W. Kurz, "Microstructural effects on the sliding wear resistance of a cobalt-based alloy," Wear, no. 174, pp. 81-91, 1994.

[38] H. Yu, R. Ahmed, H. de Villiers Lovelock, and S. Davies, “Tribo-Mechanical Evaluations of Cobalt-Based (Stellite 4) Alloys Manufactured via HIPing and Casting,” Proceedings of the World Congress on Engineering 2007 Vol II WCE 2007, July 2 - 4, 2007, London, U.K.

[39] M.X. Yao, J.B.C. Wu, Y. Xie, “Wear, corrosion and cracking resistance of some W- or Mo-containing Stellite hardfacing alloys,” Materials Science and Engineering: A, Volume 407, Issues 1–2, 25 October 2005, Pages 234-244.

[40] W. Xu, R. Liu, P.C. Patnaik, M.X. Yao, X.J. Wu, “Mechanical and tribological properties of newly developed Tribaloy alloys,” Materials Science and Engineering A, 452-453, 2007, 427-436.

[41] SE Mason, RD Rawlings, “Effect of iron additions on microstructure and mechanical properties of Ni–Cr–Mo–Si hardfacing alloy,” Materials Science and Technology, Volume 5, Number 2, February 1989 , pp. 180-185(6).

[42] A Halstead, RD Rawlings, “The effect of iron additions on the microstructure and

properties of the “Tribaloy” Co-Mo-Cr-Si wear resistant alloys,” J. Mater. Sci., 20 (1985), p. 1693.

[43] Abouei V, Saghafian H, Kheirandish S, Ranjbar K, “A Study on the Wear Behaviour of Dual Phase Steels,” Journal of Materials Sciences and Technology, 23 (2007).

[44] Halis Çelik, Mehmet Kaplan, “Effects of silicon on the wear behaviour of cobalt-based alloys at elevated temperature,” Wear, Volume 257, Issues 5–6, September 2004, Pages 606-611.

[45] Iulian Radu, D.Y. Li, R. Llewellyn, “Tribological behavior of Stellite 21 modified with yttrium,” Wear, Volume 257, Issue 11, December 2004, Pages 1154-1166.

[46] Iulian Radu, D.Y. Li, “Investigation of the role of oxide scale on Stellite 21 modified with yttrium in resisting wear at elevated temperatures,” Wear, Volume 259, Issues 1–6, July–August 2005, Pages 453-458.

[47] Linchun Wang, D.Y. Li, “Effects of yttrium on microstructure, mechanical properties and high-temperature wear behavior of cast Stellite 6 alloy,” Wear, Volume 255, Issues 1–6, August–September 2003, Pages 535-544.

[48] Iulian Radu, D.Y. Li, “The wear performance of yttrium-modified Stellite 712 at elevated temperatures,” Tribology International, Volume 40, Issue 2, February 2007, Pages 254-265.

[49] Y.D. Zhang, C. Zhang, H. Lan, P.Y. Hou, Z.G. Yang, “Improvement of the oxidation resistance of Tribaloy T-800 alloy by the additions of yttrium and aluminium,” Corrosion Science, Volume 53, Issue 3, March 2011, Pages 1035-1043.

[50] Samit Kapoor, “High-Temperature Hardness and Tribological Properties of Stellite Alloys,” Master’s Thesis, Department of Mechanical & Aerospace Engineering, Carleton University, 2011.